Universidad de León
Departamento de Ingeniería y Ciencias Agrarias

Determinación de acciones en silos metálicos: simulación, diseño de modelos experimentales e instrumentación

TESIS DOCTORAL

Autor: D. Ángel Ruiz Padín, Ingeniero Agrónomo

Directores: D. Pedro Aguado Rodríguez, Dr. Ingeniero Agrónomo
D. Ángel Couto Yáñez, Dr. Ingeniero Agrónomo
D. Alberto Tascón Vegas, Dr. Ingeniero Agrónomo

2013

Índice

1. Introducción

1.1. Introducción general y justificación de la unidad temática

El objetivo general perseguido por la línea de investigación que ha obtenido como resultado inmediato los cuatro artículos que configuran la presente tesis es la determinación de acciones en silos en casos de especial dificultad, o poco conocidos o investigados hasta la fecha.

Así, el primer artículo, ***"Dust explosions in vented silos: Simulations and comparisons with current standards"***, publicado en *Powder Technology 208 (2011) 717-724*, trata de la determinación de acciones en el caso de explosiones de polvo en silos, de capital importancia en el diseño de los silos para graneles agrícolas o agroalimentarios debido a su propensión a la formación de polvos combustibles.

Los tres artículos siguientes: ***"Design and instrumentation of a mid-size test station for measuring static and dynamic pressures in silos under different conditions – Part I: Description "***, publicado en *Computers and Electronics in Agriculture 85 (2012) 164-173*, ***"Design and instrumentation of a mid-size test station for measuring static and dynamic pressures in silos under different conditions – Part II: Construction and validation"*** , publicado en *Computers and Electronics in Agriculture 85 (2012) 174–187* , y ***"Experimental study of the pressures exerted by wheat stored in slender cylindrical silos, varying the flow rate of material during discharge. Comparison with Eurocode 1, part 4"***, publicado en *Powder Technology 237 (2013) 450–467*, corresponden al diseño, validación, y primeros resultados de investigación, respectivamente, de una estación de ensayo para la determinación de acciones en un silo de tamaño real. La instalación es novedosa en su concepción, por su versatilidad y modularidad; en su instrumentación, debido al tipo de sensores empleado y la electrónica asociada; y en las posibilidades de ensayo, pues permite la realización de ensayos con graneles agrícolas saturados (para la determinación de acciones de hinchamiento, muy poco conocidas hasta la fecha).

En los apartados siguientes se introduce de forma más extensa cada uno de los cuatro artículos que configuran la presente tesis, presentando los antecedentes que motivan su realización así como una descripción sucinta del trabajo realizado.

1.2. Introducción al artículo I

Muchos de los materiales almacenados en silos producen polvo combustible. Las explosiones de polvo se producen cuando se dispersa el polvo en el aire en forma de nube y reacciona con el oxígeno en presencia de una fuente de ignición, generando una reacción de combustión violenta. Estos materiales incluyen muchos productos agrícolas y alimenticios (cereales, malta, harina, almidón de maíz, azúcar, etc).

De acuerdo con la Directiva ATEX 1999/92/CE, las medidas contra explosiones deben cumplir tres principios (en orden de prioridad): la prevención de la formación de atmósferas explosivas, la evitación de ignición y la mitigación de los efectos de una explosión. En grandes silos es inevitable que se produzcan mezclas de aire/polvo durante el llenado o vaciado, y por lo tanto, las explosiones de polvo representan un serio peligro. La lucha contra posibles fuentes de ignición es por tanto esencial. Sin embargo, en muchas situaciones no es posible eliminar de forma absoluta las fuentes de ignición, y han de tomarse medidas para mitigar el daño.

El Eurocódigo 1, parte 4, "Acciones en estructuras. Silos y depósitos." (EN 1991-4) contempla las cargas producidas por las explosiones, que se clasifican como acciones accidentales, y prescribe que el daño potencial debe ser limitado por ventilación, supresión o contención. La ventilación es la medida de protección más común en silos, debido a sus más favorables características técnicas y económicas, y de hecho suele ser la única opción en grandes silos.

En un silo cerrado sin dispositivos de ventilación, la presión producida por la explosión de una nube de polvo puede llegar a 10 bar (1.000 kPa), con el riesgo de daños graves o incluso la destrucción completa del silo. El alivio de la presión a través de una abertura de ventilación (paneles de venteo) tiene por objeto prevenir la aparición de estas presiones inaceptables. Sin embargo, la ventilación de los silos no siempre es sencilla, y con frecuencia surgen complicaciones que hacen que la prestación de esa protección sea difícil o incluso imposible. Por ejemplo, los grandes silos de metal utilizados en la agricultura y la industria alimentaria por lo general tienen la parte superior de las paredes y la cubierta de baja resistencia, haciendo la instalación de los paneles de venteo técnicamente difícil y costosa.

El área de los paneles de venteo se pueden determinar siguiendo las recomendaciones de las normas EN 14491 y NFPA 68, que son las comúnmente usadas en Europa y América

del Norte respectivamente. Estas normas resultan contradictorias en ciertas situaciones. Dependiendo de la relación de longitud a diámetro (L/D) del silo, el área de los paneles de venteo resultante de la aplicación de la norma EN 14491 puede ser casi el doble que el obtenido con la NFPA 68.

Las ecuaciones de la norma EN 14491 consideran para el cálculo del área de los paneles de venteo un recinto completamente lleno por una nube de polvo en régimen turbulento con una concentración de polvo óptima. Sin embargo, en muchas situaciones prácticas (por ejemplo, en la mayoría de los silos empleados en la agricultura y la industria alimentaria: grandes silos con llenado por caída libre o mecanismo de alimentación mecánica), los procedimientos empleados en la norma europea tienden a sobrevalorar la intensidad de explosión. La propia norma especifica que para nubes de polvo no homogéneas de baja concentración de polvo, en condiciones de turbulencia baja a moderada, se puede reducir el área de ventilación, pero no proporciona ningún valor o fórmula alternativa para el cálculo, sino que indica que se determine por ensayos.

Las simulaciones numéricas podrían proporcionar un método alternativo para la determinación del área de los paneles de venteo en estas situaciones. Con el desarrollo de los recursos computacionales, los métodos numéricos se han convertido en herramientas de gran alcance en muchos campos de investigación en ingeniería. La simulación basada en los principios de la dinámica de fluidos computacional (CFD) se ha convertido en una metodología ampliamente adoptada para resolver problemas complejos con respecto al calor, flujo de fluidos, y en menor medida para explosiones de polvo.

El objetivo principal del presente trabajo consistió en simular explosiones de polvo en silos con ventilación mediante un código CFD comercial, el DESC (Dust Explosion Simulation Code), desarrollado específicamente para las explosiones de polvo, para determinar la magnitud de las presiones resultantes. Conociendo estas presiones, resulta posible a analizar el comportamiento de la estructura de un silo en el caso de una explosión mediante la utilización del método de los elementos finitos (FEM), que ya se ha utilizado con éxito para estudiar los requerimientos de diseño de los silos para otros tipos de carga. Adicionalmente, se compararon las presiones de explosión, así como el área de lo paneles de venteo necesarios para aliviarlas, resultantes de las simulaciones, con los valores previstos en las normas EN 14491 y NFPA 68.

El objetivo final de esta investigación es el de resolver las dificultades técnicas en la protección de los silos contra explosiones de polvo, para solucionar los problemas de diseño de silos a ellas asociados.

1.3. Introducción al artículo II

Numerosos investigadores han desarrollado modelos teóricos para predecir el comportamiento del material almacenado en silos, modelos que precisan de ensayos experimentales para ser validados, lo cual en numerosas ocasiones no se ha realizado en la práctica debido al elevado coste y trabajo que supone el diseño y construcción de estaciones de ensayo. En otras ocasiones se han extraído conclusiones a partir de ensayos realizado en silos a escala, sin embargo es ampliamente conocido que los errores de escala hacen en muchas ocasiones que los resultados obtenidos difieran considerablemente del comportamiento a tamaño real.

A nivel mundial existen muy pocas estaciones experimentales de ensayo y muy pocos ensayos realizados en silos a tamaño real, se trata de instalaciones y ensayos que han exigido un gran esfuerzo y de los cuales se han obtenido resultados de gran importancia. Sin embargo, a día de hoy, aún existen numerosas incertidumbres susceptibles de ser investigadas para llegar a predecir el comportamiento del material almacenado en este tipo de estructuras de modo suficientemente fiable. El problema de estas instalaciones se debe a que el diseño de silos en la práctica admite múltiples configuraciones lo que hace que las condiciones de contorno y parámetros a controlar sea muy elevado.

En este artículo se describe el diseño de una estación de ensayo de presiones en silos a tamaño real. El diseño versátil de la misma permite adaptar su geometría a las configuraciones más comúnmente presentadas en la práctica para silos esbeltos, permitiendo la realización de ensayos con fondo plano o con tolva y combinar ambos casos con la descarga centrada o excéntrica. Además, para cada una de estas configuraciones es posible el estudio del comportamiento del material en diferentes condiciones, estado estático, estado dinámico de carga o descarga, variación de la velocidad de carga o descarga, presiones de hinchamiento en el caso de material almacenado saturado con soluciones acuosas, simulación del aumento de la altura del silo, etc.

La versatilidad de la misma pretende servir como herramienta de validación para los modelos teóricos existentes y al mismo tiempo, obtener nuevos datos de modo que sirva

para dar un paso más en el conocimiento del comportamiento del material almacenado en este tipo de estructuras.

1.4. Introducción al artículo III

El presente artículo es la continuación del desarrollado previamente por los autores sobre el diseño de una estación de ensayo para la determinación de las acciones de los materiales almacenados en silos. Siguiendo dicho diseño se ha construido una estación de ensayo a tamaño real. Inicialmente no se ha dotado a la instalación del equipamiento completo, sino de un equipamiento básico que permita validar el diseño para posteriormente completarlo con el resto de elementos. En esta publicación se exponen las principales características de dicha instalación y los resultados obtenidos en los primeros ensayos. Los resultados son comparados con los valores obtenidos con la normativa europea de cálculo de acciones en silos.

Para la medida de presiones y desplazamientos en los ensayos y estaciones anteriormente citados es común el empleo de células de presión, células de campo libre, galgas extensométricas y medidores de desplazamiento.

A diferencia de otros ensayos realizados previamente, la estación aquí citada presenta la novedad de que las presiones en el interior del silo se determinan a partir de células de carga; así, las presiones normales a la pared se determinan a partir de células de carga de flexión mientras que las presiones verticales se determinan a partir de células de carga de tracción/compresión, elementos usados comúnmente en el pesaje industrial. Otra novedad que aporta es la versatilidad de la misma, ya que permite el ensayo tanto de silos con fondo plano como con tolva, el estudio de la descarga centrada y excéntrica, la simulación de silos con mayor relación altura/diámetro o incluso el estudio del hinchamiento del material cuando este se humedece.

El resultado de este novedoso diseño es que permite obtener la mayoría de los parámetros que rigen el comportamiento del material almacenado y comparar y validar mediante ensayos reales los diferentes modelos teóricos usados y la normativa vigente.

Aunque de los ensayos realizados ya se pueden extraer algunas conclusiones novedosas acerca de las leyes que rigen los empujes en el interior de este tipo de estructuras, teniendo en cuenta la versatilidad de la estación de ensayo, los diferentes tipos de ensayo que pueden realizarse y los distintos materiales susceptibles de ser ensayados, la finalidad que

se persigue con esta publicación es, únicamente, la de demostrar que el diseño teórico de la estación de ensayo expuesto en la anterior publicación es válido para la medida de presiones en silos y que este brinda múltiples posibilidades para el avance de las investigaciones en esta materia.

1.5. Introducción al artículo IV

En esta publicación se exponen los resultados de una serie de ensayos experimentales de presiones en la pared en silos cilíndricos de acero obtenidos cuando el material almacenado es trigo, realizados en la estación de ensayo cuyo diseño y validación se expone en los dos artículos anteriores.

Se realizaron un total de 20 ensayos, con tres secuencias de funcionamiento: tipo I, llenado – estático – vaciado (7 ensayos); tipo II, llenado – estático – vaciado parcial – estático – vaciado completo (12 ensayos); y tipo III, llenado – estático – vaciado parcial – estático – rellenado – estático – vaciado parcial – estático – rellenado – estático – vaciado completo (1 ensayo). Para cada uno de los ensayos, se estudió el comportamiento del material almacenado en estado estático y durante la descarga y se experimentó con diferentes flujos de material en la descarga. Además se ensayó el efecto en las presiones de descargas parciales además de completas. Los resultados fueron comparados con los valores obtenidos con la normativa europea de cálculo de acciones en silos.

2. Resultados y discusión

2.1. Resumen global de resultados

Con respecto a la determinación de acciones en silos mediante simulación, los resultados obtenidos mediante el código DESC para el cálculo de explosiones de nubes de polvo indicaron que en las condiciones habituales en los grandes silos agrícolas, las normas EN 14491 y NFPA 68 sobrevaloran la magnitud de las sobrepresiones en presencia de dispositivos de venteo. Estos resultados deben ser empleados con precaución, dado que la magnitud de las sobrepresiones obtenidas resulta muy dependiente de los parámetros de la nube de polvo supuestos para la simulación. Adicionalmente, se obtuvieron valores de la magnitud de las subpresiones potenciales, para cuya determinación no existe formulación en las normas citadas remitiendo éstas a ensayos experimentales de imposible realización en la práctica.

Con respecto al diseño, validación y utilización de una estación experimental de ensayo de silos para la determinación de acciones, el principal resultado fue la ejecución de la estación en sí misma, a partir del diseño ideado. Durante la validación del diseño se descubrió un fenómeno de reasentamiento del grano, con período creciente, desconocido hasta la fecha. La primera serie de ensayos tras la validación ha proporcionado resultados del comportamiento del material durante la descarga parcial no documentados previamente. En algunos de los ensayos, las acciones (presiones) registradas resultaron superiores a las obtenidas por aplicación de la normativa vigente.

En los apartados siguientes se detallan de forma más extensa los resultados de cada uno de los cuatro artículos que configuran la presente tesis.

2.2. Resultados y discusión del artículo I

Las dimensiones de los silos simulados fueron: diámetro (D) 6 m, relación altura diámetro (L/D) 1,5-2-2,5 (L: 9, 12 y 15 m), área de venteo 0 a 8 m^2, presión de activación de venteo (P_{stat}) 0,05 y 0,10 bar. Los valores de explosividad empleados fueron los correspondientes a un llenado del silo con almidón de maíz, por tratarse de un material homogéneo y habitual en los ensayos de explosiones en silos. Se ensayaron dos tipos de condiciones iniciales para la nube de polvo: condición 0, con concentración de polvo de 300 g/m^3 e intensidad

relativa de turbulencia del 112%; y condición 1, con concentración de polvo de 500 g/m^3 e intensidad relativa de turbulencia del 80%.

En las simulaciones realizadas, las presiones registradas en diferentes puntos de control fueron casi de la misma misma magnitud, concluyéndose que la distribución de la presión en los silos durante las explosiones resulta uniforme. Hubo dos instantes a lo largo de los gráficos de tiempo-presión en los que se registraron diferencias triviales en diferentes puntos de control: cuando los paneles de venteo acababan de abrir, lo que lleva a una rápida disminución de la presión, y cuando la presión alcanzó un segundo valor pico y comienza a bajar. Analizando las secuencias de tiempo-temperatura registradas en distintos puntos de control, se observó que la llama se propaga más lentamente que la presión.

En algunas de las simulaciones se observaron fases de presión negativa sobre la curva de presión-tiempo; los valores máximos alcanzados fueron de -0,02 bar. Estas presiones negativas mostraron las siguientes tendencias: aumentaron con la relación L/D del silo; para la misma geometría de silo aumentaron con el área de ventilación, y se incrementaron cuando la presión de activación en los paneles de venteo disminuyó. Estas subpresiones pueden producir importantes esfuerzos de compresión en las paredes del silo, provocando el fallo por pandeo . Por lo tanto, se concluye que no es suficiente considerar sólo la sobrepresión máxima desarrollada por explosiones en el cálculo de la estructura de un silo, sino también las subpresiones.

Los silos de metal, que tienen paredes más delgadas que los silos de hormigón, son especialmente vulnerables a los esfuerzos de compresión inducidos por la formación de vacíos parciales. Sin embargo, ni la norma europea (EN 14491), ni la americana (NFPA 68), ni el Eurocódigo 1, parte 4, “Acciones en estructuras. Silos y depósitos”, proponen un método para predecir las posibles subpresiones. Las simulaciones por ordenador pueden ser una herramienta muy útil para predecir el valor de las subpresiones potenciales.

La comparación con las normas EN 14491 y NFPA 68 se realizó mediante curvas área de venteo vs. presión. Las tendencias de las curvas de las simulaciones fueron similares a las resultantes de la aplicación de ambas normas. Sin embargo, los valores de la sobrepresión (P_{red}, presión de explosión reducida por venteo) obtenidos en las simulaciones para la condición 0 fueron menores que los obtenidos con ellas. Para valores bajos de P_{red}, las diferencias fueron significativas en comparación con las áreas de venteo previstas por la norma NFPA 68, y muy grandes en comparación con las de la norma EN 14491. La curva

de las simulaciones para la condición 0 es aproximadamente paralela a la curva de norma NFPA 68.

Para la condición 1, los resultados de las simulaciones coincidieron bien con los valores previstos por la norma NFPA 68, existiendo muy poca diferencia entre sus curvas. Los valores de P_{red} obtenidos por simulación fueron algo menores que los de la norma NFPA 68 para silos de 9 m de altura y ligeramente mayores para los silos de 12 m y 15 m de altura. Sin embargo, las diferencias siguieron siendo elevadas con la norma EN 14491 para valores bajos de P_{red}, a pesar de ser la condición 1 más desfavorable que la condición 0.

Las diferencias entre las simulaciones y las normas podrían explicarse por las condiciones de la nube de polvo inicial consideradas. En este trabajo, la concentración de polvo, la velocidad del aire y la turbulencia fueron ajustados a los medidos durante el proceso de llenado mecánico de un silo real. Estos valores fueron muy bajos en comparación con los valores medidos en los ensayos estándar de explosión en laboratorio, en los que la nube de polvo se crea mediante la descarga de contenedores de polvo presurizados. Estos contenedores presurizados son también el método empleado para crear nubes de polvo en los ensayos de ventilación de explosiones, empleando un número de contenedores proporcional al volumen del silo, y en los que las normas se basan parcialmente.

Por otra parte, las diferencias significativas entre las normas EN 14491 y la NFPA 68 para valores bajos de P_{red} pueden ser explicados por la corrección del área de venteo para recipientes alargados que prescribe la norma EN 14491 cuando $P_{red} < 1{,}5$ bar y $L/D > 1$. Esta corrección depende de la relación L/D y de P_{red}, y conduce a incrementos del área de ventilación muy elevados si P_{red} es muy baja. Por lo tanto, valores más bajos de P_{red} resultan en una corrección del área de venteo más grande para una relación L/D dada. Esta corrección es la misma que se propuso en los años 90 por la segunda versión de la norma alemana VDI 3673. Las ecuaciones de la NFPA 68 también introducen una corrección para recipientes alargados cuando $L/D > 2$, pero impone incrementos más moderados del área de venteo que la EN 14491 cuando P_{red} es muy bajo, y no prescribe corrección del área para $L/D \leq 2$. Para los silos estudiados en este trabajo, las grandes diferencias entre las áreas de ventilación propuestas por la norma EN 14491 y la NFPA 68 para valores bajos de P_{red} son debidos principalmente al tipo de corrección aplicada por la relación L/D.

La variación de la presión de activación de los paneles de venteo (P_{stat}) no tuvo un efecto importante sobre las sobrepresiones registradas. Para una P_{stat} de 0,05 bar se observó una

reducción media del 4,33% en P_{red} con respecto a las simulaciones con P_{stat} de 0,1 bar. Estos resultados concuerdan muy bien con la reducción media del 4,02% en P_{red} obtenida con la norma NFPA 68 cuando la presión de activación se reduce de 0,1 bar a 0,05 bar. Ambos estándares asumen que una menor presión de activación del dispositivo de ventilación produce una P_{red} inferior debido a la liberación más rápida de gases de combustión calientes y polvo no quemado. Sin embargo, la norma EN 14491 considera como valor mínimo de P_{stat} 0,1 bar, y exige que las áreas de ventilación sean calculadas con ese valor aún cuando sea menor.

La concentración de polvo tuvo una fuerte influencia sobre la sobrepresión reducida de explosión. P_{red} aumentó cuando la concentración estaba más cerca de la concentración óptima (aproximadamente 750 kg/m^3 para el polvo de almidón de maíz utilizado en las simulaciones), un resultado previsible. La influencia de las condiciones de las nubes de polvo iniciales sobre P_{red} resultó mayor cuando el área de ventilación era pequeña. Por otro lado, las diferencias entre las normas EN 14491 y la NFPA 68 se redujeron cuando P_{red} fue alta, aumentando notablemente cuando fue baja

Para bajas sobrepresiones ($P_{red} \leq 0,3$ bar), que son comunes para los silos cilíndricos metálicos, las áreas de ventilación necesarias de acuerdo con las simulaciones numéricas resultaron aproximadamente la mitad de las consideradas por la norma EN 14491.

Las simulaciones realizadas confirman la idea generalizada de que las áreas de ventilación calculadas de acuerdo con la norma EN 14491, que se basa en la norma anterior VDI 3673, son muy conservadoras en comparación con las que realmente podrían ser necesarias en la mayoría de grandes silos. Se deben exceptuar de esta consideración algunos escenarios posibles que podrían implicar temporalmente condiciones de alta concentración de polvo y alta turbulencia (como una explosión de polvo secundaria). Debe tenerse en cuenta que la ecuación general en la norma EN 14491 *"se aplicará a los recintos individuales cuando se hayan tomado medidas (aislamiento de explosiones) para evitar la propagación de la llama entre recintos"*. Por consiguiente, cuando se hayan implementado medidas de aislamiento, la posibilidad de explosiones secundarias es remota, y parece claro que la EN 14491 sobredimensiona las áreas de ventilación para grandes silos aislados, en particular cuando la turbulencia no es alta y la nube de polvo no es homogénea.

Los resultados obtenidos mediante simulación por ordenador con el código DESC se deben utilizar con extrema precaución, ya que resultan muy dependientes de las condiciones

iniciales de la nube de polvo (concentración de polvo, velocidad del aire y turbulencia). Por tanto, la realización de simulaciones precisas requerirá la determinación exacta de las características de las nubes de polvo, mediante su medición en situaciones reales en grandes silos.

2.3. Resultados y discusión del artículo II

El resultado de éste artículo es el propio diseño de la estación de ensayo, que se describe a continuación. Se realizó el diseño para el ensayo de silos cilíndricos esbeltos ya que es la configuración más comúnmente empleada en la industria, aunque el diseño e instrumentación también sería válido para construir estaciones de ensayo para silos de sección cuadrada, rectangular o incluso poligonal, empleando los mismos principios y adaptándolos a la geometría elegida.

La instalación se compone de 2 silos, uno de ensayo y otro para almacenamiento del material granular a ensayar. El llenado y vaciado de los mismos se realiza interconectando los dos silos mediante dos sinfines movidos por motores eléctricos. Para la medida de presiones en la pared y fondo del silo de ensayo bajo diferentes condiciones, este se instrumenta con células de carga situadas en puntos estratégicos del mismo.

La geometría del silo que se describe es cilíndrica, y se compone de 3 partes independientes y desmontables, una parte inferior o fondo donde se sitúa la salida del material almacenado, un cuerpo cilíndrico o parte central y una tapa o coronación en la parte superior.

La parte inferior se compone de 4 piezas, por una parte, un juego de 3 tolvas intercambiables, una con descarga centrada, otra con descarga totalmente excéntrica y otra con una excentricidad de la boca de salida intermedia. Las 3 tolvas se refuerzan con un anillo en la zona de unión con el cilindro de la parte central. La cuarta pieza está formada por un fondo plano, en éste se disponen a su vez tres bocas de salida (centrada, intermedia y excéntrica)

El cuerpo del silo está formado por un cilindro reforzado en su base y coronación con dos anillos. Mediante estos anillos se independiza la parte central, ya que irán apoyados sobre células de carga verticales de forma que se puedan determinar de manera independiente las fuerzas verticales que se produzcan en ella.

La parte superior la forma una tapa reforzada con un anillo de acero en su perímetro. Dicho anillo servirá de apoyo de la misma en las tres células de carga verticales que la independizan del cilindro. Las tres células de carga en la parte superior permitirán conocer las cargas verticales en la pared con respecto a la parte superior, lo que será de utilidad cuando se introduzcan cargas en la parte superior del silo. La tapa no es plana ya que en ella se dispone un alojamiento para colocar una membrana hinchable con objeto de introducir cargas adicionales en la parte superior del grano.

La medida de presiones en la pared del cilindro se realiza en cuatro generatrices y a distintas alturas. La medida de presiones en la tolva se realiza inmediatamente debajo de la transición, en la prolongación de las generatrices de medición del cilindro anteriormente citadas. Para la medida de presiones normales a la pared en las distintas zonas se utilizan células de carga de flexión. Para ello se realizan aberturas en la pared donde se situarán chapas con la misma forma del hueco existente y mismo espesor de la pared, estas serán del mismo material que la pared y se encontrarán totalmente enrasadas en la parte interna del silo.

En dichas chapas se acoplan las células de carga paralelas al cilindro, lo cual permitirá medir la fuerza horizontal aplicada sobre una superficie de área conocida. Entre los bordes de la chapa y la pared se dispone una mínima holgura para evitar rozamiento y asegurarnos que la chapa gravita únicamente sobre la célula de flexión. Existen en el mercado células de carga de este tipo que sufren deformaciones muy pequeñas, entre 0,3 y 0,5 mm en estado de carga límite, con lo cual se evita el posible error en la interpretación de presiones que podría provocar el desplazamiento de la pared del silo conectada a las mismas debido a la falta de rigidez de estas.

La medida de presiones verticales se realiza con células de carga de tracción-compresión. La medida de fuerzas verticales actuando sobre la pared es posible ya que las tres partes que forman el cuerpo del silo (tapa, cilindro y tolva) se encuentran independizadas, es decir, los anillos de refuerzo de las mismas se encuentran muy próximos pero no llegan a tocarse en ningún punto. La interconexión física para que el silo funcione como un conjunto se realiza mediante el apoyo de los anillos de refuerzo en las células de carga de tracción-compresión.

Se realiza la medición en puntos situados en tres niveles de altura colocando en cada nivel tres células de carga espaciadas 120º en la circunferencia. La tolva se apoya sobre tres

células de carga (L0), lo que nos permitirá medir el peso total del material almacenado. El cilindro se apoya en otras tres células de carga (L1), situadas sobre las anteriores, lo que nos permitirá medir la fuerza vertical actuante sobre la pared. En la parte superior del cilindro se sitúan otras tres células de carga (L2) sobre las que se apoyará la tapa del silo, lo cual permitirá introducir cargas en la parte superior para la simulación de presiones en silos con una relación altura/diámetro mayor, evitando la necesidad de construir un cilindro de mayor altura. Este sistema también permitirá el estudio del empuje de hinchamiento del material almacenado bajo diferentes presiones de confinamiento. Para ello, en el alojamiento existente en la tapa superior se colocará una membrana elástica hinchable con el fin de aplicar la sobrepresión establecida en el experimento en la parte superior.

Al igual que las células de carga de flexión, las células de carga de tracción-compresión de este tipo existentes en el mercado, tienen una deformación a carga máxima muy pequeña, menor de 0,5 mm, con lo cual no existe el riesgo que durante el ensayo entren en contacto los anillos que independizan las tres partes del silo, para ello es importante que en la elección de la separación entre los anillos se tenga en cuenta la deformación a carga máxima de la célula elegida.

La descarga se realiza mediante tornillos sin fin acoplados a dos motores de corriente alterna. Para el control de la velocidad de llenado y descarga se regula la velocidad de rotación de los mismos mediante variadores electrónicos de frecuencia (VFD, *Variable Frequency Drive*).

Para el control de la instalación se usa un protocolo de comunicación estándar con interfaz RS485. Para ello se diseña un software SCADA (*Supervisory Control And Data Adquisiton*) específico. La señal analógica que envía cada célula de carga (mV/V) es procesada por un conversor A/D en una lectura digital que se transmite por la red RS485, los conversores existentes en el mercado son capaces de procesar y volcar varias lecturas por segundo.

La lectura y almacenamiento de los datos enviados por las células de carga, así como el control de la velocidad de rotación de los motores se realiza desde el PC, mediante el software SCADA, la aplicación, diseñada específicamente para tal fin, permite elegir el intervalo de tiempo ente lecturas (desde décimas de segundo), almacenándolas en un fichero de texto. Al mismo tiempo permite actuar sobre los variadores electrónicos de frecuencia y establecer la velocidad de llenado o vaciado deseada en cada experimento.

El valor de las presiones normales a la pared se obtiene directamente de la lectura de las células de flexión situadas en las 4 generatrices de la pared del cilindro y tolva, para ello, se divide el valor de la fuerza obtenido en cada célula por la superficie de la pared sobre la que actúa. De esta forma conocemos en cada instante la presión normal a la pared del cilindro y tolva en los puntos donde se sitúan las células.

El valor medio de la presión normal a la pared del cilindro, en la unión silo tolva, en cada instante t, se obtiene de la lectura de las células de flexión situadas en las 4 generatrices del cilindro. La superficie de pared sobre la que actúa cada célula situada en el cilindro es constante. La comparación de lecturas entre las cuatro células de carga situadas en ese nivel permitirá detectar si la distribución de presiones normales a la pared es axil-simétrica o no, el patrón de distribución que siguen y su valor máximo en caso de distribuciones no axilsimétricas. De igual modo se pueden obtener dichas presiones a distintas alturas del cilindro, realizando el mismo análisis en todos los niveles en que se sitúan células de flexión.

La presión vertical media en la parte inferior del cilindro (unión silo tolva) se obtiene de la lectura de las células de carga de tracción/compresión situadas en el nivel L1. Por comparación de los valores obtenidos por las células de carga podremos conocer además si la presión vertical en la pared es axilsimétrica o no.

La presión vertical media del material almacenado a nivel de la unión silo-tolva se obtiene de la lectura de las células de tracción/compresión situadas en los niveles L0 y L1. Este parámetro nos permite conocer la carga transferida por el grano al fondo del silo (en el caso de silos de fondo plano) o a la tolva.

La media de la fuerza de rozamiento del material almacenado contra la pared del cilindro se puede conocer en cada instante, puesto que conocemos la evolución en el tiempo de la superficie del cilindro en contacto con el material almacenado, ello es posible al ser conocida la velocidad de llenado y de vaciado. De la misma forma se puede determinar el valor medio del coeficiente de rozamiento grano pared. El silo es de acero, con lo cual los resultado de rozamiento grano pared serán aplicables a silos con pared lisa, sin embargo sería posible estudiar la influencia del coeficiente de rozamiento grano pared en los empujes, para ello bastaría con alterar la rugosidad de la pared revistiéndola interiormente con láminas flexibles de distintas rugosidades o cualquier otro método que modifique la rugosidad de la pared. Del mismo modo, también es posible la simulación de uniones

soldadas, para el caso del estudio de silos construidos de este modo, simulando las imperfecciones. El Eurocódigo propone determinar estos parámetros a base de ensayos de laboratorio, en esta estación de ensayo se puede determinar directamente.

La simulación de mayores alturas de almacenamiento se consigue transmitiendo una presión vertical adicional al material almacenado en la parte superior del silo. Ello permitirá el estudio de presiones estáticas y dinámicas de vaciado al inicio de la descarga. Para ello, en la tapa del silo se dispone un alojamiento para albergar una membrana hinchable. La sobrepresión que transmite dicha membrana al material almacenado es función de la presión de hinchado de la misma y se puede obtener a partir de la lectura de las células de tracción/compresión situadas en el nivel L2.

Para determinar la presión vertical del material almacenado en la unión silo tolva deberá tenerse en cuenta que la lectura de las células de carga del nivel L2 será negativo (tracción) frente al positivo (compresión) de las células de carga de los niveles L1 y L0.

De esta forma se podrá analizar el efecto que produce una sobrepresión sobre el material almacenado y su influencia en las presiones horizontales. Para obtener la presión vertical por unidad de longitud en la base del cilindro habrá que tener en cuenta además las fuerzas verticales adicionales que actuarían sobre la pared del cilindro debidas al rozamiento del grano con las paredes y el al propio peso del cilindro que se simula.

Determinados materiales susceptibles de almacenamiento en este tipo de estructuras se hinchan al ser humedecidos o saturados con soluciones acuosas, lo cual provoca un aumento en las presiones en el interior del silo. Para el estudio de las presiones de hinchamiento se construye una membrana impermeable con la misma forma y dimensiones que el interior del silo y se satura el material almacenado con la solución acuosa a ensayar. Para evitar que la membrana, al ofrecer resistencia al hinchamiento, falsee las lecturas de las células de carga, las chapas de la pared para la lectura de presiones, en este ensayo, no se encuentran enrasadas con la pared interior del cilindro, si no que se colocan de modo que sobresalgan ligeramente hacia el interior del silo. La determinación de las presiones y los distintos parámetros del material almacenado se determinará según lo descrito en los apartados anteriores para material almacenado en condiciones normales. El estudio del hinchamiento bajo distintas presiones de confinamiento del material almacenado es posible transmitiéndole la sobrepresión deseada al mismo en la parte superior del silo, con el procedimiento ya descrito.

2.4. Resultados y discusión del artículo III

Para la evaluación y validación de la estación de ensayo cuyo diseño se recoge en el artículo previo, se realizaron 12 ensayos consistentes en la toma de datos en tres fases: durante el llenado del silo, en estado estático y durante la descarga. El llenado del silo se realizó centrado y a velocidad constante, y una vez finalizada esta fase se dejó el material en el interior del silo durante distintos intervalos de tiempo. Para realizar la descarga se abrió totalmente la trampilla de la boca de salida del silo, de modo que en los primeros instantes se producía una descarga libre hasta que se llenaba la tolva de recogida del sinfín de vaciado y a partir de este punto la descarga se producía a velocidad constante.

El comportamiento y valor que alcanzaron los distintos parámetros analizados fue similar en los 12 ensayos. Para evitar un número elevado de figuras o gráficos sobrecargados, en el artículo publicado solo se detallaron los resultados que se obtuvieron en dos de los ensayos realizados, cuya diferencia fue el tiempo de permanencia del material en estado estático en el interior del silo, que en el primero fue de 21,8 horas y en el segundo 1,6 h.

Del análisis de las presiones normales a la pared del silo y presiones verticales del material almacenado a nivel de la unión silo tolva, resultó en ambos ensayos que la presión normal a la pared alcanzó los mayores valores durante la descarga en la pared de tolva al nivel de la unión silo-tolva, lo cual coincide con la normativa europea y con ensayos en silos reales existentes a nivel internacional.

Analizando la variación en el tiempo de las presiones normales a la pared y la presión vertical en el material almacenado al nivel de la unión silo tolva, en el intervalo entre el fin del llenado y el comienzo de la descarga, es decir, en estado estático, se observó que la presión vertical en el material almacenado al nivel de la unión silo tolva aumentaba con el tiempo, y lo mismo ocurría con la presión normal a la pared de la tolva. En el caso de las presión normal a la pared del cilindro, ocurría lo contrario, disminuyendo con el tiempo. Es decir, las paredes del cilindro van descargándose, aumentando el peso que descansa sobre la tolva.

Así, en estado estático, las presiones en el interior del silo no permanecen constantes, observándose un proceso de reasentamiento del material en el interior del silo, que se produce de forma repentina y en intervalos de tiempo cada vez más espaciados. Este comportamiento resulta un descubrimiento novedoso. Es un fenómeno acerca del cual no se ha encontrado ninguna referencia ni en la normativa ni en las numerosas publicaciones

internacionales sobre silos consultadas, por lo que se considera que debe ser investigado en profundidad para dilucidar los principios físicos que provocan este comportamiento.

Las figuras que muestran la evolución temporal de las presiones a lo largo de todo el ensayo reflejaron que la instrumentación diseñada era correcta y adecuada a los objetivos de la estación. La lectura de los distintos sensores fue coherente, entre sí y con respecto a su evolución temporal.

El corto intervalo de tiempo fijado para la lectura de datos durante el ensayo (0,5 s) permitió observar que la sobrepresión que se produce durante la descarga no es instantánea para luego descender gradualmente, sino que se alcanza un valor máximo y se mantiene casi constante durante unos segundos.

Las posibilidades de ensayo dinámico fueron patentes en el análisis de las lecturas durante la descarga. Así, se observó que la lectura de las células situadas en la parte inferior del silo reflejaban el inicio de la descarga de forma instantánea, mientras que la célula de la parte superior empieza a variar su lectura aproximadamente un segundo más tarde. Esto se puede interpretar como una medida de la velocidad de la onda de sobrepresión, que se propaga desde la parte inferior hasta la parte superior del silo. El máximo incremento de presiones se produjo en la pared de la tolva al nivel de la unión silo-tolva, llegando a duplicar la presión en estado estático.

Comparando las presiones máximas obtenidas durante los ensayos en estado estático y las presiones máximas obtenidas durante la descarga con el Eurocodigo 1 parte 4, los valores obtenidos en los ensayos fueron inferiores a los obtenidos con el método de cálculo propuesto por la norma.

Analizando las presiones de vaciado, se observó que estas no siguen un patrón regular en el incremento de presiones en la pared con respecto a las presiones en estático, sino que la curva sufre unas ondulaciones y estas se producen a la misma altura en los dos ensayos cuyos resultados figuran en el artículo y en el resto de ensayos realizados. En un principio se atribuyó a una mala calibración de las células situadas a ese nivel o a la existencia de rozamiento entre las placas que transmiten la presión a las células y la pared del silo, por lo que se comprobó la holgura existente y se recalibraron las células, encontrándose que se volvía a producir el mismo fenómeno. Por último, se intercambiaron las células entre los distintos niveles de la pared y el fenómeno volvió a aparecer. La explicación podría estar en el modo de propagación de las sobrepresiones durante el vaciado, desde la parte inferior

a la superior del silo como se ha comentado anteriormente, provocando incrementos de presión en determinadas zonas y permaneciendo la presión casi constante o incluso disminuyendo en otras.

En el análisis de los datos obtenidos en los 12 ensayos realizados consistentes en llenado concéntrico, estado estático y descarga centrada, no se encontraron diferencias de presiones significativas entre los diferentes ensayos para la generatriz ensayada, lo que permite suponer que en el silo diseñado no se produce asimetría de presiones normales a la pared a lo largo de la circunferencia del cilindro, asimetrías sí observadas por diversos autores aun siendo la descarga centrada. La ausencia de las mismas podría tener su explicación en las condiciones de diseño del silo, construido con un estricto control de la geometría; y de las condiciones ambientales, ya que el silo se encuentra en el interior de un laboratorio.

2.5. Resultados y discusión del artículo IV

Los ensayos se realizaron con trigo (*Triticum aestivum*) variedad Galera R2, con pureza mínima del 98%. Las propiedades de este material habían sido previamente determinadas experimentalmente en los laboratorios de la Escuela conforme al método propuesto en el Eurocódigo 1, parte 4. Los valores obtenidos fueron: peso específico, 8,38 kN /m^3; ángulo de rozamiento interno, 34,22º; coeficiente de fricción con pared de acero, 0,20; y humedad, 10,3%. Usando este material granular se realizaron 21 ensayos de llenado y vaciado centrados del silo.

En un primer grupo de ensayos (tipo I, ensayos 1 a 7), tras llenar el silo con el material granular, se mantuvo en estado estático en torno a 5 minutos y a continuación se procedió al vaciado del mismo variando la cantidad de flujo de grano entre los distintos ensayos. Para realizar el vaciado se pusieron primero en marcha los motores que mueven los tornillos sinfín y se abrió después la compuerta de la boca de salida, encontrándose en todos los ensayos la tolva del tornillo sinfín libre de material. La variación de la cantidad del flujo de grano se consiguió variando la posición de la tajadera de la boca de salida, ensayándose 4 posiciones de la misma: P_I, totalmente abierta (ensayos 1 y 2), P_{II} (ensayos 3 y 4), P_{III} (ensayos 5 y 6) y P_{IV} (ensayo 7).

En un segundo grupo de ensayos, (tipo II, ensayos 8 a 20), al igual que en los descritos anteriormente, se varió el flujo de grano con las mismas cuatro aperturas de la tajadera de

salida, pero con una modificación con respecto a los anteriores consistente en que el vaciado se realizó en dos etapas: en una primera etapa se abrió la tajadera de la boca de salida del grano con los motores del dispositivo de vaciado apagados, con lo que el vaciado se interrumpía una vez colmatada la tolva del dispositivo de vaciado volviendo a encontrarse el material granular en estado estático (el tiempo de permanencia en esta fase se varió entre los distintos ensayos) y en una segunda se reinició el vaciado con la tolva llena.

Por último, se realizó un ensayo (tipo III, ensayo 21) consistente en llenar el silo, realizar una descarga parcial de unos 2,10 kN y volver a rellenar hasta el nivel inicial, repitiendo el proceso dos veces. Cada una de las 2 descargas parciales se realizó en siete etapas de aproximadamente 0,3 kN cada una. Para ello se abrió la compuerta de salida del grano hasta la posición 3 (P_{III}) con el dispositivo de vaciado encendido, de modo que no llegase a colmatarse la tolva de recogida del mismo, se descargaron aproximadamente 0,3 kN de grano y se cerró la compuerta, se mantuvo en estado estático 5 minutos aproximadamente y se repitió el proceso, realizando la descarga parcial de los 2,1 kN en 7 etapas, a continuación se rellenó el silo hasta el nivel inicial y se repitió el proceso, y por último se volvió a llenar el silo y se hizo una descarga completa del mismo en una única etapa.

En todos los ensayos se observó que durante la descarga la totalidad del material almacenado se encuentra en movimiento (*mass flow*).

Resultados de los ensayos tipo I

En los ensayos de tipo I, se observó que la presión normal a la pared sufría una variación considerable al iniciarse la descarga, alcanzando los mayores valores en la pared de tolva, al nivel de la unión silo-tolva, en coincidencia con la normativa europea y con otros ensayos en silos reales. Ese incremento llegó a alcanzar hasta un 179,8% en la pared de la tolva y hasta un 89,3% en la parte inferior del cilindro. En las células de la parte inferior del cilindro el incremento de presión fue siempre positivo, mientras que en la parte superior del cilindro se registró que a determinadas alturas la presión permanecía casi constante o incluso descendía. La interpretación de este comportamiento, que se repitió en los ensayos tipos II y III, fue que durante la descarga se produce una variación en la compactación del grano a diferentes alturas; permitiendo formular la hipótesis de que en un silo de longitud infinita este fenómeno consistente en aumentar la presión en determinadas zonas en detrimento de otras se repetiría a intervalos a lo largo de la altura de silo.

En estado estático, la presión vertical en el material almacenado al nivel de la unión silo tolva aumentó con el tiempo, al igual que la presión normal a la pared de la tolva. En el caso de las presiones normales a la pared del cilindro ocurrió lo contrario, disminuyendo con el tiempo. Así, en estado estático, las paredes del cilindro van descargándose, aumentando el peso que descansa sobre la tolva debido al reasentamiento del grano en el interior del silo.

En lo que respecta al flujo durante la descarga, se observó en primer lugar como para la misma posición de la boca de salida el flujo varia ligeramente entre unos ensayos y otros, debido a que la apertura de la tajadera es manual hasta una marca realizada en la misma con lo cual no es exactamente la misma abertura para cada posición ensayada. También se observó como en los ensayos con la boca de salida en P_I y P_{II} la cantidad de flujo es prácticamente la misma, debido a que esta cantidad de flujo coincide con el máximo que es capaz de evacuar el dispositivo de descarga, con lo que en los ensayos en P_I, en los primeros instantes el flujo es mucho mayor (descarga libre), llegando a colmatarse la tolva del dispositivo de vaciado, momento a partir del cual la descarga continua a un flujo constante coincidente con el máximo que es capaz de evacuar el tornillo sin fin, mientras en los ensayos con la boca de salida en P_{II}, la abertura de la misma evacua un flujo hacia la tolva del dispositivo de vaciado coincidente aproximadamente con el máximo que es capaz de evacuar. En los ensayos P_{III} y P_{IV} el flujo evacuado es inferior al que es capaz de evacuar el dispositivo de vaciado con lo que la tolva del mismo nunca llega a colmatarse.

Analizando el máximo de presiones normales a la pared registradas durante la descarga al nivel de la unión silo-tolva en función del flujo de descarga, se observó que las presiones en la pared disminuyen linealmente al aumentar la velocidad de descarga, mientras que las presiones máximas alcanzadas en la tolva son prácticamente constantes e independientes de la velocidad de descarga. Así, de acuerdo a los resultados obtenidos y contrariamente a lo que podría pensarse, una descarga rápida no implica una mayor sobrepresión en la pared del silo.

Resultados del ensayo tipo II

En los ensayos del tipo II, los resultados en la fase de llenado y en la primera fase en estado estático fueron comparables y similares a los obtenidos en los ensayos tipo I.

En la primera descarga en los ensayos en los que la compuerta de salida se encuentra en posición PI se evacuan aproximadamente 45 kN de trigo mientras que en los ensayos con la compuerta en PII, PIII, y PIV entorno a 26 kN. Esta diferencia es debida a que con la trampilla en PI la boca de salida está totalmente abierta y se llena completamente la tolva del dispositivo de vaciado, mientras que con la boca de salida en el resto de posiciones la descarga se realiza por una pequeña abertura, llegando un momento en que el material alcanza el nivel de la misma y la tapona dejando de fluir el grano. Se observó, al igual que en los ensayos anteriores, que para la misma posición de la boca de salida el flujo varia ligeramente entre unos ensayos y otros, lo cual se debe al mismo motivo explicado anteriormente para los ensayos tipo I.

El estado de presiones que se alcanza tras la primera descarga no se recupera al estado estático anterior cuando el material almacenado vuelve a permanecer en reposo (incluso en los ensayos 11, 16 o 20 en los que el segundo estado estático se prolonga durante más de 70 h el estado de presiones inicial sigue sin alcanzarse). Este hecho se trata de un descubrimiento novedoso que creemos que será de gran utilidad en el desarrollo nuevas teorías y métodos numéricos de cálculo de presiones durante el vaciado en silos ya que demuestra que el movimiento del material en el interior del silo durante la primera descarga provoca la compactación del mismo en determinadas zonas en detrimento de otras y las principales variaciones de presión que se producen en el interior del mismo se deben fundamentalmente a este fenómeno y no al aumento de volumen debido al deslizamiento lateral de las partículas en entre sí durante la descarga, fenómeno conocido como dilatancia, ya que de ser así se recuperaría el estado inicial al detener la misma.

La presión normal a la pared sufre una variación considerable al iniciarse la primera descarga, alcanzando valores y distribución de presiones en el interior del silo similares a las descritas para los ensayos tipo I, sin embargo, la variación de presión tras la segunda descarga es mucho menor y esta variación de presión se recupera al volver al estado estático por lo que creemos que este segundo incremento de presión es el que debe de atribuirse a la dilatancia.

A diferencia de lo que ocurría en los ensayos tipo I, en los que en las células de la parte inferior del cilindro el incremento de presión es siempre positivo mientras que en la parte superior del cilindro se registra que a determinadas alturas la presión permanecía casi constante o incluso descendía, en este tipo de ensayos se observaron presiones inferiores a las existentes en estado estático en las células situadas en posiciones bajas.

Al igual que en los ensayos tipo I, las presiones en la parte inferior de la pared disminuyen linealmente al aumentar la velocidad de descarga , mientras que las presiones en la tolva son prácticamente constantes e independientes de la velocidad de descarga. Se concluye así, al igual que en el caso anterior, que una descarga lenta no conlleva una disminución de presiones con respecto a una descarga rápida.

Otra de las principales conclusiones obtenidas en los ensayos tipo II es que con la descarga de una pequeña cantidad de material del silo (en los ensayos la cantidad descargada osciló entre los 1,7 y 3,2 %), se produce un estado de sobrepresiones en el mismo con unos máximos similares al que se produciría si realizamos la descarga completa, estado de sobrepresiones que ya no se recupera hasta que hayamos vaciado el silo y además en la segunda descarga las presiones máximas alcanzarán aun mayor valor. Este aspecto debería tenerse en cuenta en el diseño de silos ya que en la práctica no siempre se realiza la descarga de todo el material almacenado en el silo de una vez, siendo frecuente que se realice en distintas fases en función de las necesidades de material almacenado o en función de los pedidos.

Resultados del ensayo tipo III

En el ensayo tipo III, como era de esperar a la vista de los resultados anteriores, tras la primera descarga el estado estático de presiones con respecto al alcanzado al finalizar el primer llenado ya no se recupera. En la unión silo-tolva se observó un descenso de presiones tras las distintas descargas sucesivas, pero ese descenso es debido al vaciado progresivo del silo. Analizando las descargas sucesivas se observó como aparecían picos de presiones que rápidamente se recuperaban al volver al estado estático. Creemos que estos incrementos de presiones puntuales son los que se deben al aumento de volumen debido deslizamiento lateral de las partículas granulares entres si, fenómeno conocido como dilatancia. Es decir en el interior del silo durante la descarga ocurre un proceso similar al que ocurriría si sometemos un material granular poco denso a un esfuerzo cortante en un aparato triaxial, el corte hace que el material aumente su peso específico, tras sucesivos cortes se logra un peso específico que podríamos denominar crítico, y una vez alcanzado este, los sucesivos cortes provocarán un incremento de volumen.

De la interpretación de los resultados deducimos que al inicio de la primera descarga el material granular se compacta en las zonas inferiores del silo aumentando su peso específico hasta alcanzar un valor crítico y este fenómeno es el principal responsable del

incremento de presiones en esta zona, estado que no se recupera al detener la descarga. Llegado a este estado, las descargas sucesivas ya no provocan un aumento del peso específico en estas zonas sino un aumento de volumen por el deslizamiento de las partículas entre si, y este sería es el responsable de los picos de presiones que se producen y que vuelven al valor inicial al detener la descarga. El descenso de presión en zonas superiores se debería a la migración de material de las mismas hacia las zonas que se compactan y creemos que en un silo de longitud infinita a lo largo de la altura del mismo se alternarían zonas con incremento y descenso de presión.

Con respecto a la comparación de los resultados obtenidos en los ensayos con los resultantes de los cálculos prescritos por el Eurocódigo 1, parte 4, se obtuvieron valores inferiores a los de la norma en la mayor parte de los casos. En el estado estático que sigue al primer llenado, y para los tres tipos de ensayo, a cualquier altura y en todos los casos las presiones fueron inferiores a las obtenidas según el método de cálculo propuesto por el Eurocódigo. En la fase de descarga, la presión normal en la pared del cilindro obtenida en los ensayos se encontró siempre por debajo de la propuesta por el Eurocódigo, incluso al nivel de la unión silo-tolva. Sin embargo, al mismo nivel, las presiones normales a la pared de la tolva superaron al Eurocódigo en 8 de los ensayos, llegando a alcanzar un valor superior en un 11,56% al obtenido con el método de cálculo propuesto por el mismo.

3. Conclusiones

3.1. Conclusiones generales

La línea de investigación seguida permitió avanzar en el conocimiento de las acciones en silos en casos poco estudiados. Por una parte, la simulación numérica mediante dinámica de fluidos computacional, objeto del primer artículo, ha demostrado ser una herramienta poderosa para la determinación de acciones en las explosiones de nubes de polvo en silos, permitiendo la cuantificación de las sobrepresiones y subpresiones; acciones que pueden ser incorporadas al subsiguiente proceso de cálculo estructural con otras herramientas. Por otra parte, la estación experimental de ensayo de silos diseñada, validada y utilizada en los tres siguientes artículos ha satisfecho cumplidamente los objetivos y expectativas propuestos al inicio de la investigación, conseguidos ya con su ejecución, habiéndose obtenido adicionalmente conclusiones sobre el comportamiento de los materiales en los silos novedosas y previamente no publicadas como el fenómeno de reasentamiento del material, o la no recuperación del estado inicial de presiones tras una descarga parcial.

En los apartados siguientes se exponen de forma más extensa las conclusiones de cada uno de los cuatro artículos que configuran la presente tesis.

3.2. Conclusiones del artículo I

Las áreas de ventilación y las sobrepresiones asociadas resultantes de las simulaciones realizadas fueron inferiores a las previstas por la norma europea EN 14491, resultando próximas a las obtenidas aplicando la norma americana NFPA 68. Las diferencias con respecto a los valores establecidos en la norma EN 14491 fueron elevadas para valores bajos de la sobrepresión reducida de explosión (P_{red}), que es el escenario más común en grandes silos cilíndricos de acero.

Los resultados deben extrapolarse con precaución, ya que las simulaciones DESC son absolutamente dependientes de las características del flujo y la concentración de polvo supuesta para la nube de polvo inicial. La caracterización exacta de las propiedades de las nubes de polvo en grandes volúmenes, junto con la validación experimental, parecen necesarias para la relización de simulaciones precisas. Las incertidumbres asociadas a los datos de entrada son uno de los puntos débiles de las simulaciones CFD.

Algunas de las simulaciones muestran presiones negativas de hasta -0,2 bar en ciertos puntos de la onda de presión. La norma EN 1991-4 advierte sobre el problema de las subpresiones que aparecenen en los silos ventilados, pero no propone ningún medio para estimarlos, ni tampoco las normas EN 14491 o NFPA 68. Las presiones negativas, aunque sean de magnitud reducida, producen tensiones de compresión que podrían conducir a la deformación y ruina del silo si no se consideran en el diseño. Las simulaciones numéricas pueden ser muy útiles para estimar estas subpresiones.

El programa DESC ha demostrado ser una herramienta muy útil para estudiar cómo protegerse contra explosiones de polvo en silos y para mejorar el conocimiento de las explosiones de polvo y sus consecuencias. Las simulaciones ofrecen una serie de ventajas: pueden generar una gran cantidad de información para cualquier punto de interés, las condiciones iniciales pueden ser variadas, y las simulaciones son mucho más baratas que la realización de experimentos reales de explosión. El programa también podría servir para la planificación de pruebas reales de explosión y extrapolar los resultados a otras situaciones.

La mejora del diseño de silos ventilados requiere investigación adicional del proceso de venteo y de las características de las nubes de polvo. Debe incluir experimentos y simulaciones realistas que con el equipo real que se utiliza actualmente en la industria.

Las simulaciones numéricas pueden ser una herramienta poderosa para ayudar a los ingenieros a diseñar métodos de mitigación de explosiones y el cálculo de las estructuras de silos ventilados.

3.3. Conclusiones del artículo II

En este artículo se presenta un diseño novedoso para la construcción de una estación de ensayo de silos a tamaño real. Dicha estación permite obtener los siguientes parámetros:

- Presiones laterales en la pared vertical de los silos
- En silos con tolva, presiones en las zonas próximas a la transición
- Fuerzas de rozamiento en la pared vertical
- Presiones verticales medias
- Coeficientes de rozamiento con la pared medios para distintos materiales y tipos de pared.

- Relación K entre presiones horizontales y verticales

Por otra parte, se pueden realizar ensayos en las siguientes condiciones:

- Silos con tolva o fondo plano
- Vaciado con distintas excentricidades
- Llenado y vaciado con distintas velocidades
- Distintas relaciones altura/diámetro variando la presión en la parte superior
- Hinchamiento de los materiales almacenados debido a la humedad

Por tanto, en la estación se pueden investigar los parámetros que rigen el comportamiento del material almacenado bajo diferentes condiciones de contorno. En un solo silo de ensayo se pueden obtener gran parte de los datos necesarios para el cálculo de estas estructuras, lo que resulta de máxima utilidad para avanzar en las investigaciones en esta materia. Por un lado, los datos obtenidos permiten comprobar los métodos de cálculo desarrollados, y, por otro, obtener parte de los parámetros utilizados en los mismos. La ventaja de obtener ciertos parámetros en un silo estriba en que las condiciones son más aproximadas a las reales.

La posibilidad de medir tanto presiones laterales como verticales en distintos puntos de la pared del silo permite obtener los valores de las presiones horizontales, verticales y de rozamiento en la pared. Conocidas las presiones de rozamiento y las horizontales también se pueden determinar los coeficientes de rozamiento medios que se producen en la pared del silo. Por otra parte, además de diferentes materiales almacenados, se pueden realizar ensayos con diferentes tipos de pared.

La posibilidad de intercambiar el fondo del silo permite analizar fondos planos y con tolva, además de distintas excentricidades del vaciado. Los datos obtenidos en estas condiciones son esenciales dado que son los que condicionan el diseño de los silos. Por otra parte, debido a la posibilidad de regular la velocidad en los motores de carga y descarga, se puede analizar la influencia de la velocidad de llenado y vaciado en los parámetros descritos anteriormente.

Además, el silo cuenta con la posibilidad de introducir cargas en la parte superior, pudiéndose simular así silos de mayor altura de almacenamiento. De esta forma se pueden

estudiar las variaciones de los datos obtenidos para diferentes relaciones altura diámetro con un silo de altura reducida.

Una de las hipótesis de cálculo sobre las que existen menos datos a nivel internacional es la aquella en la que el material almacenado se hincha debido a la humedad. Las presiones producidas son muy elevadas y, sin embargo, apenas existen datos experimentales o procedimientos de cálculo de las mismas. El silo desarrollado está preparado para ensayar materiales incluso en condiciones de saturación, obteniéndose por tanto los parámetros descritos anteriormente en estas condiciones.

3.4. Conclusiones del artículo III

El diseño de estación de ensayo realizado por los autores de esta publicación y expuesto en el artículo anterior es válido para la medida de presiones en silos y brinda múltiples posibilidades para futuras investigaciones.

Antes de la descarga, es decir durante el proceso de llenado y permanencia del material en el interior del silo las mayores presiones normales a la pared del cilindro se producen justo al final del llenado, mientras que en la pared de la tolva ocurre lo contrario ya que la presión normal a la misma va aumentando con el tiempo durante el almacenaje.

Las mayores presiones en el interior del silo se producen en los primeros instantes de la descarga, esto coincide con los ensayos reales realizados por numerosos autores y con la normativa europea de silos, siendo el lugar donde mayores presiones normales a la pared se producen en la pared de la tolva, al nivel de la unión silo-tolva. Si tenemos en cuenta la pared del cilindro, al nivel de la unión silo-tolva es donde también se producen las mayores presiones normales a la pared, aunque estas son muy inferiores a las alcanzadas en la tolva. En los ensayos realizados las presiones normales a la pared de la tolva son del orden del 180% superiores a las obtenidas en la pared del cilindro.

Durante el estado estático el material almacenado sufre un proceso de reasentamiento, descargándose las paredes del cilindro y aumentando la presión normal a la pared de la tolva y la presión vertical en el material almacenado al nivel de la unión silo tolva. Ese proceso de reasentamiento se produce a pulsos, a intervalos de tiempo cada vez más grandes.

La observación del patrón que siguen la evolución de las presiones en estado estático debidas al reasentamiento del grano y el que siguen las sobrepresiones a lo largo de la generatriz vertical del cilindro durante el vaciado induce a pensar que el incremento de presiones en determinadas zonas del silo no es consecuencia de un comportamiento caótico sino que obedece a determinadas leyes físicas que aún no se encuentran suficientemente estudiadas.

El Eurocódigo 1, parte 4, en el apartado 1.1.2.5, dice que "*where discharge devices are used (for example feeders or internal flow tubes) solids flow is smooth and central*". Consideramos que este aspecto debería ser investigado ya que, como es nuestro caso, a veces estos mecanismos tienen una tolva de recogida, produciéndose una descarga libre en los primeros instantes, justo cuando se producen las mayores presiones durante la descarga.

3.5. Conclusiones del artículo IV

En estado estático las presiones en el interior del silo no son constantes ya que el grano sufre un proceso de reasentamiento a intervalos cada vez más espaciados, descargándose la pared del cilindro e incrementando la presión en la pared de la tolva.

La disminución del flujo del material granular durante la descarga no lleva asociado una disminución de presiones en la pared del silo sino más bien todo lo contrario.

Con la descarga de una pequeña cantidad de material del silo (en los ensayos la cantidad descargada osciló entre los 1,7 y 3,2 %), se produce un estado de sobrepresiones en el mismo con unos máximos similares al que se produciría si realizamos la descarga completa, estado de sobrepresiones que ya no se recupera al estado estático anterior y además en la segunda descarga las presiones máximas alcanzarán aun mayor valor.

Al inicio de la descarga el material granular sufre un proceso de compactación aumentando el peso específico en determinadas zonas en detrimento de otras y a este efecto se debe la principal variación de presiones en el interior del silo durante la descarga. Si se para la descarga en este instante el silo no recupera el estado de tensiones anterior. Una vez el material ha alcanzado un determinado grado de compactación que podríamos denominar "crítico", las variaciones de presión durante la descarga se deben al fenómeno conocido como dilatancia, es decir al incremento de volumen provocado por el deslizamiento lateral de las partículas granulares entre si.

Durante la descarga las presiones normales a la pared de la tolva al nivel de la unión silo-tolva pueden llegar a superar a las obtenidas según el método de cálculo propuesto por el Eurocódigo 1, parte 4.

ANEJO 1

Copia del artículo I,

Dust explosions in vented silos: Simulations and comparisons with current standards,

publicado en

Powder Technology 208 (2011) 717–724

Powder Technology 208 (2011) 717–724

Contents lists available at ScienceDirect

Powder Technology

journal homepage: www.elsevier.com/locate/powtec

Dust explosions in vented silos: Simulations and comparisons with current standards

Alberto Tascón *, Ángel Ruiz, Pedro J. Aguado

Departamento de Ingeniería y Ciencias Agrarias, ESTI Agraria, Universidad de León, Av. Portugal 41, 24071 León, Spain

ARTICLE INFO

Article history:
Received 30 June 2010
Received in revised form 6 December 2010
Accepted 27 January 2011
Available online 3 February 2011

Keywords:
Dust explosion
Silo
Venting
CFD
DESC

ABSTRACT

Dust explosions represent a serious hazard to personnel and equipment in industries and silo facilities that handle combustible materials. Venting devices are the most common protective systems employed in silos, although their use may pose problems in large and low-strength silos. The main aim of the present work was to simulate dust explosions in silos using a commercial CFD program, the DESC code, to determine the pressures developed in vented explosions with vent areas of different sizes. Dust cloud characteristics were taken from studies carried out by the FSA (Research Centre for Applied System Safety and Industrial Medicine, Germany) in a 12 m^3 silo with a mechanical feeding system. The pressures and associated vent areas in these simulations were compared to those contemplated in two venting standards. The simulated explosion pressures showed the expected trends for the associated vent areas and agreed reasonably well with the values contemplated in NFPA 68 (2007) [5]. However, when the reduced explosion overpressure was low, the vent area contemplated in EN 14491 (2006) [4] was much larger than in the present simulations.

© 2011 Elsevier B.V. All rights reserved.

1. Introduction

Many materials stored in silos produce combustible dust. Dust explosions occur when such dust is dispersed in the air as a cloud and reacts with oxygen in the presence of an ignition source, generating a violent combustion reaction in the form of flame propagation. These materials include agricultural and food products (grain, malt, flour, maize starch, sugar, etc.), synthetic organic materials (plastics, pigments, pesticides, etc.), metals (aluminium, magnesium, etc.) and coal [1].

In accordance with the ATEX Directive 1999/92/EC [2], the measures taken against explosions by the employers should adhere to three principles (in order of priority): the prevention of the formation of explosive atmospheres, the avoidance of ignition, and the mitigation of the effects of an explosion.

In large silos it is unavoidable that dust/air mixtures are produced by the bulk material during the filling or empting of the vessel. Therefore, dust explosions represent a serious hazard. Fighting potential ignition sources that could trigger dust clouds is therefore essential. Nevertheless, in many situations it is not enough to try to eliminate ignition sources, and measures for mitigating the damage that might be produced have to be considered.

Eurocode 1, part 4, "*Actions on structures. Silos and tanks*" (EN 1991-4) contemplates the loads produced by explosions [3], classified as accidental actions, and proposes that potential damage be limited by venting, suppression or containment. Venting is the most common protective measure used in silos owing to its more favourable technical and economic features; indeed, they are usually the only option in large silos. In a closed vessel with no venting device, dust explosion pressures can reach 7–10 bar (700–1000 kPa), placing silos at risk of severe damage or even complete destruction. Pressure relief through a vent opening aims to prevent the appearance of these unacceptably high pressures.

The sizes of vent areas can be determined following the recommendations in standards EN 14491 [4] and NFPA 68 [5], which are commonly used in Europe and North America respectively. Comprehensive lists of other methods for dust explosion vent design have been compiled by Abbasi and Abbasi [6], Barton [7] and Eckhoff [1]. However, the venting of silos is not always simple, and complications frequently arise that render the provision of such protection difficult or even impossible. For example, the large metal silos used in the agricultural and food industry usually have a low-strength roof and upper wall, making the installation of venting devices technically difficult and costly. This could lead the employers to believe that venting is not the solution to the problem of dust explosions in silos; the danger that then arises is that no mitigation measures might be taken at all.

The aforementioned dust explosion venting standards, both of which have recently become effective, are, in certain situations, more than a little contradictory. For example, Fig. 1 compares standards NFPA 68 [5] and EN 14491 [4] with respect to barley dust in a 1000 m^3 silo and with a very low reduced explosion overpressure[1] (P_{red}) of

* Corresponding author at: Departamento de Agricultura y Alimentación, Universidad de La Rioja, Av. Madre de Dios 51, 26006, Logroño, Spain. Tel.: +34 941 299 733; fax: +34 941 299 721.
E-mail address: alberto.tascon@unirioja.es (A. Tascón).

[1] P_{red} is the maximum overpressure generated by an explosion in a vessel protected by venting or suppression [4]. The silo should be able to resist such P_{red}.

0032-5910/$ – see front matter © 2011 Elsevier B.V. All rights reserved.
doi:10.1016/j.powtec.2011.01.015

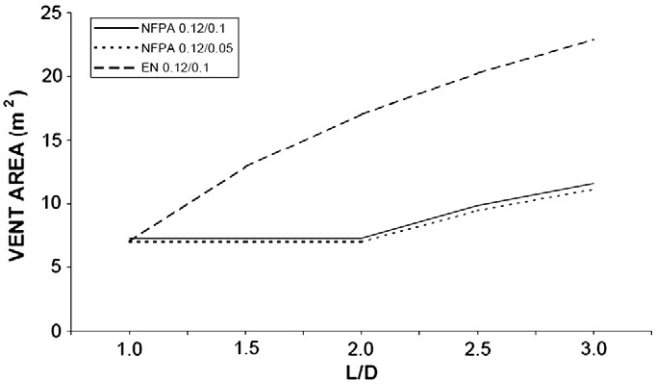

Fig. 1. Comparison of vent areas required by NFPA 68 [5] and EN 14491 [4] for barley storage (P_{max} = 7.1 bar, K_{st} = 50 bar·m/s). V = 1000 m^3. P_{red} = 0.12 bar. Activation pressure (P_{stat}) = 0.1 and 0.05 bar.

0.12 bar. Depending on the length-to-diameter (L/D) ratio, the vent area contemplated in EN 14491 [4] can be around twice that suggested by NFPA 68 [5]. A comparison of these standards in terms of their application to silos was recently reported by Tascón et al. [8].

The equations in EN 14491 [4] are used for calculating vent areas for an enclosure completely filled by a turbulent dust cloud of optimum dust concentration. However, in some practical situations, for example in most silos (especially large silos filled by a free-fall or mechanical feeding mechanism), the test procedures employed in European standards tend to overstate explosion intensities. EN 14491 [4] specifies that, for non-homogeneous dust clouds of low dust concentration under conditions of low to moderate turbulence, a reduced vent area can be used. However, no value or alternative formula is provided for calculating this area. Rather, the standard requires it be determined by explosion venting trials. In principle, numerical simulations could provide an alternative means of determining vent areas in these situations.

With the development of computational resources, numerical methods have become powerful tools in many research and engineering fields. Simulation based on the principles of computational fluid dynamics (CFD) has become a widely adopted methodology for solving complex problems regarding heat and fluid flow. A number of researchers have already published interesting reports on the application of CFD-tools to dust explosions [9–12].

The main aim of the present work was to simulate dust explosions in vented silos using a commercial CFD-code, the DESC (Dust Explosion Simulation Code), which is specific for dust explosions, in order to predict the pressure build-up over time. Knowing these pressures would allow researchers to analyse the behaviour of a silo's structure in the event of an explosion through the use of the finite-element method (FEM); this has already been successfully used to study silo design requirements for different types of load [13]. In the present work the explosion pressures and the necessary vent sizes to deal with them, as determined in simulations, were compared with the values predicted in EN 14491 [4] and NFPA 68 [5]. The ultimate aim of this research is to solve technical difficulties in the protection of silos against dust explosions and to solve pertinent silo design problems.

2. Methodology

A commercial CFD software – the Dust Explosion Simulation Code (DESC) – has been available from GexCon since the end of 2005. This code was the result of a project supported by the European Commission involving 11 participants. Further details on the DESC project can be found elsewhere [14].

DESC is based on the CFD programme for gas explosions known as FLACS (FLame ACceleration Simulator). It is a finite volume code in which transport equations for the mass, momentum, enthalpy, fuel, mixture fraction, turbulent kinetic energy and the turbulent energy dissipation rate of the fluid flow (in this case the mixture dust/air in an exploding silo) are solved on a structured Cartesian grid; all solid objects (in this case the silo and its components) are mapped to this grid using a distributed porosity concept [15]. The results of standardized tests in 20-litre explosion vessels [16,17] have to be used to extract the necessary input combustion parameters. Scenarios taking into account the geometry of the problem, the characteristics of the grid, the ignition point and ignition energy, monitoring points and output variables etc., are defined in the pre-processor CASD. The results of simulations are presented in the post-processor Flowvis. The combustion and turbulence models used in the programme and the approach adopted for DESC development are those described by Skjold et al. [12,18].

In the present work, dust explosions in silos were simulated using DESC (version 1.0b3) running under the Linux operating system (Mandriva). The intention was to simulate cylindrical flat-bottomed silos with mechanical feeding systems — the most common type of silo used to store grain and other granular and powdered products in the agricultural and food industries in Spain.

In the simulations, the silos were 6 m in diameter and either 9, 12 or 15 m in height. The grid defined was three-dimensional with cells 0.2 m in size. The geometry of the silos, including the vent panels, the ignition point and the monitoring points, was fitted to the grid. The usual conical roof of this type of silos was transformed into a prolongation of the cylindrical silo wall with the same volume and a flat roof; it is not possible to set vent panels on a conical surface in DESC. Eight inertialess pressure relief panels were contemplated in the flat roof, each one of 1 m^2 (see Fig. 2). The total vent area could be set from 0 m^2 to 8 m^2 by setting the activation pressure of the vents to either a common value for commercial vent panels or to a value much higher than the maximum explosion pressure of the dust (P_{max}). Simulations were carried out for activation pressures of 0.1 bar and 0.05 bar, both of which represent common static activation overpressures (P_{stat}) of commercial vent panels.

The ignition was located at 0.50 m above the silo bottom. The ignition energy was set to 10 kJ, which is the standard energy used in explosion severity tests [16,17]. Furthermore, such ignition energy has previously been used in numerous experimental tests in large vessels [19–21]. However, real ignition sources can generate much lower or considerably greater energies [1]. In consequence, other researchers decided to select higher or lower values than 10 kJ for their experiments [9,22–24]. In the present simulations with DESC the standard energy of 10 kJ was considered appropriate for comparison purposes.

To observe the variation in the values of essential parameters during the explosion, several monitoring points were selected along

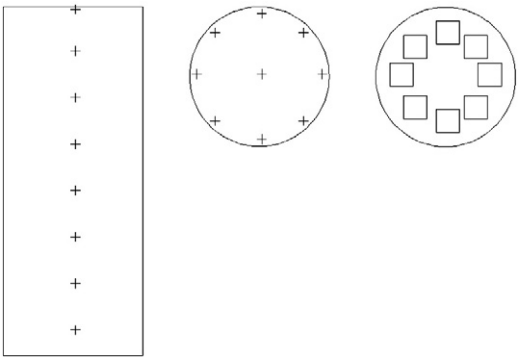

Fig. 2. Silo 6 m in diameter and 15 m in height. The vertical cross-section shows the monitoring points along the z-axis (on the left); the horizontal cross-section shows the monitoring points near the roof (in the middle); the top view shows the vent panels in the roof (on the right).

the vertical axis of the cylinder, one every 2 m, and eight others situated on a plane near the roof, one for every 45° (see Fig. 2). The monitoring points near the roof were used to study in detail what happens to the structure of the roof during an explosion.

The intention was to simulate silos under real industrial conditions with mechanical feeding, the bulk material entering into the silo by free fall (the most commonly used filling system for large cylindrical steel silos in Spain). However, in DESC it is not possible to simulate the mechanical filling of a vessel by the free-fall of a bulk granular material through a pipe after arrival via a conveyor (screw, bulk elevator or conveyor belt) and the consequent dust cloud. Thus, the approach adopted for all simulations was to consider an initial dust cloud which completely filled the silo and to set the dust cloud characteristics according to such filling system.

Maize starch ($P_{max} = 8.63$ bar and $K_{st} = 149$ bar·m/s) was contemplated in all simulations. Its explosion characteristics were input in the DESC program's fuel file as supplied by GexCon. The silo was considered completely filled by a dust cloud — in principle the most dangerous of situations. This approach was based on the following rule stated by the formulae in EN 14491 [4] and NFPA 68 [5]: the larger the volume, the greater the vent area required. However, in a complete structural analysis for the design of a silo, account should be taken of the effects of load combinations, for example the pressures exerted by the stored material in a partially filled silo plus the explosion pressures developed in the free volume above the bulk solid [25].

A great challenge was deciding upon the initial level of turbulence and concentration of the dust cloud generated in the silo. There is a lack of published data in this area with respect to large vessels in the practical, industrial setting. Given the absence of data regarding real dust clouds in large silos, those of Hauert, Vogl and Radant [20,26,27], gathered in comprehensive experiments involving a 12 m^3 steel silo at the FSA (Forschungsgesellschaft für Angewandte Systemsicherheit und Arbeitsmedizin, Research Centre for Applied System Safety and Industrial Medicine) as part of the European CREDIT (Cooperative Research of Exploding Dusts on Industrial Terrains) project [28], were adopted.

Hauert et al. used the Laser-Doppler-Anemometry (LDA) technique to measure the flow field in the silo, calculating both the mean velocity and the RMS turbulence velocity. A dust concentration measuring probe was developed by FSA, based on the principle that an attenuation of the intensity of a light beam is produced when it penetrates a cloud with solid particles. The measuring equipments were placed at different heights and also at different positions in radial direction into the 12 m^3 silo. Three different ways of feeding the silo were implemented: a pneumatic conveying system with axial or tangential release and a mechanical system (free-fall after a screw conveyor). Maize starch was one of the materials used in the experiments in the FSA silo.

Dust concentrations, mean air velocities and RMS turbulence velocities were set to those measured in the FSA 12 m^3 silo when fed mechanically with maize starch, considering average values for the whole volume of the silo. Thus, the present simulations involved a simplified initial dust cloud. The data were obtained from the CREDIT Final Technical Report [27], averaging the values for the whole volume of the FSA 12 m^3 silo. The input turbulence variable in DESC is the relative turbulence intensity, which can be calculated as the ratio of the turbulence intensity (RMS turbulence velocity, m/s) to the mean flow velocity (m/s). Table 1 shows the average dust concentration and flow characteristics chosen for the simulations (*condition set 0*). The mean air velocity measured in the FSA 12 m^3 silo was exceptionally low. As a result, the relative turbulence intensity (%) was very high, although the turbulence intensity (m/s) measured in the silo was also quite low.

The characteristics of the flow in the 12 m^3 silo reported by FSA were those related to the longitudinal axis of the silo, i.e., the axial components of the flow characteristics. DESC only permits one input value for the initial turbulence and flow velocity, and considers the turbulence to be isotropic. The FSA researchers verified that the tangential components of the turbulence show approximately the same behaviour as the axial components and that the latter seem to be higher [27]. Therefore the axial values reported by the FSA were taken as the input flow values.

Table 1
Initial dust cloud conditions selected for the simulations.

Parameters	Condition set 0	Condition set 1
Dust concentration	300 g/m^3	500 g/m^3
Air velocity	0.15 m/s	0.15 m/s
Relative turbulence intensity	112%	80%

The approach adopted for the present simulations may seem something of an oversimplification, but it provided a starting point. It also errs on the side of safety since it involves the transformation of a non-homogeneous cloud with high/low local dust concentrations into a homogeneous cloud.

The level of turbulence and the dust concentration in a silo are related to the capacity of the filling system. In the work performed by the FSA the maximum capacity of the mechanical filling system was adapted to the size of the silo (12 m^3), i.e., a screw of capacity 3.6 tons/h [27]. The largest silo considered in the present work was 424 m^3 in volume (6 m in diameter, 15 m in height), i.e., thirty-five times as large as the experimental silo of the FSA. However, the capacity of the filling system would not be increased by thirty-five times in a real silo of these dimensions in the agricultural and food industry; at most the capacity of the filling system would be some 25–75 tons/h. In consequence, in the present work it was considered that lower average velocity and turbulence values could be expected for silos much larger than the FSA 12 m^3 silo, although at certain points near the pipe inlet and along the trajectory of the particles they might be higher. In the absence of more published data regarding real dust clouds in large silos, the works by Hauert, Vogl and Radant were considered appropriate for such silos.

In further simulations, *condition set 1*, a higher concentration for the initial dust cloud (500 g/m^3) and a reduction in the initial relative turbulence intensity (80%) were considered. This might correspond to silos with layers of dust settled on the walls, which would be dispersed in the air by turbulence produced by the filling process and the explosion itself, increasing the average dust concentration. Silo walls made of corrugated steel plates can hold large dust deposits, thicker than those on polished or smooth walls. The former are widely used for the storage of grain and similar materials because of their better mechanical behaviour; indeed, most agricultural silos have corrugated walls. The reduction in turbulence was supported by the aforementioned reasoning that, in silos larger than the 12 m^3 FSA silo (i.e., those simulated in the present work) the ratio of the volume to the capacity of the mechanical feeding system often increases, reducing the average turbulence. A value of 0.80 (80%) was selected by the authors.

Two sets of conditions regarding the initial conditions of the dust cloud were therefore considered: *condition set 0*, in which the values reported by the researchers of the FSA, averaged for the whole volume of the experimental silo, were used; and *condition set 1*, in which a higher dust concentration and a lower turbulence were assumed. Tables 1 and 2 describe the characteristics of the simulations considered in this work.

Finally the maximum explosion overpressures obtained by the computer simulations and their related vent areas were compared to the values predicted by EN 14491 [4] and NFPA 68 [5]. With respect to EN 14491 [4], the general equation for isolated enclosures with a maximum reduced explosion overpressure ($P_{max,red}$) of <1.5 bar was used to calculate the associated vent area. For NFPA 68 [5], the general equation for calculating the minimum necessary vent area with low or medium turbulence was used; the correction for L/D values of >2 was used when necessary.

Table 2
Characteristics of the DESC simulations.

Parameters	Numerical values
Silo diameter (D)	6 m
Length-to-diameter ratio (L/D)	1.5–2–2.5
Volume (V)	254.5 m^3–339.3 m^3–424.1 m^3
Vent area (A)	From 0 m^2 to 8 m^2
Activation pressure of the venting devices (P_{stat})	0.05–0.1 bar
Ignition energy	10 kJ
Ignition point	0.5 m (bottom)
Dust (maize starch)	P_{max} = 8.63 bar, K_{st} = 149 bar·m/s

Prior to the calculations presented in this paper, some simulations were carried out to study the sensitivity of the results with respect to the grid resolution defined in DESC. A vessel 2 m in diameter and 3 m in height, with no vents, was considered for such simulations. The ignition, 10 kJ, was located at the silo bottom. It was assumed that the vessel was completely filled by a quiescent dust cloud of 700 kg/m^3 (maize starch, P_{max} = 8.63 bar and K_{st} = 149 bar·m/s). Three different grid resolutions were considered: 0.10 m, 0.20 m and 0.50 m. Table 3 presents some results of these simulations. It was found that the overpressures were almost identical but the differences in the maximum rate of pressure rise ($(dP/dt)_{max}$) were significant. The values of $(dP/dt)_{max}$ depended on the grid resolution and clearly converged following a correct trend. There was a difference in $(dP/dt)_{max}$ of 2.56% between the simulation with 0.20 m cells and the simulation with 0.10 m cells.

Taking into account the limitations in processing speed and memory capacity, a grid of 0.20 m was considered accurate enough to simulate dust explosions in much larger silos than this previous one.

3. Results and discussion

The results of the numerical DESC simulations are provided as graphs and text files with the values of the different variables calculated for the simulated explosion. Special interest was paid to the overpressures and temperatures generated since the ultimate aim of this research is to be able to carry out structural analyses of vented silos.

Fig. 3 shows the comparison of the overpressure time histories for four different vent areas in a silo 6 m in diameter and 9 m in height. Note that the pressure in bars denotes gauge pressure, i.e., pressure above atmospheric pressure. Fig. 3 therefore shows the overpressures that were recorded at a monitoring point situated in the middle of the silo (at 5.10 m from the bottom) over the z-axis.

In the simulations performed in this work, the pressures recorded at different monitoring points were nearly the same. Thus, the distribution of the pressure in the silos during the explosions was uniform. There are two instants along the pressure–time graphs when trivial differences were recorded at different monitoring points: when the vent panels had just opened, which led to a rapid decline in pressure, and when the pressure reached the second peak value and started to go down (see Fig. 4).

Fig. 5 shows the temperature time histories recorded at different monitoring points. Results in Figs. 4 and 5 correspond to the same simulation and they demonstrate that the flame propagated slower than the pressure, reaching the monitoring points along the z-axis in sequence.

Table 3
Overpressure and maximum rate of pressure rise obtained by computer simulation for three different grid resolutions. D = 2 m. L = 3 m.

Grid	P	$(dP/dt)_{max}$
0.10 m	8.80 bar	26.52 bar/s
0.20 m	8.80 bar	25.84 bar/s
0.50 m	8.82 bar	18.37 bar/s

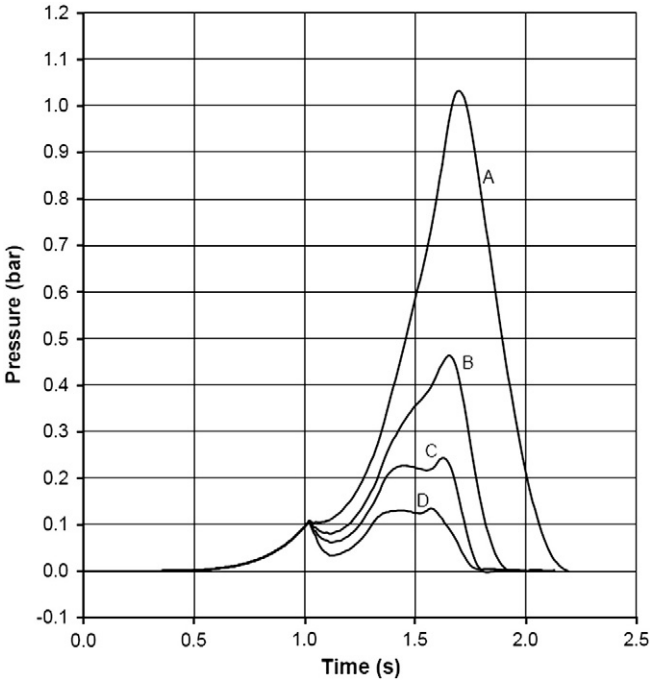

Fig. 3. Overpressure time histories. Maize starch. D = 6 m. L = 9 m. P_{stat} = 0.1 bar. Condition set 0. Vent area = 2 m^2 (A), 3 m^2 (B), 4 m^2 (C) and 5 m^2 (D).

In some of the simulations negative pressure phases were seen over the pressure-time curve; the maximum values reached were about −0.02 bar. These negative pressures showed the following trends: they increased with the L/D ratio of the silo; for the same silo geometry they increased with the vent area; and they increased as the activation pressure on the vent panels decreased.

The underpressures developed could induce the strong compression of the silo walls, making it necessary to understand their structural behaviour if buckling failures are to be avoided. Thus, it may not be enough to only take into account the maximum overpressure developed

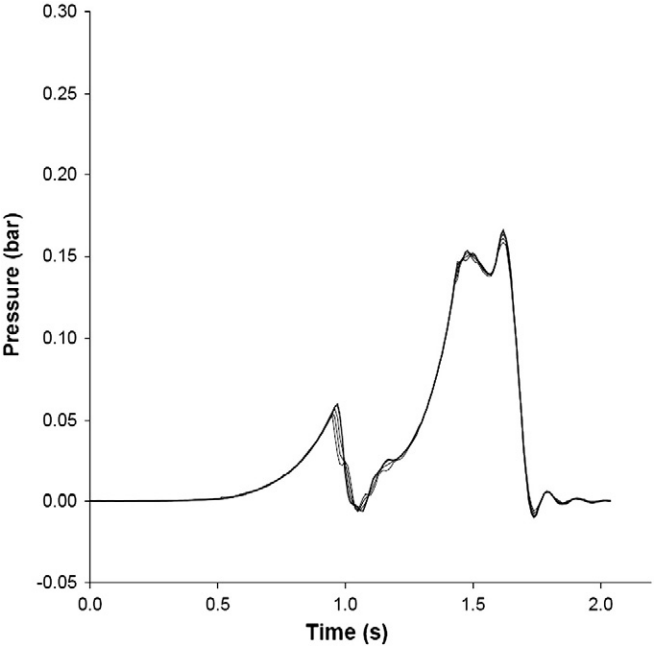

Fig. 4. Overpressure time histories recorded at six monitor points situated along the vertical axis of the silo. Maize starch. D = 6 m. L = 12 m. Activation overpressure = 0.05 bar. Vent area = 7 m^2. Condition set 0.

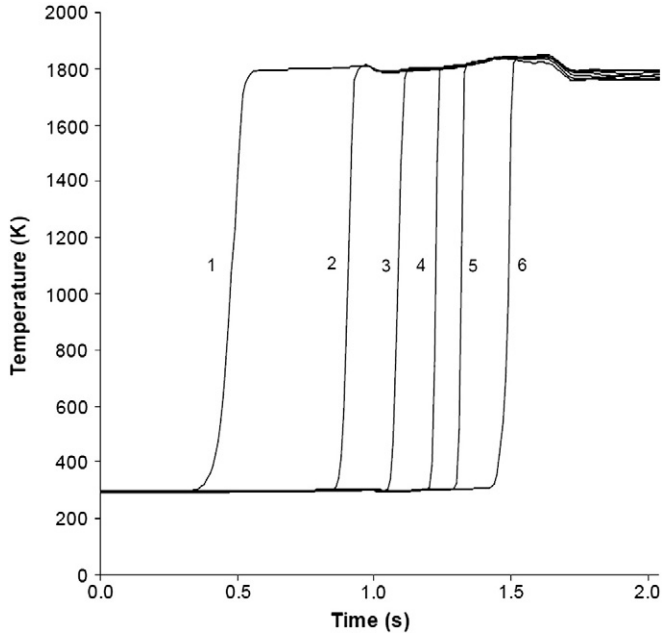

Fig. 5. Temperature time histories recorded at six monitor points situated along the vertical axis of the silo. Maize starch. D = 6 m. L = 12 m. P_{stat} = 0.05 bar. Vent area = 7 m^2. Condition set 0.

by vented explosions when designing a silo's structure. Metal silos, which have much thinner walls than concrete silos, could be particularly vulnerable to compressive stresses induced by the formation of partial vacuums. However neither venting standard EN 14491 [4] nor NFPA 68 [5], nor Eurocode 1, part 4, "*Actions on structures. Silos and tanks*" [3], propose any method for predicting potential underpressures that might improve silo design. This concern is different to the negative pressures developing in vessels fitted with explosion doors, which is described in EN 14491 [4] and NFPA 68 [5] and controlled by using vacuum breakers to avoid the deformation of the walls after the doors have closed the vented area. Computer simulations could be a useful tool for predicting the value of potential underpressures.

Figs. 6 and 7 show the correlations of the maximum reduced explosion overpressures (P_{red}) obtained by computer simulation using the DESC code with the corresponding vent areas for silos 9 m in height. Figs. 8 and 9 show the same for silos 12 m in height, and Figs. 10 and 11 show the same for silos 15 m in height. The results were compared to the vent areas required by standards EN 14491 [4] and NFPA 68 [5]. Both

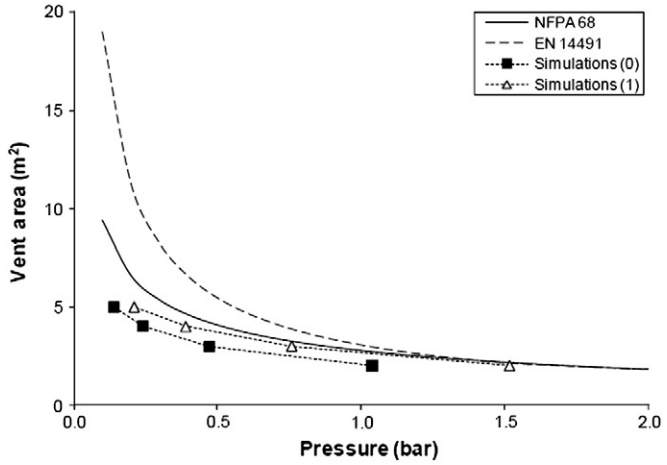

Fig. 6. Correlation of the reduced explosion overpressure with the vent area. Comparison of results obtained by computer simulation with the values contemplated in EN 14491 [4] and NFPA 68 [5]. Maize starch. D = 6 m. L = 9 m. P_{stat} = 0.1 bar.

condition sets 0 and *1* are contemplated in these figures (Simulations(0) and Simulations(1)). The overpressures plotted are the maximum values recorded by any monitoring point during the explosion process.

The trends of the curves for the DESC simulations are similar to those arising from standards EN 14491 [4] and NFPA 68 [5]. However the overpressure values obtained by DESC for *condition set 0* were lower than those predicted by either. For low overpressure values, the differences were significant compared to those vent areas predicted by standard NFPA 68 [5], but notably greater compared to those vent areas set out by EN 14491 [4]. The curve for the DESC simulations adhering to *condition set 0* is approximately parallel to the curve for standard NFPA 68 [5].

The differences between the DESC simulations and standards EN 14491 [4] and NFPA 68 [5] may be explained by the initial dust cloud conditions considered. In this work, dust concentration, air velocity and turbulence were set to those measured during the mechanical filling process of a small real silo. The mean velocity and the RMS turbulence velocity registered in such situation were very low in comparison with the values measured in explosion laboratory tests [27,29], in which the dust cloud is created by the discharged of pressurized dust containers. These pressurized containers were also the method to create dust clouds in the explosion venting test series on which the present standards are partially based, setting a number of containers proportional to the volume of the vessel [19].

On the other hand the significant differences between EN 14491 [4] and NFPA 68 [5] for low overpressure values may be explained by the vent area correction for elongated vessels which is required by EN 14491 [4] when $P_{red} < 1.5$ bar and $L/D > 1$. Such correction[2] depends on the L/D ratio and the P_{red} and it imposes a notably increment of vent area if P_{red} is very low [8]. Thus, a lower P_{red} results in a larger vent area correction for a fixed L/D ratio. This correction is the same one which was proposed in the 90s by the second version of the German guideline VDI 3673 [30]. The equations in NFPA 68 [5] also introduce a correction for elongated vessels when $L/D > 2$ but it imposes more moderate increments of vent area than EN 14491 [4] when P_{red} is very low [8]. There is no correction of the vent area for $L/D \leq 2$ in NFPA 68 [5]. For the silos studied in this paper, the great differences between the vent areas proposed by EN 14491 [4] and NFPA 68 [5] for very low overpressure values are mainly due to the type of L/D correction applied.

For the simulations adhering to *condition set 1*, the results matched the values predicted by NFPA 68 [5] very well; indeed, there was little difference between their curves. The overpressure values obtained by DESC were lower than those found in NFPA 68 [5] for silos 9 m in height, and slightly greater for silos 12 m and 15 m in height. Even for *condition set 1*, which is more unfavourable than *condition set 0*, the results obtained were far from the values considered by EN 14491 [4] when the P_{red} value was small.

The variation of the activation pressure of the venting panels (P_{stat}) in the present work had no important effect on the overpressures recorded. When panels with an opening pressure of 0.05 bar were contemplated, a mean reduction of 4.33% in the explosion overpressure (minimum of 0.75%; maximum of 11.40%, standard deviation of 3.67) was seen with respect to simulations in which it was 0.1 bar, except in one simulation, which produced an irrelevant increment of 0.30%. These results agreed very well with the mean reduction of 4.02% in the overpressure P_{red} according to NFPA 68 [5] when P_{stat} is reduced from 0.1 bar to 0.05 bar (see Fig. 1). Both standards [4,5] assume that a lower activation pressure of the venting device produces a lower explosion overpressure due to the prompter release of hot combustion gasses and also unburnt dust. However, EN 14491

[2] Correction for elongated vessels in EN 14491: $\Delta A = A' \cdot (-4.305 \cdot \log P_{red} + 0.758) \cdot \log L/D$. Vent area for cubic vessels: A′. Total vent area for elongated vessels: $A = A' + \Delta A$.

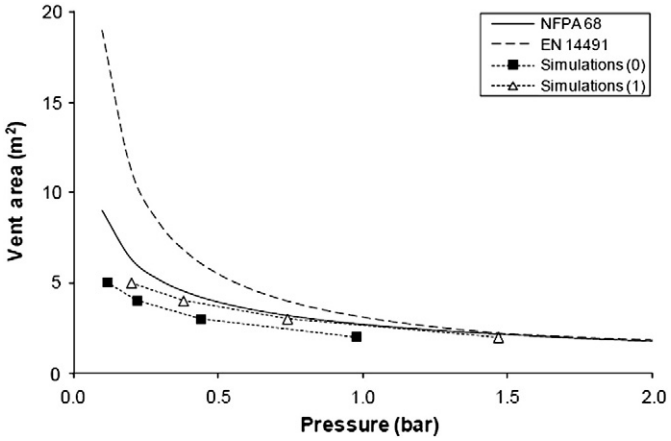

Fig. 7. Correlation of the reduced explosion overpressure with the vent area. Comparison of results obtained by computer simulation with the values contemplated in EN 14491 [4] and NFPA 68 [5]. Maize starch. D = 6 m. L = 9 m. P_{stat} = 0.05 bar.

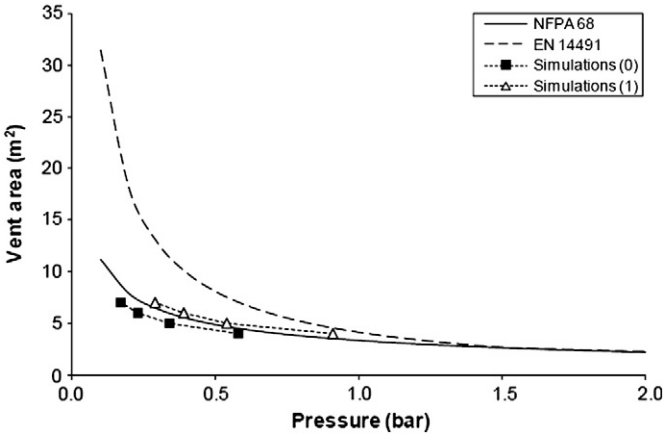

Fig. 9. Correlation of the reduced explosion overpressure with the vent area. Comparison of results obtained by computer simulation with the values contemplated in EN 14491 [4] and NFPA 68 [5]. Maize starch. D = 6 m. L = 12 m. P_{stat} = 0.05 bar.

[4] considers a minimum value of P_{stat} = 0.1 bar and requires the vent areas be determined for that value when P_{stat} < 0.1 bar.

According to the results, the dust concentration had a strong influence on the reduced explosion overpressure. The overpressure increased when the concentration was nearer to the optimum concentration (approximately 750 kg/m^3 for the maize starch used in the simulations), a foreseeable result.

The influence of the initial dust cloud conditions on the reduced explosion overpressure seemed to be stronger when the vent area was small (and the overpressure high). On the other hand, the differences between EN 14491 [4] and NFPA 68 [5] reduced when the overpressure was high and notably increased when it was low.

For low overpressures ($P_{red} \leq 0.3$ bar), which are common for metallic, cylindrical silos, the vent areas necessary according to the numerical simulations adhering to *condition set 0* were approximately half those considered by EN 14491 [4]. For example, in Fig. 6, when the venting area was 3 m^2 the overpressure obtained by DESC was 0.47 bar, while for NFPA 68 [5] it was 0.89 bar, and for EN 14491 [4] it was 1.03 bar. For *condition set 1* the P_{red} obtained by DESC was 0.76 bar.

The present computer simulations confirm the widespread idea that vent areas calculated according to EN 14491 [4] which is based on the previous standard VDI 3673 (2002) [31], are very conservative compared with what might really be necessary for most large silos. In fact this has already been investigated in a number of experiments [32,33]. However, some potential scenarios could involve conditions of temporarily high turbulence and dust concentration levels. An example would be a secondary dust explosion. Thus, the results obtained by computer simulation should be used with extreme caution since they reflect given levels of turbulence and dust concentration. It should be noted that the general equation in EN 14491 [4] "shall apply to single enclosures where appropriate measures (explosion isolation) have been taken to prevent flame propagation between enclosures". Consequently, when isolation measures have been implemented, the likelihood of secondary explosions is remote, and it seems clear that EN 14491 [4] notably oversizes vent areas for large isolated silos when the turbulence is not high and the dust cloud not homogeneous.

The results of the present DESC simulations were very dependent on the initial conditions of the dust cloud (dust concentration, air velocity and turbulence). Further measurements of dust cloud characteristics in large silos therefore seem to be necessary for accurate computer simulations.

4. Conclusions

The vent areas and associated overpressures obtained in the present simulations were lower than those contemplated by European standard

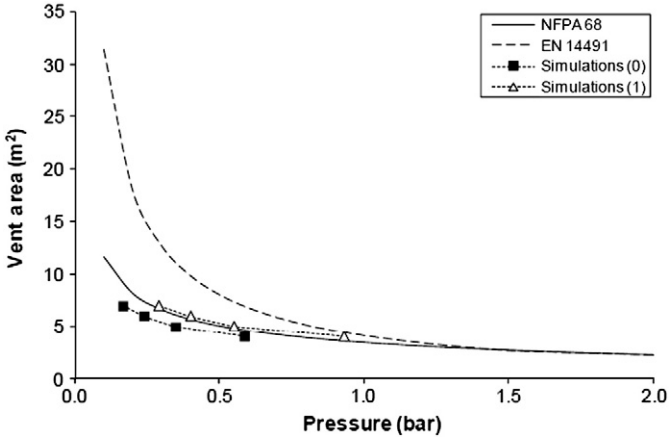

Fig. 8. Correlation of the reduced explosion overpressure with the vent area. Comparison of results obtained by computer simulation with the values contemplated in EN 14491 [4] and NFPA 68 [5]. Maize starch. D = 6 m. L = 12 m. P_{stat} = 0.1 bar.

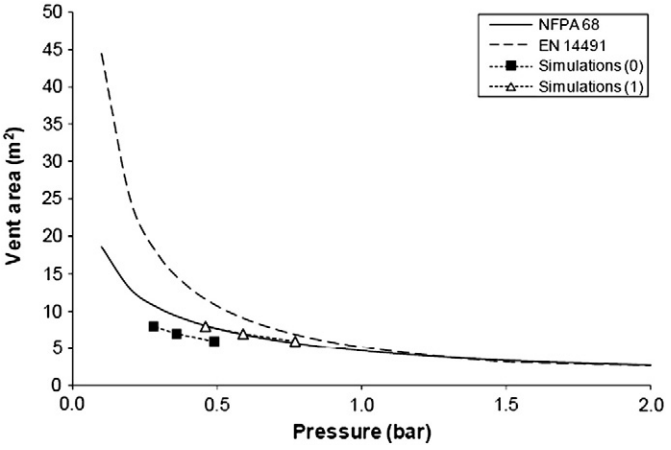

Fig. 10. Correlation of the reduced explosion overpressure with the vent area. Comparison of results obtained by computer simulation with the values contemplated in EN 14491 [4] and NFPA 68 [5]. Maize starch. D = 6 m. L = 15 m. P_{stat} = 0.1 bar.

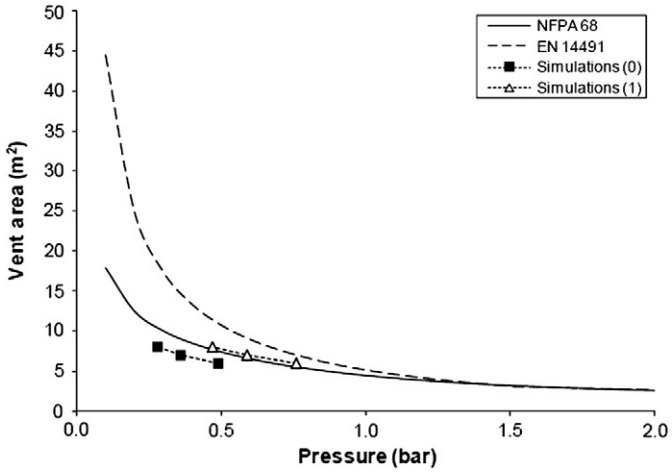

Fig. 11. Correlation of the reduced explosion overpressure with the vent area. Comparison of results obtained by computer simulation with the values contemplated in EN 14491 [4] and NFPA 68 [5]. Maize starch. D = 6 m. L = 15 m. P_{stat} = 0.05 bar.

EN 14491 [4] but agreed quite well with those of American standard NFPA 68 [5]. The differences with respect to the values set out in EN 14491 [4] were large when the reduced explosion overpressure P_{red} was low, which is the most common scenario in large, cylindrical, steel silos.

The present results should be extrapolated with caution since DESC simulations are absolutely dependent on the flow characteristics and the dust concentration assumed for the initial dust cloud. The characterization of dust cloud properties in large volumes, together with experimental validation, would therefore seem necessary if accurate simulations are to be continued. The uncertainties related to the input data are one of the weak points of CFD simulations. Experimental verification is intended to be carried out by the authors, although comparison of DESC simulations with several experiments described in literature has already been carried out, indicating a reasonably good agreement [12,14,18]. There are also uncertainties associated with the chosen approach to the original development of DESC; these are discussed by Skjold [12,14,18].

Some of the present scenarios showed negative pressures of up to −0.2 bar to appear at certain points of the pressure wave. It may therefore not be enough to simply consider the maximum overpressure developed by the vented explosion if silos are to be correctly deigned. EN 1991-4 [3] warns about the problem of underpressures arising in vented silos, but it proposes no means of estimating them, nor does EN 14491 [4] nor NFPA 68 [5]. Negative pressures, although not very high, produce compressive stresses that could lead to buckling failures if the design of a silo does not take them into account. Numerical simulations might be very useful for estimating these underpressures.

The DESC program has proven to be a very useful tool for studying how to protect against dust explosions – in this case in silos – and for improving our knowledge on dust explosions and their consequences. Simulations offer a number of advantages: they can generate a great deal of information for any point of interest, the initial conditions can be varied, and simulations are much cheaper than performing real explosion experiments. The program could also serve for planning real explosion tests and extrapolating the results to other situations.

Improving the design of vented silos will require further research into the venting process and the characteristics of the dust clouds. This must include realistic experiments and simulations involving the actual equipment currently used in industry. Numerical simulations could be a powerful tool for helping engineers design explosion mitigation methods and calculating the structure of vented silos.

Acknowledgements

The authors express their deepest gratitude to the late Dr. Frank Hauert (FSA) for providing information on the CREDIT Project. Acknowledgements are also due to the Education Council of the Community of Castilla y León (Spain) and the European Social Fund, for funding this work via project LE010B05 and via a research grant.

References

[1] R.K. Eckhoff, Dust Explosions in the Process Industries, third ed.Gulf Professional Publishing, USA, 2003.
[2] Directive 1999/92/EC of the European Parliament and of the Council of 16 December 1999 on minimum requirements for improving the safety and health protection of workers potentially at risk from explosive atmospheres, Off. J. Eur. Union L 23 (28.01.2000) 57–64, Brussels.
[3] EN 1991-4, Eurocode 1, Actions on structures, Part 4, Silos and tanks, European Committee for Standardization, Brussels, 2006.
[4] EN 14491, Dust explosion venting protective systems, European Committee for Standardization, Brussels, 2006.
[5] NFPA 68, Standard on explosion protection by deflagration venting, National Fire Protection Association, Quincy, MA, USA, 2007.
[6] T. Abbasi, S.A. Abbasi, Dust explosions — cases, causes, consequences, and control, J. Hazard. Mater. 140 (2007) 7–44.
[7] J. Barton, Dust Explosion Prevention and Protection: a Practical Guide, Institution of Chemical Engineers, IChemE, Rugby, UK, 2002.
[8] A. Tascón, P.J. Aguado, A. Ramírez, Dust explosion venting in silos: a comparison of standards NFPA 68 and EN 14491, J. Loss Prev. Process Ind. 22 (2009) 204–209.
[9] K. Van Wingerden, G.H. Pedersen, R.K. Eckhoff, Violence of dust explosions in integrated systems, Process Saf. Prog. 14 (2) (1995) 131–138.
[10] S. Zhong, X. Deng, Modeling of maize starch explosions in a 12 m^3 silo, J. Loss Prev. Process Ind. 13 (2000) 299–309.
[11] P. Kosinski, A.C. Hoffmann, An investigation of the consequences of primary dust explosions in interconnected vessels, J. Hazard. Mater. A137 (2006) 752–761.
[12] T. Skjold, B.J. Arntzen, O.R. Hansen, I.E. Storvik, R.K. Eckhoff, Simulation of dust explosions in complex geometries with experimental input from standardized tests, J. Loss Prev. Process Ind. 19 (2006) 210–217.
[13] F. Ayuga, P. Aguado, E. Gallego, A. Ramírez, New steps towards the knowledge of silos behaviour, Int. Agrophysics 19 (2005) 7–17.
[14] T. Skjold, Review of the DESC project, J. Loss Prev. Process Ind. 20 (2007) 291–302.
[15] B. J. Arntzen, Modelling of turbulence and combustion for simulation of gas explosions in complex geometries, Dr. Ing. Thesis, NTNU, Trondheim, Norway, 1998.
[16] EN 14034-1, Determination of Explosion Characteristics of Dust Clouds, Part 1, Determination of the Maximum Explosion Pressure p_{max} of Dust Clouds, European Committee for Standardization, Brussels, 2004.
[17] EN 14034-2, Determination of Explosion Characteristics of Dust Clouds, Part 2, Determination of the Maximum Rate of Explosion Pressure Rise $(dp/dt)_{max}$ of Dust Clouds, European Committee for Standardization, Brussels, 2006.
[18] T. Skjold, B.J. Arntzen, O.R. Hansen, O.J. Taraldset, I.E. Storvik, R.F. Eckhoff, Simulating dust explosions with the first version of DESC, Process Saf. Environ. Prot. 83 (B2) (2005) 151–160.
[19] W. Bartknecht, Pressure venting of dust explosions in large vessels, Plant Oper. Prog. 5 (4) (1986) 196–204.
[20] F. Hauert, A. Vogl, S. Radant, Dust cloud characterization and its influence on the pressure–time–history in silos, Process Saf. Prog. 15 (3) (1996) 178–184.
[21] S. Höchst, W. Leuckel, On the effect of venting large vessels with mass inert panels, J. Loss Prev. Process Ind. 11 (2) (1998) 89–97.
[22] R.K. Eckhoff, K. Fuhre, Dust explosion experiments in a vented 500 m^3 silo cell, J. Occup. Accid. 6 (1984) 229–240.
[23] R.K. Eckhoff, K. Fuhre, G.H. Pedersen, Dust explosions experiments in a vented 236 m^3 silo cell, J. Occup. Accid. 9 (1987) 161–175.
[24] R. DeGood, K. Chatrathi, Comparative analysis of test work studying factors influencing pressures developed in vented deflagrations, J. Loss Prev. Process Ind. 4 (1991) 297–304.
[25] J. Eibl, Actions, in: C.J. Brown, J. Nielsen (Eds.), Silos, Fundamentals of Theory, Behavior and Design, E and FN Spon, London, 1998, pp. 275–311.
[26] F. Hauert, A. Vogl, S. Radant, Measurement of turbulence and dust concentration in silos and vessels, Proc. 6th Int. Coll. on Dust Explosions, Shenyang, 1994, pp. 71–80.
[27] F. Hauert, A. Vogl, Measurement of dust cloud characteristics in industrial plants, CREDIT-Project, Final Technical Report, FSA, Mannheim, 1995.
[28] N. Gibson, Problems in the control of dust explosions: an overview of the CEC CREDIT project, J. Loss Prev. Process Ind. 9 (4) (1996) 291–302.
[29] A.E. Dahoe, R.S. Cant, B. Scarlett, On the decay of turbulence in the 20-liter explosion sphere, Flow Turbul. Combust. 67 (2001) 159–184.
[30] R. Siwek, New revised VDI guideline 3673 "Pressure release of dust explosions", Process Saf. Prog. 13 (4) (1994) 190–201.
[31] VDI 3673, Pressure Venting of Dust Explosions, Verein Deutscher Ingenieure, Düsseldorf, Germany, 2002.
[32] R.K. Eckhoff, Sizing of dust explosion vents in the process industries. Advances made during the 1980s, J. Loss Prev. Process Ind. 3 (1990) 268–279.
[33] R.K. Eckhoff, Influence of initial and explosion-induced turbulence on dust explosions in large vented silo cells, Saf. Sci. 16 (1993) 511–525.

Alberto Tascón: Ph.D. Agricultural Engineer. Researcher during 5 years in the Department of Agricultural Engineering at the University of León. Member of the Spanish Technical Committee AENOR CTN 163 for "Potentially explosive atmospheres — Explosion prevention and protection" and the European Technical Committee CEN TC305 WG03 "Systems and devices for explosion prevention and protection" on behalf of ADIX Ingeniería. Co-investigator in four research projects funded by Government bodies and companies about silo design and dust explosions in silos.

Ángel Ruiz: MSc Agricultural Engineer. Consultant on civil engineering, hydraulics and hydrology during 7 years. At present Professor in hydraulics and irrigation systems, School of Agricultural Engineering, University of León.

Pedro J. Aguado: Ph.D. Agricultural Engineer. Professor in technical projects, quality management and rural infrastructures, School of Agricultural Engineering, University of León. Member of the Spanish Technical Committee AENOR CTN 157 "Projects". Member of the Construction Committee of the Spanish Engineering Institute. More than 15 journal papers on silo design, granular materials and dust explosions. More than 80 conference papers. Eight research projects as primary investigator. Supervisor of three doctoral theses on the field of silo design. Leader of a research team placed at the University of León.

ANEJO 2

Copia del artículo II,

Design and instrumentation of a mid-size test station for measuring static and dynamic pressures in silos under different conditions – Part I: Description,

publicado en

Computers and Electronics in Agriculture 85 (2012) 164–173

Computers and Electronics in Agriculture 85 (2012) 164–173

Contents lists available at SciVerse ScienceDirect

Computers and Electronics in Agriculture

journal homepage: www.elsevier.com/locate/compag

Design and instrumentation of a mid-size test station for measuring static and dynamic pressures in silos under different conditions – Part I: Description

A. Couto *, A. Ruiz, P.J. Aguado

Department of Agricultural Engineering and Sciences, ESTI Agricultural, University of Leon, Av. Portugal 41, 24071 León, Spain

ARTICLE INFO

Article history:
Received 18 November 2011
Received in revised form 6 March 2012
Accepted 4 April 2012

Keywords:
Test silo
Silo design
Silo pressures
Hopper eccentricity
Flat bottom

ABSTRACT

Very few experimental installations in the world have full-scale silos, and very few assays have been conducted on them. Consequently, numerous unresolved questions remain which require further research in order to be able to reliably predict the behaviour of the material stored in these kinds of structures.

In this article, we describe the design of a full-scale test station for assaying pressure in silos. The installation basically consists of a full-scale, cylindrical silo equipped with load cells to measure pressure and variable-frequency drives connected to each of the electric motors driving the filling and discharge screw conveyors, in order to study the effect on pressure of the speed at which the silo is filled or discharged. As a result of this novel design, it is possible to obtain most of the parameters which control the behaviour of stored material and to compare and validate the different theoretical models used for performing calculations and establishing current standards.

The versatility of the silo design also makes it possible to adapt the geometry to the conditions which, in practice, are present most frequently in slender silos, enabling assays to be conducted for flat bottom and hopper silos, and combining both of these conditions with central and eccentric outlets. Furthermore, for each of these configurations it is also possible to study the behaviour of the material under different conditions, including static state, dynamic filling and discharge state, variations in filling and discharge speeds, pressure caused by swelling in the case of material stored when moist or saturated with aqueous solutions, and to perform simulations of an increase in silo height.

© 2012 Elsevier B.V. All rights reserved.

1. Introduction

The question of the structural design of silos used for storing granular material has been a subject of enquiry since the end of the 19th century (Janssen, 1895). However, despite the advances in knowledge which have been achieved to date, many of the problems observed in practice remain unresolved (Ayuga, 2008; Dogangun et al., 2009; Nielsen, 2008) since the laws which control the behaviour of granular material and the pressures it exerts on internal silo walls are still not completely understood.

Numerous researchers have developed theoretical models (Artoni et al., 2009; Ayuga et al., 2001; Briassoulis, 2000; Gillie and Holst, 2003; Goodey et al., 2003, 2006; Guaita et al., 2003; Juan et al., 2006; Khelil, 2002; Knebel and Schweizerhof, 1995; Martinez et al., 2002; Matchett, 2006; Matchett et al., 2008; Ooi and Rotter, 1991; Pircher et al., 2001; Song, 2004; Song and Teng, 2003; Vidal et al., 2005, 2006, 2008; Winterstetter and Schmidt, 2002; Wu and Schmidt, 1992; Yang and Hsiau, 2001) to predict the behaviour of material stored in this kind of structure, using different boundary conditions. Such models require validation through experimental assays: however, in practice these are rarely performed due to the high costs and effort involved in designing and constructing test stations. Furthermore, many of the parameters of the stored material required by these theoretical models in order to predict behaviour (Moya et al., 2002, 2006) have been insufficiently studied.

Other researchers have conducted assays on model silos built to scale (Ahn et al., 2008; Askegaard and Munch-Andersen, 1985; Chou and Hsu, 2003; Chou et al., 2002; Coetzee and Els, 2009; Grudzien et al., 2010, 2011; Nedderman and Tüzün, 1979; Niedostatkiewicz et al., 2009; Rotter et al., 1989; Sielamowicz et al., 2005; Sielamowicz et al., 2006, 2010; Sielamowicz and Czech, 2010; Wu et al., 2009; Wójcik and Tejchman, 2009) in order to reach their conclusions. However, it is well-known that errors of scale have often led to results which differ considerably from behaviour at full scale (Chen et al., 2007; Nielsen and Askegaard, 1977).

Very few experimental installations in the world have full-scale silos (Brown et al., 2000; Härtl et al., 2008; Ramirez et al., 2010c; Schurich et al., 2001; Teng and Lin, 2005; Teng et al., 2001; Zhao and Teng, 2004a; Zhong et al., 2001), and very few assays have been conducted on them (Chen et al., 2005, 2007; Härtl et al., 2008; Ooi et al., 1990; Teng et al., 2005; Wu et al., 2009; Yang

* Corresponding author. Tel./fax: +34 987 29 10 00x5243.
E-mail addresses: acouy@unileon.es (A. Couto), aruip@unileon.es (A. Ruiz), pedro.aguado@unileon.es (P.J. Aguado).

0168-1699/$ - see front matter © 2012 Elsevier B.V. All rights reserved.
http://dx.doi.org/10.1016/j.compag.2012.04.009

and Hsiau, 2001). Such installations and assays require considerable effort, but have produced very important results. Nevertheless, numerous unresolved questions remain which require further research in order to be able to reliably predict the behaviour of the material stored in these kinds of structure. The problem with these structures is that many different types of silo design are possible in practice, resulting in a very high number of boundary conditions and parameters requiring study.

In this article, we describe the design of a full-scale test station for assaying pressures in silos. Due to the versatility of the test silo design, it is also possible to adapt the geometry to the conditions which, in practice, are present most frequently in slender silos, enabling assays to be conducted for flat bottom and hopper silos, and combining both of these conditions with central and eccentric outlets. Furthermore, for each of these configurations it is also possible to study the behaviour of the material under different conditions, including static state, dynamic loading and discharge state, variations in loading and discharge speeds, pressure caused by swelling in the case of material stored when moist or saturated with aqueous solutions, and to perform simulations of an increase in silo height, etc.

This same versatility also offers the possibility of using the test silo as a tool for validating existing theoretical models, whilst at the same time obtaining new data which will contribute to furthering knowledge on the behaviour of material stored in these kinds of structure.

2. Description

The design and instrumentation of the test station was conducted entirely by the research team at the Department of Agricultural Engineering and Sciences, University of León, Spain. In this article we describe the design of a test station for slender cylindrical silos, since this is the form most frequently used in the industry, although the design and instrumentation would also be valid for construction of a test station for square, rectangular and even polygonal silos using the same principals and adapting them to the chosen geometry.

2.1. General description of the test station

The installation consists of 2 silos, one for conducting assays and the other for storing the granular material used in assays. The silos are connected by two screw conveyors powered by electric motors, to facilitate filling and discharge of the same (Fig. 1). In order to measure pressures on the walls and at the base of the test silo under different conditions, load cells are positioned at strategic points of the test silo (Fig. 4).

2.2. Geometry of the test silo

The geometry of the silo described is cylindrical, and it consists of three independent segments which can be dismantled; the lower segment, or base, where the outlet for stored material is located, a central segment, or cylindrical body, and a roof, or cover, which comprises the upper segment (Fig. 2).

The lower segment consists of four pieces, including a set of three interchangeable hoppers, one for central discharge, another for completely eccentric discharge and the last providing intermediate outlet eccentricity. The three hoppers are reinforced with a ring at the silo-hopper transition. The fourth piece comprises a flat bottom which in turn has three outlet holes (central, intermediate and eccentric) (Figs. 2, 3 and 7).

The body of the silo consists of a cylinder reinforced at the top and bottom with rings which rest on the vertical load cells, thus separating the cylinder from the other segments and making it possible to determine the vertical forces produced in the central segment independently (Figs. 2, 7 and 8).

The upper segment consists of a roof reinforced around the perimeter with a steel ring, which is also mounted on three vertical load cells and separates the upper segment from the central segment. The three load cells in the upper segment provide information on vertical wall pressure when additional pressure is exerted on the upper segment. The roof is not flat, since it contains the housing for an inflatable membrane which can be used to exert additional pressures on the upper surface of the grain (Figs. 2 and 8).

The test silo constructed to validate this design, described in detail in the second part of this publication, was constructed using steel plates 3 mm thick whilst the reinforcement rings for the cylinder, hopper and roof were 50 mm wide and 10 mm thick. Following the nomenclature employed in Fig. 9 in this article, the dimensions were: $h_c = 2.00$ m; $h_h = 0.73$ m; $h_b = 2.73$ m; $d_c = 1.00$ m; $\beta = 34.30°$; $e_0 = 0$ m. According to the Eurocode classification, this corresponds to a slender silo, since the cylinder height/diameter ratio is equal to 2 ($h_c/d_c = 2$).

2.3. Instrumentation

2.3.1. Measuring horizontal pressures

The pressures exerted on the cylinder wall are measured at four generatrices and at different heights. Pressures exerted on the hopper are measured immediately below the transition, at the prolongation of the generatrices for measuring the cylinder.

To measure normal wall pressures at different points, double bending beam load cells are used. To this end, openings are made in the wall, into which panels of exactly the same shape as the opening, made of the same material as the wall and of the same thickness, are inserted. These panels are completely flush with the inner side of the silo wall.

Load cells parallel to the cylinder are connected to these panels, in order to measure the horizontal force exerted on a known surface area. A very small tolerance is allowed between the edges of the panels and the wall in order to avoid friction and ensure that the panel rests only on the double bending beam load cells (Fig. 5).

Load cells of this type, which undergo small deformations of between 0.3 and 0.5 mm when at limit load, are available on the market. This avoids any possible error when interpreting pressures which could arise from displacement of the silo walls connected to the load cells due to the lack of rigidity of these devices (Fig. 6).

2.3.2. Measuring vertical forces

Vertical forces are measured by tension/compression load cells (Molenda et al., 2009). Measurements are taken at points located at three different heights by three load cells placed at each height, 120° apart around the circumference of the cylinder (Fig. 4).

The hopper is mounted on three load cells, thus enabling measurement of the total weight of the stored material. The cylinder is mounted on a further three load cells, located above the previous three, enabling measurement of the vertical force exerted on the wall (Fig. 7), this enables the value of the frictional forces to be obtained, which in turn is used to obtain average vertical pressures at a determined level. In addition, this also permits values for the vertical force on the wall at the silo-hopper transition junction caused by friction between the stored material and the cylinder walls to be obtained.

Another three load cells are located in the upper segment of the cylinder, and provide the mounting for the silo roof, making it possible to exert additional pressure on the upper segment in order to simulate pressures in silos with a higher h_c/d_c ratio, thus avoiding the need to construct a taller cylinder. As a result, the effect of an overpressure on the stored material can be analysed, as can its

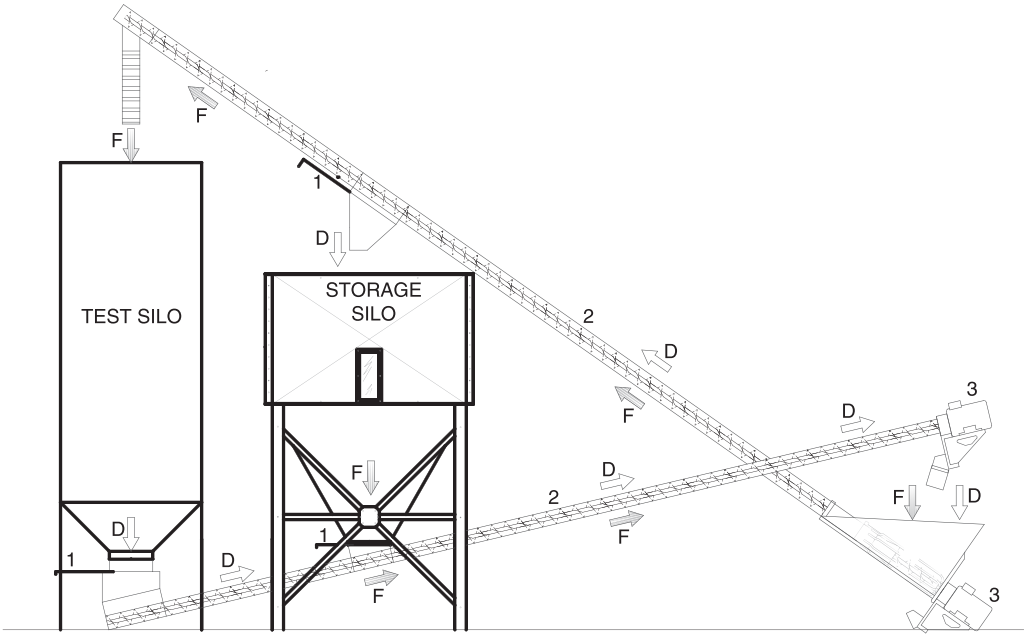

Fig. 1. General Test Station silo installation. 1: Slide gate; 2: screw conveyor; 3: AC motor; F: filling; D: discharge.

Fig. 2. Geometry of the test silo.

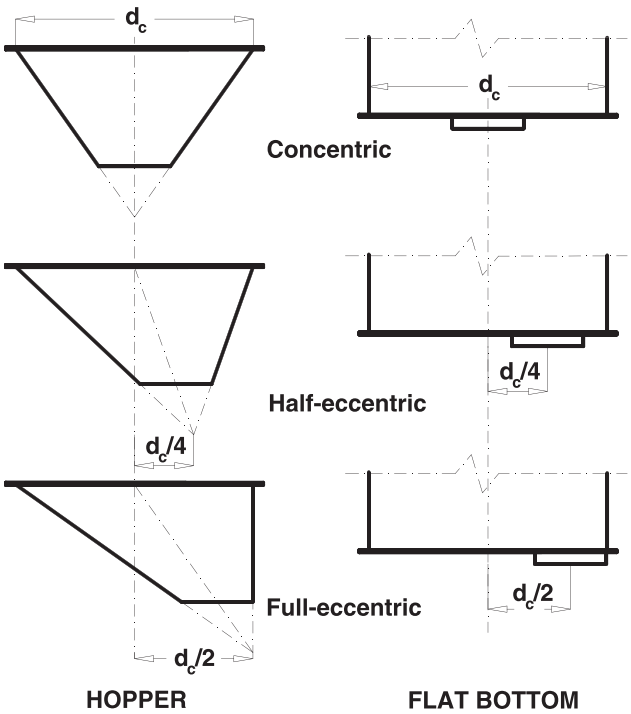

Fig. 3. Discharge in hopper and flat bottom silos.

influence on the horizontal pressures. However, in order to obtain the vertical pressure per unit length at the silo-hopper transition junction it is also necessary to take into account the additional vertical forces acting on the cylinder wall due to friction between the grain and the simulated cylinder walls, as well as the weight of the simulated cylinder itself.

This system also makes it possible to study the pressure exerted by swelling of material stored under different confinement pressures. To this end, an elastic inflatable membrane is housed in the roof, in order to apply the additional pressure specified in the experiment in the upper segment (Fig. 8).

As with the double bending beam load cells, there are tension/compression load cells of this kind available on the market which undergo small deformations of less than 0.5 mm at limit load, thus avoiding the risk of coming into contact with the rings separating the three segments of the silo during the assay. It is therefore important to consider the deformation of the load cell chosen at limit load when determining the separation between rings (Figs. 6–8), and the design should be sufficiently rigid to prevent either horizontal or vertical deformation of the rings.

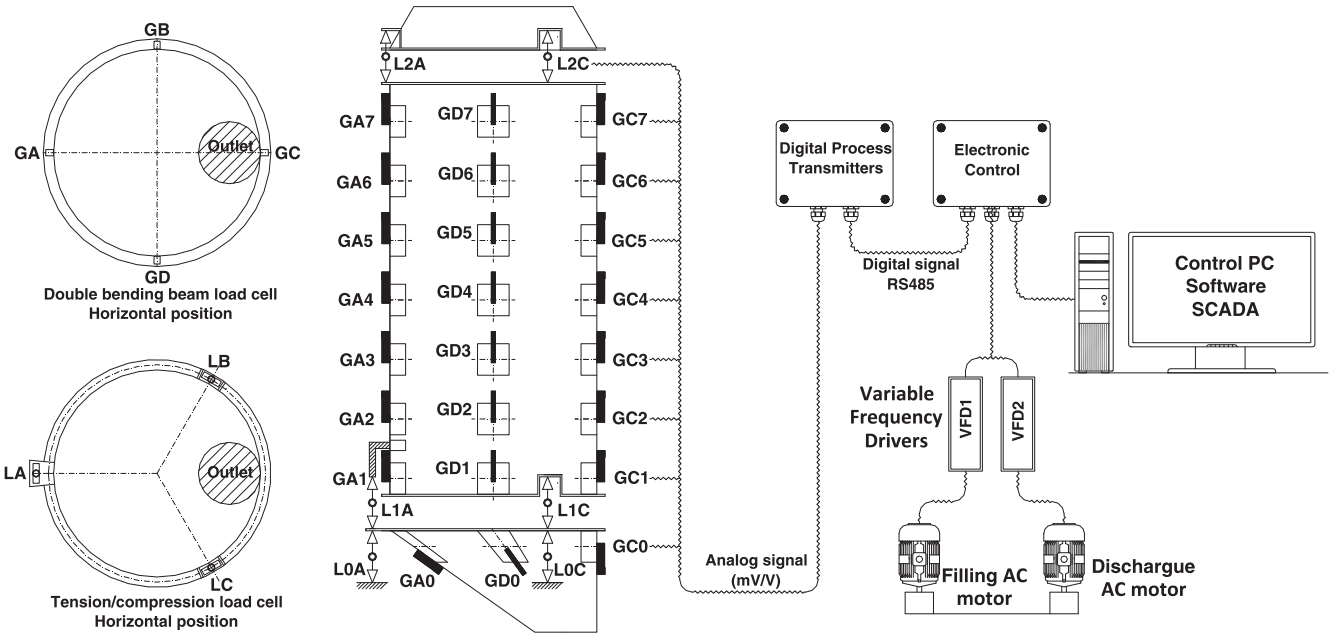

Fig. 4. Instrumentation.

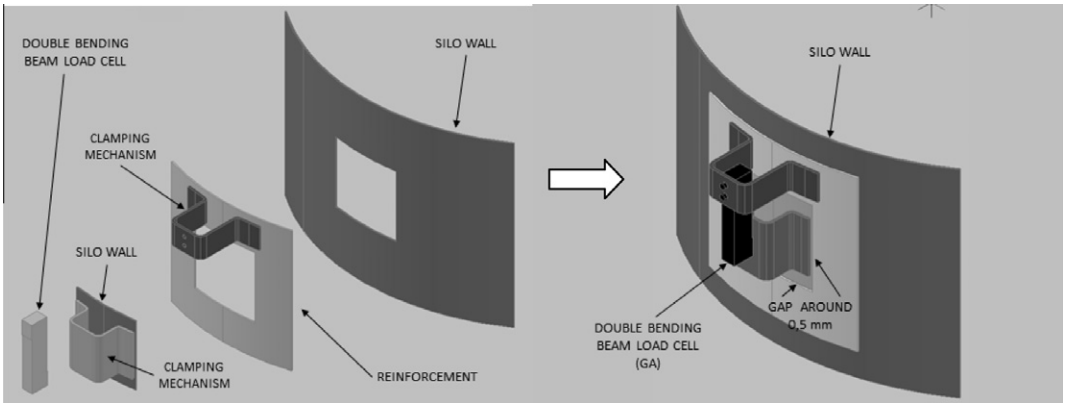

Fig. 5. Double bending beam load cell assembly.

2.3.3. Control filling and discharge speed

Filling and discharge is performed using screw conveyors connected to two A/C motors. Filling and discharge speed is controlled by variable-frequency drives (VFD) which regulate conveyor rotation speed.

2.3.4. Communication protocol

The installation could be controlled using a standard communication protocol with an RS485 interface. For this, it would be necessary a specific SCADA (Supervisory Control and Data Acquisition). The analog signal sent by each load cell (mV/V) would be processed by an A/D converter into a digital readout which is transmitted by the RS485 network. The converters currently available on the market are capable of processing and uploading various readouts per second.

Reading and storage of the data sent by the load cells, together with motor rotation speed control, is performed by a PC using the SCADA software application specifically designed for this purpose. This application facilitates selection of the time interval between readings (from tenths of seconds), storing them in a text file. At the same time, it also provides the ability to control the variable-frequency drives and set the filling or discharge speed desired in each experiment.

2.3.5. Calibration

See Part 2, apart 2.3.5.

3. Data processing

3.1. Nomenclature

The nomenclature employed is in accordance with that used in the Eurocode (CEN, 2006), but also includes specific aspects of this installation which are not considered in the code.

To avoid repetition, only those equations which are not given in the second part of these two publications will be included in this section. The different parameters involved in these equations and which are either not considered in the Eurocode or are expressed differently, are defined as follows:

– $F_{L1x,t}$: vertical force exerted on the load cells located at level L1 at each time t, kN.

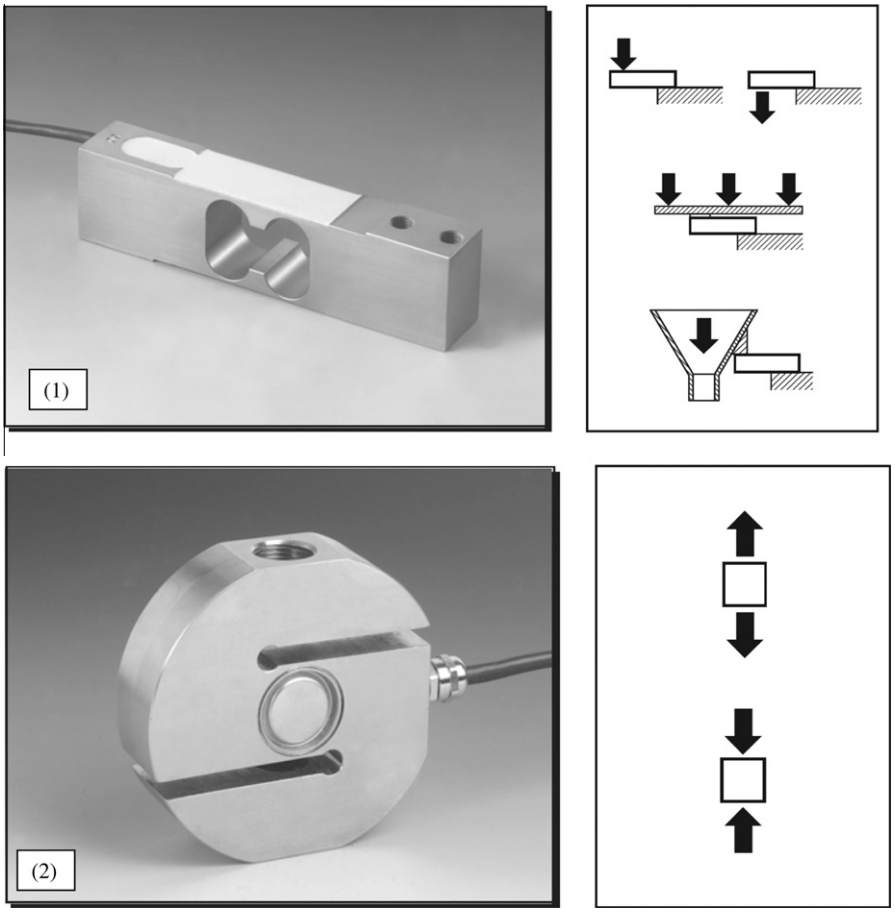

Fig. 6. Example of a double bending beam load cell (1) and tension/compression load cell (2) made by Técnicas de Electrónica y Automatismos, S.A., Spain.

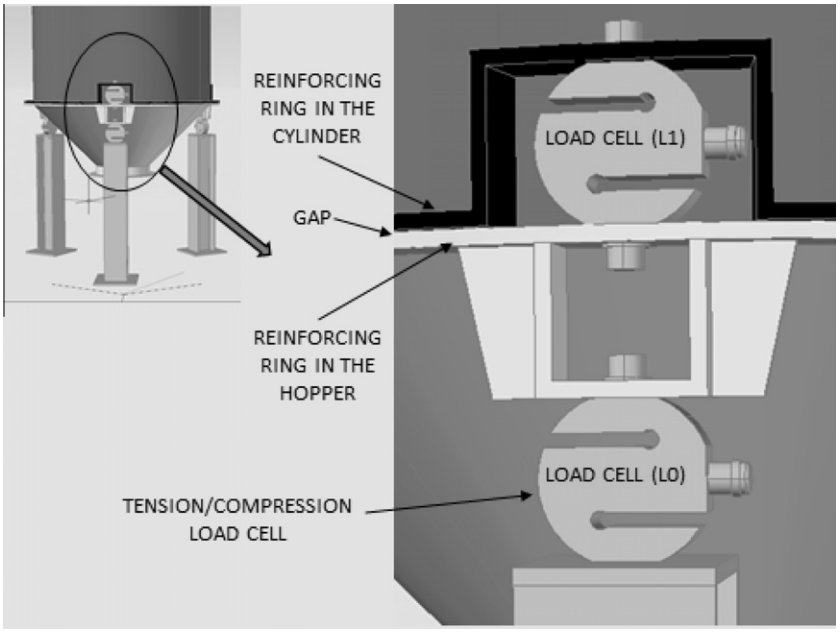

Fig. 7. Double bending beam load cell assembly at the bottom.

- $p_{vt,t}$: vertical stress in the stored material at the silo-hopper transition at time t, kN/m^2.
- $p_{w,t}$: mean value of wall frictional traction at time t, kN/m^2.
- $S_{c,t}$: cylinder surface in contact with stored material at time t, m^2.
- sp_v: additional vertical pressure exerted on the stored material in the upper segment of the silo, kN/m^2.
- W_{hsm}: weight of stored material between the outlet and the silo-hopper transition, zero in the case of flat bottom, kN.

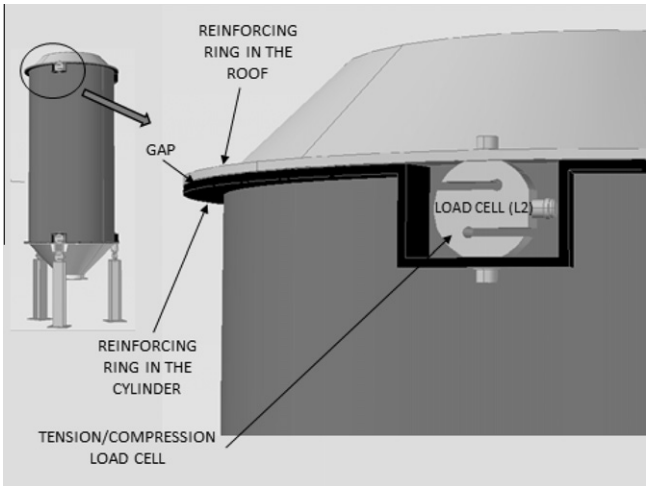

Fig. 8. Double bending beam load cell assembly at the top.

3.2. Normal wall pressures

Values for normal wall pressures are obtained directly from readings provided by the double bending beam load cells located at the four cylinder and hopper wall generatrices, by dividing the force value obtained by each cell by the wall surface on which that force is acting. Thus it is possible to obtain normal cylinder and hopper wall pressure at each time at the points where the load cells are located.

3.3. Normal cylinder wall pressure at the silo-hopper transition

The mean value for normal cylinder wall pressure at the silo-hopper transition at each time t, is obtained from readings of the double bending beam load cells located at the four level 1 cylinder generatrices given that the surface on which they act is known and constant (see Eq. (1) Part II).

Comparison of readings from the four load cells located at this level provides information on whether normal wall pressures are axial-symmetric or not, on the distribution pattern present and on maximum values in the case of non-axial symmetric distribution.

Similarly, these pressures can be obtained for different heights within the cylinder, using the same analysis for all levels at which the double bending beam load cells are located.

3.4. Normal hopper wall pressure at the silo-hopper transition

The mean value for normal hopper wall pressure at the silo-hopper transition at each time *t* is obtained from readings provided by the double bending beam load cells located at the four cylinder generatrices at level 0 (see Eq. (2) Part II).

As in the case of the cylinder wall, a comparison of readings from the four load cells will provide information on whether the distribution of normal wall pressures is axial-symmetric or not, on the distribution pattern present and on maximum values in the case of non-axial symmetric distribution.

3.5. Vertical force on the cylinder wall by unit of length

The mean vertical force in the lower segment of the cylinder (silo-hopper transition) by unit of length at each time *t*, is obtained from readings provided by the tension/compression load cells located at level L1. Since the cylinder rests on these three cells, this value is obtained by dividing the sum of the values obtained by the perimeter of the circumference. This force at the base of the cylinder is due to the weight of the stored material and the frictional force it exerts on the walls. Since the cylinder weight is known, the vertical force due to friction can easily be deduced (see Eq. (3) Part II).

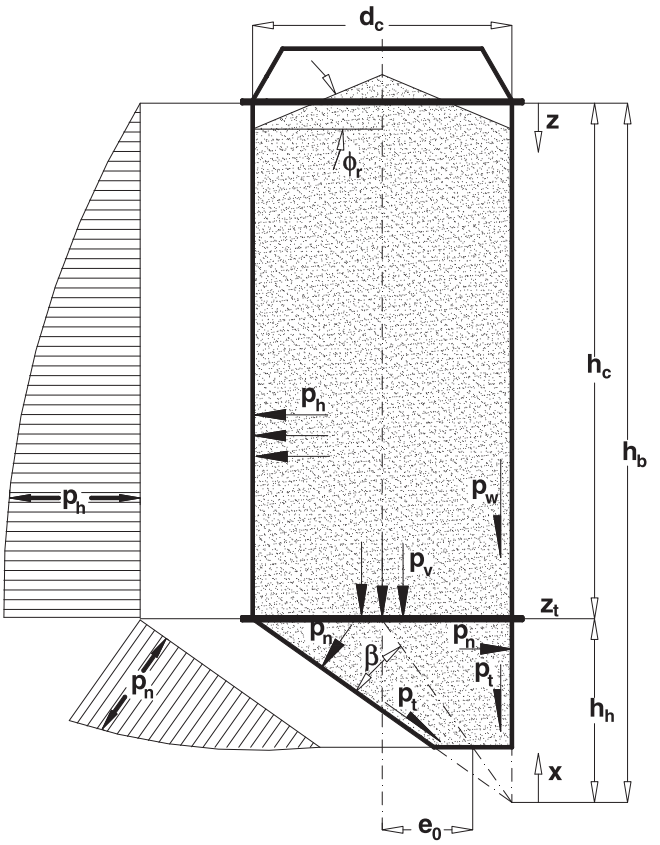

Fig. 9. Symbols.

Through comparison of the values obtained by the load cells, information is obtained as to whether vertical wall pressure is axial symmetric or not.

3.6. Vertical pressure of stored material at the silo-hopper transition

The mean vertical pressure of stored material at the silo-hopper transition for each time t, is obtained from readings provided by the tension/compression load cells located at levels L0 and L1 (see Eq. (4) Part II).

From this parameter, the pressure exerted by the grain on the base of the silo (in the case of flat bottom silos) or on the hopper, is obtained.

3.7. Wall frictional traction

The mean value of the frictional force exerted on the cylinder wall by stored material can be obtained for each time t; since filling and discharge speed is known, evolution over time of the cylinder surface in contact with the stored material can be deduced (see Eq. (5) Part II).

3.8. Wall friction coefficient

Mean value for the grain-wall friction coefficient are obtained using the expression shown in Section 2.5.5. in Part 2 (see Eq. (6) Part II).

The test silo is made of steel and consequently, the results obtained for grain-wall friction are applicable to smooth-walled steel silos. However, it would be possible to study the effects of the grain-wall friction coefficient on pressures by altering the roughness of the walls, facing them with flexible sheets of different degrees of roughness, or using any other method which modifies wall roughness. Similarly, it would be possible to simulate soldered joints in order to study silos constructed in this manner, simulating wall imperfections.

The Eurocode (CEN, 2006) suggests determining these parameters from laboratory parameters; however, in this test station it is possible to determine them directly.

3.9. Lateral pressure ratio K

The lateral pressure ratio K (ratio of mean horizontal to mean vertical pressure) should be determined at a particle packing density and stress level corresponding to the position of stored material in the silo where maximum vertical stress after filling occurs (CEN, 2006).

With this test station, the K coefficient can be obtained under static and dynamic conditions, and variability under these conditions during filling or discharge can be studied (see Eq. (7) Part II).

3.10. Simulation of pressures in silos with a higher h_c/d_c ratio

Simulation of greater storage heights is achieved through exerting additional vertical pressure in the upper segment of the silo.

This technique makes it possible to study static and dynamic discharge pressures at the start of discharge.

To this end, the silo roof contains housing for an inflatable membrane. The inflation pressure of this membrane determines the additional pressure it exerts on stored material, and is obtained from the readings of the tension/compression cells located at level L2, using the following expression:

$$sp_v = \frac{(F_{L2A} + F_{L2B} + F_{L2C})}{A} \quad (1)$$

To determine the vertical pressure exerted by stored material on the silo-hopper transition, it should be borne in mind that the readings from load cells at level L2 will be negative (tension) compared with the positive readings (compression) obtained from the load cells at levels L1 and L0, and consequently is determined using the following expression:

$$p_{vt,t} = \frac{(F_{L0A,t} + F_{L0B,t} + F_{L0C,t}) + (|F_{L2A,t} + F_{L2B,t} + F_{L2C,t}|) - (F_{L1A,t} + F_{L1B,t} + F_{L1C,t}) - W_{hsm}}{A} \quad (2)$$

Similarly, wall frictional traction is determined using the following expression:

$$p_{w,t} = \frac{(F_{L1A,t} + F_{L1B,t} + F_{L1C,t}) + (|F_{L2A,t} + F_{L2B,t} + F_{L2C,t}|)}{S_{c,t}} \quad (3)$$

3.11. Study of pressure caused by swelling

Some materials stored in this type of structure swell when moist or saturated in aqueous solutions, causing a rise in pressures exerted within the silo.

In order to study swelling pressure, an impermeable membrane is incorporated into the design with the same shape and dimensions as the interior of the silo, and the stored material is saturated with the aqueous solution to be assayed.

In order to prevent distorted load cell readings as a result of the membrane's resistance to swelling, in this assay the wall panels providing pressure readings are not flush with the inner cylinder wall but rather are placed in such a way as to protrude slightly into the silo interior.

The pressures and parameters of this stored material are determined as described in the previous sections for material stored under normal conditions.

To study swelling of stored material under various confinement pressures, the desired additional pressure is exerted on the material in the upper segment of the silo, as described in the previous section.

4. Research planning

Numerous authors have proposed complex mathematical models, principally based on the finite elements method (FEM) (Ayuga et al., 2001; Briassoulis, 2000; Gillie and Holst, 2003; Goodey et al., 2003, 2006; Greiner and Guggenberger, 1998; Guaita et al., 2003; Juan et al., 2006; Khelil, 2002; Khelil et al., 1999, 2001; Knebel and Schweizerhof, 1995; Martinez et al., 2002; Ooi and Rotter, 1991; Song, 2004; Song and Teng, 2003; Teng and Rotter, 1991a,b,c; Vidal et al., 2005, 2006, 2008; Wu and Schmidt, 1992; Wójcik and Tejchman, 2009; Zhao and Teng, 2004b) or on the discrete elements method (DEM) (Coetzee and Els, 2009; Wu et al., 2009; Yang and Hsiau, 2001; Gonzalez-Montellano et al., 2011), to analyse the behaviour of material stored inside a silo: however, the assumption of various limit conditions in these models can lead to wide variations in the pressures predicted (Goodey and Brown, 2004). Furthermore, experiments have demonstrated that the force exerted on silo walls depends to a large extent on the mechanical properties of the materials stored (Elghazouli and Rotter, 1996; Marchant, 1980) (e.g., the Poisson ratio, the dilatancy angle and the modulus of elasticity, the coefficient of friction, etc.), properties which have still not been sufficiently assayed in the case of many of the materials stored in silos, and research teams are still publishing studies in this field (Gudehus et al., 1986; Lawton, 1980; Moya et al., 2002, 2006; Ramirez et al., 2009).

It is essential to determine a suitable value for these parameters if a mathematical model is to generate reliable results, since the results will be strongly influenced by the values adopted.

One of the purposes of this full-scale test station is to study and validate these mathematical models under experimental conditions, together with the mechanical properties of stored materials they assume, under experimental conditions.

The use of load cells in the silo instrumentation resolves the complex problems of interpreting forces entailed in the use of strain gauges (Chen et al., 1996) or pressure cells (Askegaar et al., 1971; Brown et al., 2000; Ramirez et al., 2010a,b). For example, the problem caused by the lack of cell plate rigidity, which hinders pressure measurements (Ramirez et al., 2010a), does not arise since the rigidity of the type of load cell used is very high, presenting deformations of less than 0.5 mm at nominal loads, thus avoiding excessive displacement of the load cells connected to the wall, which could distort results.

The use of this type of load cell also eliminates complex calibration operations (Askegaard, 1981; Ramirez et al., 2010a,b), since it measures force rather than pressure, and it is thus sufficient to calibrate each load cell individually at one point, in the first quarter of the service load, and verifying this at another point located in the third quarter of the service load.

The possibility of interchanging hoppers with different outlet positions, or of substituting the hopper for a flat bottom, also with different outlet positions, provides multiple advantages, facilitating assays on a full-scale silo with different outlet configurations at the same test station. This, in turn, makes it possible to assay and validate the different mathematical models which have been developed to predict pressures.

Many agricultural companies use materials with a high water content, and these are sometimes stored in silos. Such materials can produce swelling pressures that must also be considered when designing the structure of the silo. Eurocode 1, part 4, (CEN, 2006) establishes a method for calculating pressures exerted by the stored materials on the silo walls, but no procedure exists for calculating the pressures caused by swelling during the storage of these materials. The test station described here provides the possibility of advancing in this field of knowledge since, as explained in Section 3.12, it is equipped to perform real assays of swelling in order to validate the theoretical models which have been developed for this phenomenon.

One parameter which has been the subject of much study is the K factor, the relationship between horizontal and vertical pressures. This parameter is a necessary factor in silo calculations in accordance with the various standards. The Eurocode 1, part 4 (CEN, 2006) proposes a method for obtaining an approximation of the K factor in the laboratory, together with an alternative equation based on the internal friction angle of the stored material, a parameter which also requires further assays. One of the advantages of making the base of the test silo independent from the walls is that the possibility is therefore offered of obtaining the real value of this parameter, since the design makes it possible to obtain horizontal and vertical pressure values at the silo-hopper transition, the area where most pressure is exerted and where pressure values are highest. Furthermore, it is also possible to design a specific experiment to study variability of this factor under different conditions.

There is general agreement between different research teams (Ahn et al., 2008; Artoni et al., 2009; Briassoulis, 2000; Chen et al., 2005; Goodey et al., 2003; Härtl et al., 2008; Martinez et al., 2002; Ooi et al., 1990; Ramirez et al., 2010c; Shalouf, 2003) and the standard (CEN, 2006), that the greatest pressures inside the silo are produced under dynamic conditions, basically during discharge. However, what is still not well understood is the magnitude that these additional pressures can reach, and the parameters which control them. With the design described here, in addition to furthering knowledge on increased pressures during discharge, it is also possible to study the effect that the speed of stored material discharge has on these pressures since, as described earlier, the revolutions of the loading and discharge screw conveyors are regulated by two variable-frequency drives. This further permits the study of free discharge, simply by disconnecting the automatic discharge system from the outlet. Although it is well-known that the pressures produced during filling of the silo are lower than those produced during discharge, this phenomenon can also be studied in the same way as discharge.

The effect of the flow pattern produced within the silo during discharge on pressures is also widely known (Chen et al., 2005, 2007; Grudzien et al., 2010; Grudzien et al., 2011; Härtl et al., 2008; Niedostatkiewicz et al., 2009; Sielamowicz and Czech, 2010; Zhong et al., 2001); in turn, flow pattern is highly influenced by eccentricity or not of discharge and whether the base of the silo is flat bottomed or has a hopper. In the test station described here, stored material can be discharged in an ordered manner using a screw conveyor and, although it is not described here, an experiment can be conducted to examine the type of flow by placing markers at known coordinates inside the silo during filling and obtaining the type of flow from the dwell time of the markers inside the silo during discharge (Chen et al., 2005, 2007; Härtl et al., 2008). It would also be possible to study the effect of discharge speed on the type of flow produced inside the silo.

Another factor which has been widely studied in thin-walled cylindrical silos is the phenomenon of bulging due to compression of the vertical silo wall (Khelil, 2002; Knebel and Schweizerhof, 1995; Rotter et al., 1989; Song and Teng, 2003; Teng and Chan, 2000; Teng and Lin, 2005; Teng et al., 2001; Winterstetter and Schmidt, 2002; Zhao and Teng, 2004a,b). With the design described here, it is possible to directly ascertain the force the vertical wall is subjected to at the silo-hopper transition, under both static and dynamic conditions. Moreover, by mounting the silo cylinder on independent load cells, it is possible to ascertain distribution of the force and, where asymmetries are observed, to obtain the mean and maximum values reached.

In the case of stored solids, grain-wall friction exerts a strong effect on thrust forces (Lawton, 1980). Other authors have studied the effect of imperfections in the silo wall (Pircher et al., 2001; Ramirez et al., 2010c; Teng and Lin, 2005; Teng et al., 2005), basically due to soldered joints. With the test station described here, it is not only possible to study friction of stored material against smooth walls but also to simulate different wall materials and even to simulate wall imperfections. To this end, the silo wall may be faced with flexible sheets presenting different degrees of roughness, or with very fine metal sheets which can simulate wall imperfections due to soldered joints.

Another important factor to consider when calculating silos is the h_c/d_c ratio (cylinder height divided by internal diameter). The Eurocode (CEN, 2006) classifies silos as: slender silos ($2 \leqslant h_c/d_c$), intermediate slenderness silos ($1 < h_c/d_c < 2$), squat silos ($0{,}4 < h_c/d_c \leqslant 1$) and retaining silos ($h_c/d_c \leqslant 4$), and proposes methods for calculating the different pressures according to the class to which the silo belongs. With the test station described here, it is possible to study the effect of this ratio on thrust force in slender silos, this kind of silo being the most commonly used in the industry and generally the only kind equipped with hoppers at the outlet.

Some research teams have studied the effect on pressure of placing inserts (Härtl et al., 2008; Wu et al., 2009; Yang and Hsiau, 2001) inside the silo in order to vary the flow pattern and observe the consequent effects on internal pressures produced during discharge. The test station described here is also suitable for conducting this kind of analysis.

5. Conclusions

In this article, we have presented a novel design for the construction of a full-scale silo test station. With this station it is possible to obtain the following parameters:

- Lateral pressure on the vertical silo wall.
- Pressure at areas close to the silo-hopper transition in silos with hoppers.
- Vertical wall frictional traction.
- Mean vertical pressure at the stored solid at transition.
- Mean wall frictional traction for different materials and wall types.
- The K ratio between horizontal and vertical pressures.

In addition, it is possible to conduct assays under the following conditions:

- Flat bottomed or hopper silos.
- Discharge with different eccentricities.
- Different filling and discharge speeds.
- Different height/diameter ratios, varying pressure from above.
- Swelling of stored material due to moisture.

Consequently, it is possible to study the parameters which control the behaviour of stored material under different boundary conditions in the same test silo, and thus obtain much of the data necessary for calculating these structures at a real scale.

Since both lateral pressures and vertical forces can be measured at different points of the silo walls, it is possible to obtain values for horizontal and vertical pressures and for wall friction. Therefore, the mean friction coefficient produced at the silo wall can be determined. In addition different types of materials and different types of walls can also be tested.

Since the silo base is interchangeable, both flat bottoms and hoppers can be analysed, as well as different discharge eccentricities. The data obtained under these conditions are crucial, given that they condition silo design. Furthermore, since it is possible to regulate the speed of filling and discharge motors, the effect of filling and discharge speed on the parameters described above can be analysed.

Moreover, additional pressure can be applied within the silo from above, in order to simulate silos with greater storage height and to study variations in the data obtained from different height/diameter ratios, using a silo of reduced height.

One of the calculation hypotheses about which least is known world-wide is swelling of material due to moisture. The pressures produced by this phenomenon are extremely high, but scant experimental data or procedures exist for calculating such pressures. The test silo described here is suitable for conducting assays with materials under conditions of saturation, thus making it possible to obtain the parameters described above under these conditions.

Acknowledgements

The authors thank the Spanish Research and Technology Commission (CICYT) (Research Project AGL2005-07430-C02-01/AGR) and the Regional Executive of Castilla y León (Research Project LE020A10-2) for financing this research.

We also thank the reviewers for their advice, which has undoubtedly contributed significantly to improving the quality of this publication.

References

Ahn, H., Basaranoglu, Z., Yilmaz, M., Bugutekin, A., Gül, M.Z., 2008. Experimental investigation of granular flow through an orifice. Powder Technology 186, 65–71.

Artoni, R., Santomaso, A., Canu, P., 2009. Simulation of dense granular flows: dynamics of wall stress in silos. Chemical Engineering Science 64, 4040–4050.

Askegaar, V., Berghold, M., Nielsen, J., 1971. Problems in connection with pressure cell measurements in silos. Bygningsstatiske Meddelelser 42, 33–&.

Askegaard, V., 1981. Design and application of stress and strain cells with small measuring errors. NDT International 14, 271–277.

Askegaard, V., Munch-Andersen, J., 1985. Results from tests with normal and shear stress cells in a medium-scale model silo. Powder Technology 44, 151–157.

Ayuga, F., 2008. Some unresolved problems in the design of steel cylindrical silos. In: Chen, J.F., Teng, J.G. (Eds.), Structures and Granular Solids: From Scientific Principles to Engineering Applications. CRC Press-Taylor & Francis Group, Boca Raton, USA, pp. 123–133.

Ayuga, F., Guaita, M., Aguado, P.J., Couto, A., 2001. Discharge and the eccentricity of the hopper influence on the silo wall pressures. Journal of Engineering Mechanics – ASCE 127, 1067–1074.

Briassoulis, D., 2000. Finite element analysis of a cylindrical silo shell under unsymmetrical pressure distributions. Computers and Structures 78, 271–281.

Brown, C.J., Lahlouh, E.H., Rotter, J.M., 2000. Experiments on a square planform steel silo. Chemical Engineering Science 55, 4399–4413.

CEN, 2006. EN 1991-4:2006. Eurocode 1: Actions on Structures. Part 4: Silos and Tanks. European Committee for Standardization, Brussels.

Chen, J.F., Ooi, J.Y., Rotter, J.M., 1996. A rigorous statistical technique for inferring circular silo wall pressures from wall strain measurements. Engineering Structures 18, 321–331.

Chen, J.F., Rotter, J.M., Ooi, J.Y., Zhong, Z., 2005. Flow pattern measurement in a full scale silo containing iron ore. Chemical Engineering Science 60, 3029–3041.

Chen, J.F., Rotter, J.M., Ooi, J.Y., Zhong, Z., 2007. Correlation between the flow pattern and wall pressures in a full scale experimental silo. Engineering Structures 29, 2308–2320.

Chou, C.S., Hsu, J.Y., 2003. Kinematic model for granular flow in a two-dimensional flat-bottomed hopper. Advanced Powder Technology 14, 313–331.

Chou, C.S., Hsu, J.Y., Lau, Y.D., 2002. The granular flow in a two-dimensional flat-bottomed hopper with eccentric discharge. Physica A: Statistical Mechanics and its Applications 308, 46–58.

Coetzee, C.J., Els, D.N.J., 2009. Calibration of discrete element parameters and the modelling of silo discharge and bucket filling. Computers and Electronics in Agriculture 65, 198–212.

Dogangun, A., Karaca, Z., Durmus, A., Sezen, H., 2009. Cause of damage and failures in silo structures. Journal of Performance of Constructed Facilities 23, 65–71.

Elghazouli, A.Y., Rotter, J.M., 1996. Long-term performance and assessment of circular reinforced concrete silos. Construction and Building Materials 10, 117–122.

Gillie, M., Holst, J., 2003. Structural behaviour of silos supported on discrete, eccentric brackets. Journal of Constructional Steel Research 59, 887–910.

Gonzalez-Montellano, C., Ramirez, A., Gallego, E., Ayuga, F., 2011. Validation and experimental calibration of 3D discrete element models for the simulation of the discharge flow in silos. Chemical Engineering Science 66, 5116–5126.

Goodey, R.J., Brown, C.J., 2004. The influence of the base boundary condition in modelling filling of a metal silo. Computers and Structures 82, 567–579.

Goodey, R.J., Brown, C.J., Rotter, J.M., 2003. Verification of a 3-dimensional model for filling pressures in square thin-walled silos. Engineering Structures 25, 1773–1783.

Goodey, R.J., Brown, C.J., Rotter, J.M., 2006. Predicted patterns of filling pressures in thin-walled square silos. Engineering Structures 28, 109–119.

Greiner, R., Guggenberger, W., 1998. Buckling behaviour of axially loaded steel cylinders on local supports – with and without internal pressure. Thin-Walled Structures 31, 159–167.

Grudzien, K., Romanowski, A., Chaniecki, Z., Niedostatkiewicz, M., Sankowski, D., 2010. Description of the silo flow and bulk solid pulsation detection using ECT. Flow Measurement and Instrumentation 21, 198–206.

Grudzien, K., Niedostatkiewicz, M., Adrien, J., Tejchman, J., Maire, E., 2011. Quantitative estimation of volume changes of granular materials during silo flow using X-ray tomography. Chemical Engineering and Processing: Process Intensification 50, 59–67.

Guaita, M., Couto, A., Ayuga, F., 2003. Numerical simulation of wall pressure during discharge of granular material from cylindrical silos with eccentric hoppers. Biosystems Engineering 85, 101–109.

Gudehus, G., Kolymbas, D., Tejchman, J., 1986. Behaviour of granular materials in cylindrical silos. Powder Technology 48, 81–90.

Härtl, J., Ooi, J.Y., Rotter, J.M., Wojcik, M., Ding, S., Enstad, G.G., 2008. The influence of a cone-in-cone insert on flow pattern and wall pressure in a full-scale silo. Chemical Engineering Research and Design 86, 370–378.

Janssen, H.A., 1895. Versuch über Getreidedruck in Sillozellen. Zeitschrift des Vereins Deutscher Ingenieure 39, 1045–1049.

Juan, A., Moran, J.M., Guerra, M.I., Couto, A., Ayuga, F., Aguado, P.J., 2006. Establishing stress state of cylindrical metal silos using finite element method: comparison with ENV 1993. Thin-Walled Structures 44, 1192–1200.

Khelil, A., 2002. Buckling of steel shells subjected to non-uniform axial and pressure loading. Thin-Walled Structures 40, 955–970.

Khelil, A., Belhouchet, Z., Roth, J.C., 1999. Behaviour of cylindrical steel shell subjected to silo loads. In: Dubina, D., Iványi, M. (Eds.), Stability and Ductility of Steel Structures. Elsevier Science, pp. 565–575.

Khelil, A., Belhouchet, Z., Roth, J.C., 2001. Analysis of elastic behaviour of steel shell subjected to silo loads. Journal of Constructional Steel Research 57, 959–969.

Knebel, K., Schweizerhof, K., 1995. Buckling of cylindrical-shells containing granular solids. Thin-Walled Structures 23, 295–312.

Lawton, P.J., 1980. Coefficients of friction between cereal grain and various silo wall materials. Journal of Agricultural Engineering Research 25, 75–86.

Marchant, J.A., 1980. An incremental stress/strain law for cohesionless granular materials. Journal of Agricultural Engineering Research 25, 421–444.

Martinez, M.A., Alfaro, I., Doblare, M., 2002. Simulation of axisymmetric discharging in metallic silos. Analysis of the induced pressure distribution and comparison with different standards. Engineering Structures 24, 1561–1574.

Matchett, A.J., 2006. Rotated, circular arc models of stress in silos applied to core-flow and vertical rat-holes. Powder Technology 162, 87–99.

Matchett, A.J., O'Neill, J.C., Shaw, A.P., 2008. Stress distributions in 2-dimensional, wedge hoppers with circular arc stress orientation – a co-ordinate-specific Lamé-Maxwell model. Powder Technology 187, 298–306.

Molenda, M., Montross, M.D., Thompson, S.A., Horabik, J., 2009. Asymmetry of model bin wall loads and lateral pressure induced from two- and three-dimensional obstructions attached to the wall. Transactions of the ASABE 52, 225–233.

Moya, M., Ayuga, F., Guaita, M., Aguado, P., 2002. Mechanical properties of granular agricultural materials. Transactions of the ASAE 45, 1569–1577.

Moya, M., Guaita, M., Aguado, P., Ayuga, F., 2006. Mechanical properties of granular agricultural materials, part 2. Transactions of the ASABE 49, 479–489.

Nedderman, R.M., Tüzün, U., 1979. A kinematic model for the flow of granular materials. Powder Technology 22, 243–253.

Niedostatkiewicz, M., Tejchman, J., Chaniecki, Z., Grudzien, K., 2009. Determination of bulk solid concentration changes during granular flow in a model silo with ECT sensors. Chemical Engineering Science 64, 20–30.

Nielsen, J., 2008. From silo phenomena to load models. In: Chen, J.F., Teng, J.G. (Eds.), Structures and Granular Solids: From Scientific Principles to Engineering Applications. CRC Press-Taylor & Francis Group, Boca Raton, USA, pp. 49–57.

Nielsen, J., Askegaard, V., 1977. Scale errors in model tests on granular media with special reference to silo models. Powder Technology 16, 123–130.

Ooi, J.Y., Rotter, J.M., 1991. Elastic predictions of pressures in conical silo hoppers. Engineering Structures 13, 2–12.

Ooi, J.Y., Pham, L., Rotter, J.M., 1990. Systematic and random features of measured pressures on full-scale silo walls. Engineering Structures 12, 74–87.

Pircher, M., Berry, P.A., Ding, X., Bridge, R.Q., 2001. The shape of circumferential weld-induced imperfections in thin-walled steel silos and tanks. Thin-Walled Structures 39, 999–1014.

Ramirez, A., Moya, M., Ayuga, F., 2009. Determination of the mechanical properties of powdered agricultural products and sugar. Particle and Particle Systems Characterization 26, 220–230.

Ramirez, A., Nielsen, J., Ayuga, F., 2010a. On the use of plate-type normal pressure cells in silos. Part 1: calibration and evaluation. Computers and Electronics in Agriculture 71, 71–76.

Ramirez, A., Nielsen, J., Ayuga, F., 2010b. On the use of plate-type normal pressure cells in silos. Part 2: validation for pressure measurements. Computers and Electronics in Agriculture 71, 64–70.

Ramirez, A., Nielsen, J., Ayuga, F., 2010c. Pressure measurements in steel silos with eccentric hoppers. Powder Technology 201, 7–20.

Rotter, J.M., Jumikis, P.T., Fleming, S.P., Porter, S.J., 1989. Experiments on the buckling of thin-walled model silo structures. Journal of Constructional Steel Research 13, 271–299.

Schurich, T., Fürll, C., Enstad, G.G., 2001. Full scale silo tests and numerical simulations of the ''cone in cone'' concept for mass flow. In: Kalman, A.L.A.H. (Ed.), Handbook of Powder Technology. Elsevier Science B.V., pp. 175–180.

Shalouf, F., 2003. Grain silos problem and solution. In: Bontempi, F. (Ed.), System-Based Vision for Strategic and Creative Design. A.A Balkema Publishers, Lisse, pp. 1017–1023.

Sielamowicz, I., Czech, M., 2010. Analysis of the radial flow assumption in a converging model silo. Biosystems Engineering 106, 412–422.

Sielamowicz, I., Blonski, S., Kowalewski, T.A., 2005. Optical technique DPIV in measurements of granular material flows, part 1 of 3-plane hoppers. Chemical Engineering Science 60, 589–598.

Sielamowicz, I., Bloñski, S., Kowalewski, T.A., 2006. Digital particle image velocimetry (DPIV) technique in measurements of granular material flows, part 2 of 3-converging hoppers. Chemical Engineering Science 61, 5307–5317.

Sielamowicz, I., Czech, M., Kowalewski, T.A., 2010. Empirical description of flow parameters in eccentric flow inside a silo model. Powder Technology 198, 381–394.

Song, C.Y., 2004. Effects of patch loads on structural behavior of circular flat-bottomed steel silos. Thin-Walled Structures 42, 1519–1542.

Song, C.Y., Teng, J.G., 2003. Buckling of circular steel silos subject to code-specified eccentric discharge pressures. Engineering Structures 25, 1397–1417.

Teng, J.G., Chan, F., 2000. Elastic buckling strength of T-section transition ringbeams in steel silos and tanks. Journal of Constructional Steel Research 56, 69–99.

Teng, J.G., Lin, X., 2005. Fabrication of small models of large cylinders with extensive welding for buckling experiments. Thin-Walled Structures 43, 1091–1114.

Teng, J.G., Rotter, J.M., 1991a. Collapse behavior and strength of steel silo transition junctions. 1. Collapse mechanics. Journal of Structural Engineering – ASCE 117, 3587–3604.

Teng, J.G., Rotter, J.M., 1991b. Collapse behavior and strength of steel silo transition junctions. 2. Collapse mechanics. Journal of Structural Engineering – ASCE 117, 3605–3622.

Teng, J.G., Rotter, J.M., 1991c. Plastic buckling of rings at steel silo transition junctions. Journal of Constructional Steel Research 19, 1–18.

Teng, J.G., Zhao, Y., Lam, L., 2001. Techniques for buckling experiments on steel silo transition junctions. Thin-Walled Structures 39, 685–707.

Teng, J.G., Lin, X., Rotter, J.M., Ding, X.L., 2005. Analysis of geometric imperfections in full-scale welded steel silos. Engineering Structures 27, 938–950.

Vidal, P., Guaita, M., Ayuga, F., 2005. Analysis of dynamic discharge pressures in cylindrical slender silos with a flat bottom or with a hopper: comparison with Eurocode 1. Biosystems Engineering 91, 335–348.

Vidal, P., Couto, A., Ayuga, F., Guaita, M., 2006. Influence of hopper eccentricity on discharge of cylindrical mass flow silos with rigid walls. Journal of Engineering Mechanics – ASCE 132, 1026–1033.

Vidal, P., Gallego, E., Guaita, M., Ayuga, F., 2008. Finite element analysis under different boundary conditions of the filling of cylindrical steel silos having an eccentric hopper. Journal of Constructional Steel Research 64, 480–492.

Winterstetter, T.A., Schmidt, H., 2002. Stability of circular cylindrical steel shells under combined loading. Thin-Walled Structures 40, 893–910.

Wójcik, M., Tejchman, J., 2009. Modeling of shear localization during confined granular flow in silos within non-local hypoplasticity. Powder Technology 192, 298–310.

Wu, Y.H., Schmidt, L.C., 1992. A boundary element method for prediction of silo pressures. Computers and Structures 45, 315–323.

Wu, J., Binbo, J., Chen, J., Yang, Y., 2009. Multi-scale study of particle flow in silos. Advanced Powder Technology 20, 62–73.

Yang, S.C., Hsiau, S.S., 2001. The simulation and experimental study of granular materials discharged from a silo with the placement of inserts. Powder Technology 120, 244–255.

Zhao, Y., Teng, J.G., 2004a. Buckling experiments on steel silo transition junctions I: experimental results. Journal of Constructional Steel Research 60, 1783–1801.

Zhao, Y., Teng, J.G., 2004b. Buckling experiments on steel silo transition junctions II: finite element modeling. Journal of Constructional Steel Research 60, 1803–1823.

Zhong, Z., Ooi, J.Y., Rotter, J.M., 2001. The sensitivity of silo flow and wall stresses to filling method. Engineering Structures 23, 756–767.

ANEJO 3

Copia del artículo III,

Design and instrumentation of a mid-size test station for measuring static and dynamic pressures in silos under different conditions – Part II: Construction and validation,

publicado en

Computers and Electronics in Agriculture 85 (2012) 174–187

Computers and Electronics in Agriculture 85 (2012) 174–187

Contents lists available at SciVerse ScienceDirect

Computers and Electronics in Agriculture

journal homepage: www.elsevier.com/locate/compag

Design and instrumentation of a mid-size test station for measuring static and dynamic pressures in silos under different conditions – Part II: Construction and validation

A. Ruiz, A. Couto *, P.J. Aguado

Department of Agricultural Engineering and Sciences, ESTI Agricultural, University of Leon, Av. Portugal 41, 24071 León, Spain

ARTICLE INFO

Article history:
Received 18 November 2011
Received in revised form 6 March 2012
Accepted 4 April 2012

Keywords:
Test silo
Test silo validation
Silo pressures
Hopper eccentricity
Flat bottom

ABSTRACT

Using the design described in the first of this pair of articles, a full-size silo pressure test station was constructed. In this present article, the main characteristics of this station are described, together with the results obtained from the first validation tests. In addition, these results are compared with the European standard on silos.

Very few experimental installations in the world have full-scale silos, and very few assays have been conducted on them. Consequently, many uncertainties remain which require further research in order to reliably predict the behaviour of material stored in this kind of structure.

The results obtained demonstrate that the theoretical design of the test station is valid for measuring silo pressures and that the station offers multiple possibilities for future research.

Although the principle aim of this article is to demonstrate that the previous theoretical design is valid, some novel conclusions can also be drawn from the tests performed. For example, observation of pressure patterns under static conditions inside the silo, and of overpressure surge patterns during silo discharge, has led us to conclude that the existence of asymmetrical pressures inside the silo is not a consequence of chaotic behaviour, but rather obeys certain physical laws which have still not been sufficiently studied.
© 2012 Elsevier B.V. All rights reserved.

1. Introduction

The present article represents the continuation of a previous article by the same authors on the design of a test station for determining the actions of materials stored in silos (Couto et al., 2012). Following this design, a full-size test station was constructed. Initially, the test station was not installed with a complete set of equipment, but rather with a basic version of the same which would be sufficient to validate the design before equipping it with the remaining components. In this article, we describe the main characteristics of the station and the results obtained from initial tests. The results are compared with values obtained using the European standard for calculating actions affecting silos (CEN, 2006).

Very few *experimental installations* in the world have *full-scale silos* (Brown et al., 2000; Härtl et al., 2008; Ramirez et al., 2010c; Schurich et al., 2001; Teng and Lin, 2005; Teng et al., 2001; Zhao and Teng, 2004; Zhong et al., 2001) and very few assays *have been conducted on them* (Askegaard and Munch-Andersen, 1985; Chen et al., 2005, 2007; Härtl et al., 2008; Ooi et al., 1990; Rotter et al., 2002; Teng et al., 2005; Wu et al., 2009; Yang and Hsiau, 2001). Such structures and tests demand a considerable investment, and although they have yielded extremely important results, many uncertainties still remain which require further research in order to reliably predict the behaviour of material stored in this kind of structure.

In order to measure pressure and displacement in the tests and stations cited above, it has been common practice to employ pressure cells, free field cells, strain gauges and displacement devices (Askegaard and Munch-Andersen, 1985; Brown et al., 2000; Chen et al., 1996, 2007; Härtl et al., 2008; Ramirez et al., 2010a,b,c; Rotter et al., 2002; Zhong et al., 2001). In contrast, the test station described here uses an innovative method for measuring pressures which is based on load cells. Thus, normal wall pressures are determined by double bending beam load cells whilst vertical pressures are determined by tension/compression load cells, instruments which are frequently used in industrial weighing. A further innovation is the versatility of the design, which can be used to test both flat bottom and hopper silos, to study centralised and eccentric discharge, to simulate silos with a greater height/diameter ratio, and even to study swelling in material when it becomes moist.

The result of this innovative design is that it can be used to obtain most of the parameters which govern the behaviour of stored material (Coetzee and Els, 2009; Moya et al., 2002, 2006; Ramirez

* Corresponding author. Tel./fax: +34 987 29 10 00x5243.
E-mail addresses: aruip@unileon.es (A. Ruiz), acouy@unileon.es (A. Couto), pedro.aguado@unileon.es (P.J. Aguado).

0168-1699/$ - see front matter © 2012 Elsevier B.V. All rights reserved.
http://dx.doi.org/10.1016/j.compag.2012.04.008

et al., 2009) and to conduct real-life tests in order to compare and validate different theoretical models and current standards.

The tests performed have led to some novel conclusions concerning the laws which govern stresses within this kind of structure. However, given the versatility of this test station, together with the different kinds of test which can be conducted and the different materials which can be tested, the sole aim of this present article is to demonstrate that the theoretical design of the test station described in an earlier article (Couto et al., 2012) is valid for performing measurements of silo pressures, and that the station offers multiple possibilities for further research in this field.

2. Material and methods

2.1. General description of the installation

The principle components of the test station consist of a silo for storing the material to be tested and another, experimental silo containing the instrumentation necessary for measuring the actions of the stored material. The stored material is transferred between both silos using two screw conveyors powered by electric motors (Fig. 1).

In order to construct a full-size prototype, a simplified version of the design described previously by the authors was used (Couto et al., 2012). This enabled validation of the performance of the theoretical design in practice whilst at the same time consuming the minimum of economic resources, in case the prototype did not work. In other words, we constructed a test station which comprised a basic version of the envisaged equipment, but which could be completed at a later stage once validity and correct performance had been confirmed. Simplifications (Fig. 6) to the theoretical design will be discussed in detail throughout the article in the corresponding sections.

2.2. Geometry of the experimental silo

The geometry and dimensions of the test silo are shown in Figs. 2 and 3. The silo is cylindrical, with a central hopper and a roof at the top. The silo body (a vertical cylinder), the hopper and the roof are independent and can be dismantled.

The silo walls were constructed from sheets of stainless steel 3 mm thick, whilst the cylinder, hopper and roof reinforcement rings were 50 mm wide and 10 mm thick. Given the dimensions and the type of material used for the walls, the silo can thus be considered a rigid, smooth-walled steel silo.

Fig. 1. General view of the test station.

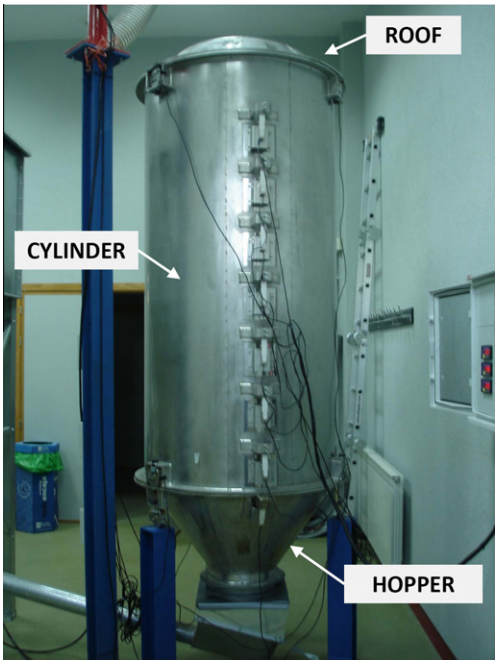

Fig. 2. Test silo.

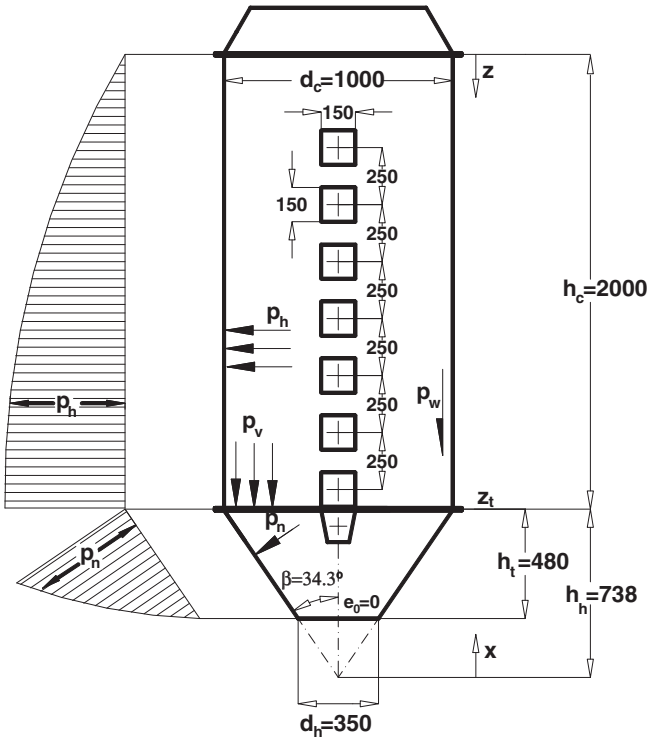

Fig. 3. Symbology and dimensions of the test silo.

According to the Eurocode classification, it corresponds to a slender silo, since the cylinder height/diameter ratio is equal to 2 ($hc/dc = 2$).

The *central part* is composed of a cylinder which is reinforced externally at the top and bottom by two rings with the dimensions described previously. These rings are mounted on the vertical load cells (Figs. 2–5), thus separating the cylinder from the hopper and the roof and enabling determination of the vertical forces produced at either extreme of the cylinder.

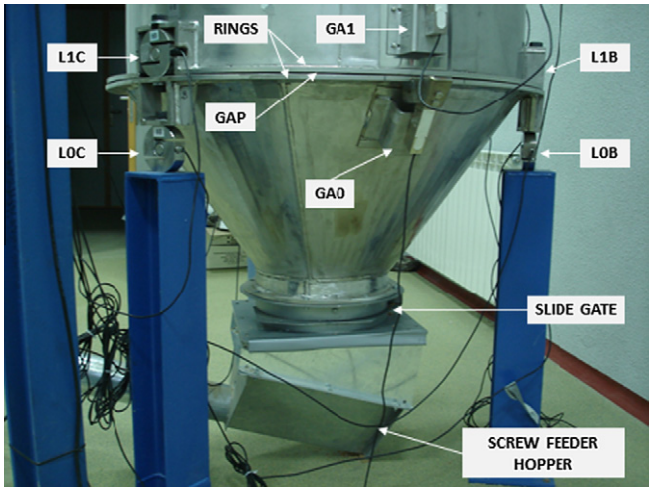

Fig. 4. Hopper details.

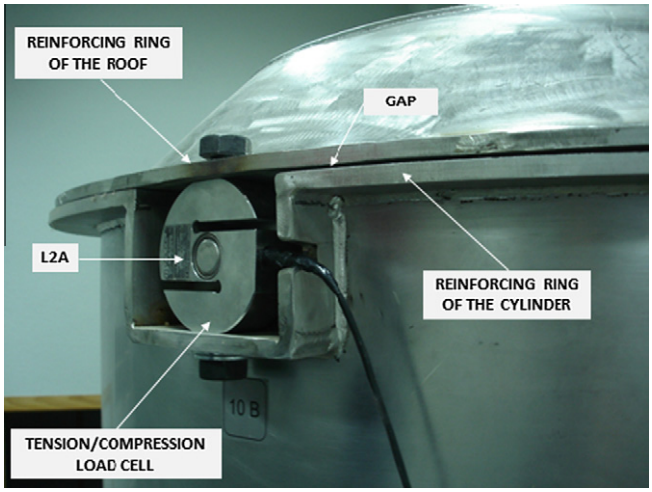

Fig. 5. Join between the roof and the cylinder.

The *lower part* consists of a truncated conical hopper, reinforced externally at the point where it joins the cylinder by a ring of the same size and thickness as the cylinder rings (Figs. 3 and 4).

The theoretical design described in Couto et al. (2012) envisaged either a set of three interchangeable hoppers for the lower part (one for centralised discharge, another for completely eccentric discharge and the last providing intermediate eccentricity), or a flat bottom with three discharge outlets. However, only a centralised discharge hopper was used when testing the prototype, since installing an eccentric discharge hopper would have required instrumentation for reading horizontal pressures in the cylinder and hopper, on at least two opposing generatrices. In all other respects, the design complied with that published previously (Couto et al., 2012), since the hopper used could be dismantled and was interchangeable with the other hoppers envisaged.

The *upper part* is identical to the theoretical design, consisting of a roof which is reinforced externally around the perimeter by a steel ring of the same dimensions as those of the cylinder rings. The ring is mounted on three vertical load cells, providing support for the upper part and separating it from the cylinder. Since the roof is not flat, it will be possible in future tests to install an inflatable membrane which can be used to exert additional pressures on the upper surface of the grain, as described in the previous article (Couto et al., 2012).

2.3. Instrumentation

2.3.1. Measuring horizontal pressures

To measure normal wall pressures, a vertical generatrix was located on the cylinder wall, along which seven readings were taken at the different heights indicated in Fig. 3, whilst hopper pressures were measured immediately below the silo-hopper transition, at the prolongation of the generatrix mentioned above for measuring cylinder pressures (Figs. 2, 3 and 6–8).

Double bending beam load cells were used to measure normal wall pressures. To this end, 150 × 150 mm openings were made in the wall, into which panels of the same curvature were inserted, leaving a small gap around the edges. This clearance was of approximately 1 mm, sufficiently large to prevent friction between the panels and the wall, and sufficiently small to prevent grains from entering the space and distorting measurement readings. The panels were attached to the load cells as indicated in Fig. 7. Hopper wall pressure readings were taken in the same way (Fig. 8).

The double bending beam load cell model employed was the UTICELL 160–15 kg, made by Técnicas de Electrónica y Automatismos, S.A., Spain.

The principle technical specifications of the model employed are as follows:

- Loads: nominal capacity 15 kg, minimum dead load 0 kg, service load 22.5 kg and safe load limit 30 kg.
- Maximum deflection at nominal capacity, between 0.3 and 0.5 mm.
- Accuracy class 3000 divisions O.I.M.L. R60 class C.

For more information on the technical specifications, see the manufacturer's web site (www.uticell.com).

2.3.2. Measuring vertical forces

In order to measure vertical forces caused by friction of the stored material against the wall, the three separate and independent parts of the silo (cylinder, hopper and roof) were connected by mounting the external reinforcing rings of each on the tension/compression load cells. The rings were very close but did not come into contact, and thus all vertical pressures were absorbed by the load cells.

Measurements were taken at points located at three different heights by placing three load cells 120° apart in transversal section at each height (Fig. 6).

The hopper was mounted on the three load cells at level 0 (LO). In this way, it was possible to measure the total weight of the silo and thus, by subtracting the weight of the structure, to determine the weight of the stored material. The cylinder was mounted on the three load cells at level 1 (L1), located above the previous cells, thus permitting measurement of vertical forces acting on the wall. Since the vertical forces acting on the wall are the frictional forces, the vertical forces inside the silo can be found by subtraction (Fig. 9).

The three load cells at level 2 (L2) were located at the upper part of the cylinder, providing the mounting for the silo roof, and these will be used in the future for the tests described in Couto et al. (2012).

The tension/compression load cell model employed was the UTICELL 650–1000 kg, made by Técnicas de Electrónica y Automatismos, S.A., Spain.

The principle technical specifications of the model employed are as follows:

- Loads: nominal capacity 1000 kg, minimum dead load 0 kg, service load 1500 kg and safe load limit 2000 kg.
- Maximum deflection at nominal capacity <0.5 mm.
- Accuracy class 3000 divisions O.I.M.L. R60 class C.

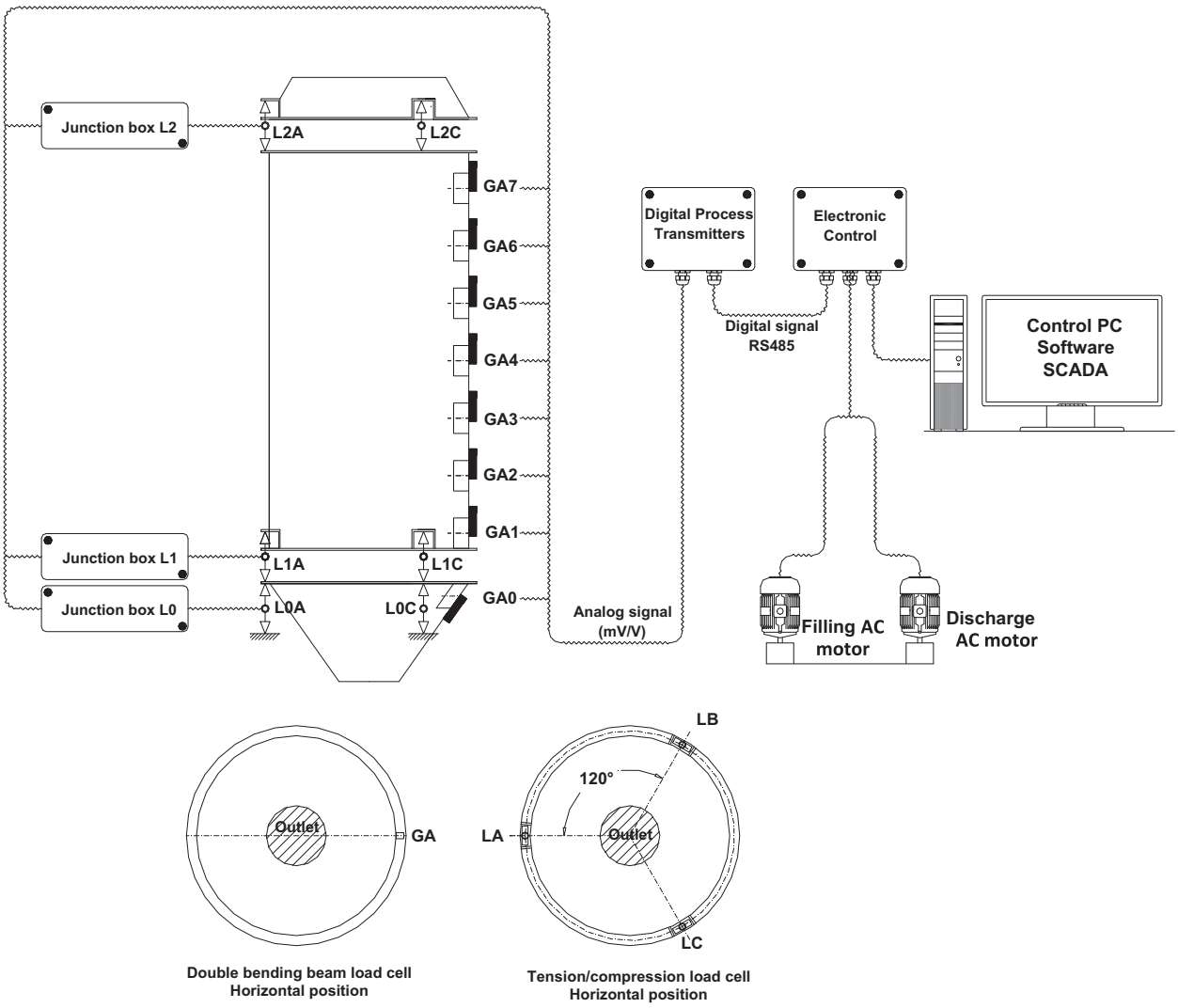

Fig. 6. Diagram of instrumentation for the load measurement system.

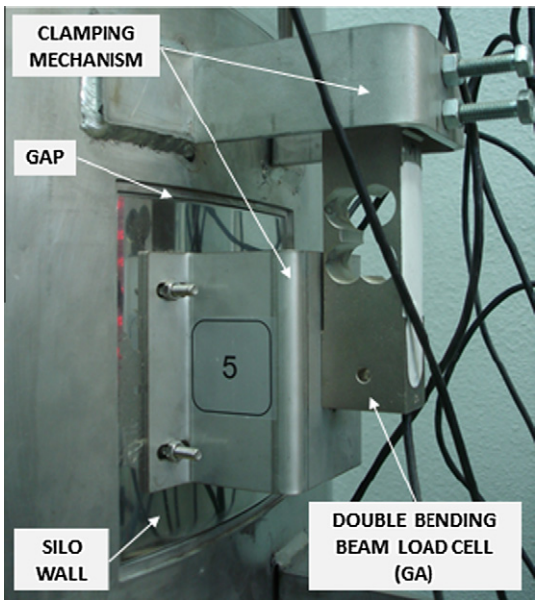

Fig. 7. Measurement of normal cylinder wall pressures.

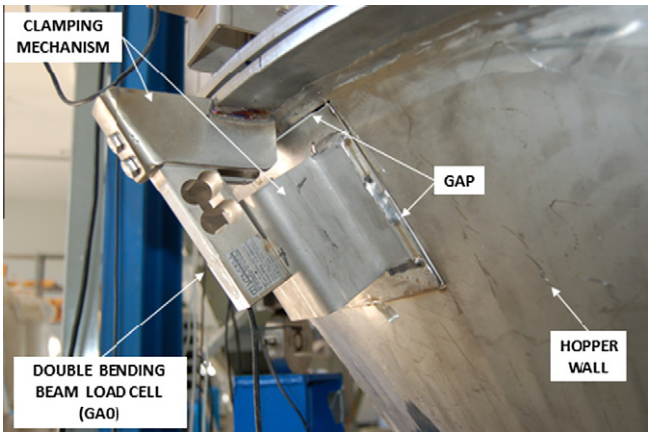

Fig. 8. Measurement of normal hopper wall pressures.

For more information on the technical specifications, see the manufacturer's web site (www.uticell.com).

The clearance between the rings maintaining the three parts of the silo separate was greater than 1 mm all around the perimeter,

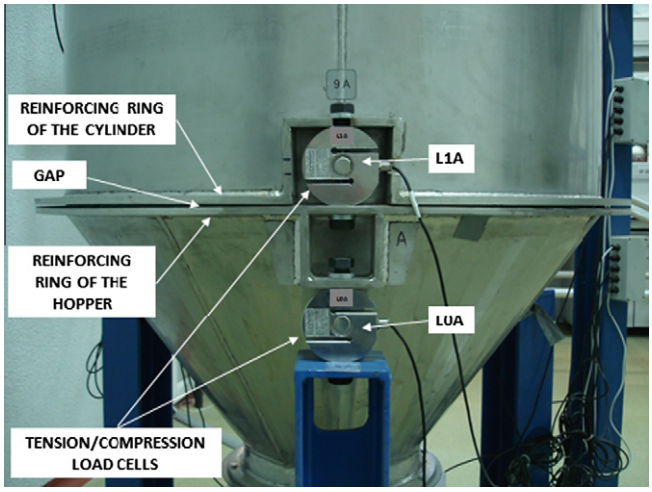

Fig. 9. Measurement of vertical pressures.

thus ensuring that the three parts would never come into contact, given the maximum deflection of the load cells (<0.5 mm).

2.3.3. Control of filling and discharge speed

Filling and discharge were performed using screw conveyors connected to two A/C motors, as described in Couto et al. (2012). However, in this first battery of tests the variable-frequency drives (VFDs) were not used, and thus filling and discharge speed could not be varied automatically. This simplification was introduced since in order to validate the model as a suitable device for reading pressure measurements during filling and discharge, the research team considered it sufficient to study the model under fixed speed conditions, leaving the study of variations in speed for future tests.

In order to prevent vibrations produced by the screw conveyors from distorting readings, contact between the screw feeder hopper (Fig. 4) and the experimental silo discharge outlet was avoided by leaving a clearance of approximately 10 mm between the two. This clearance was sealed with flexible adhesive tape to prevent grain from filtering through the opening.

In the absence of the variable-frequency drives, the tests which could be carried out with the prototype were as follows:

- Free-flowing discharge in the initial moments (from the moment of opening the slide gate located at the test silo hopper outlet until the screw feeder hopper was filled), followed by discharge at a constant speed. Two tests of this kind were performed, which are shown in the results section: as can be seen from the graphics, discharge took approximately 390 s.
- Constant speed discharge from the beginning. To achieve this, discharge was not begun until the experimental silo hopper slide gate was open and the screw feeder hopper was already full.
- Filling at constant speed.

The speed of filling and discharge could be varied manually in the tests described above by varying the extent to which the outlet slide gates on the experimental and the test silos were opened, but this could not be achieved automatically.

2.3.4. Communication protocol

The installation was controlled according to the proposal in Couto et al. (2012), using a standard communication protocol with an RS485 interface. The research team was responsible for assembly of the installation, design of the control system and development of the SCADA (Supervisory Control And Data Acquisition) software (Fig. 10).

In order to process the analog signal sent by each load cell (mV/V) and transform it into a digital readout transmitted by the RS485 network, a weight indicator frequently used in industrial weighing was employed, the DW-ST model made by DATA-CONTROL PC, S.L., Barcelona, Spain. The principle characteristics of this model are as follows:

- Accuracy class: 6000d according to EN45501/OIML R76.
- Load Cell Input with a 24 bits A/D Sigma–Delta converter.
- 1 Serial Port RS232C or RS485.

For more information on the technical specifications, see the manufacturer's web site (www.pesalia.com).

A simplified version of the design described in Couto et al. (2012) was used for test silo instrumentation (Fig. 6). This simplification consisted of connecting the set of three load cells for reading vertical pressures located at each level (L0, L1 and L2) via a junction box, where the analog signals from the three cells at each level were added together and sent to the indicator. In other words, the readings from the three vertical load cells at each level were taken in conjunction rather than separately. The reason for this was to avoid the need to buy a large number of indicators before having validated the prototype. Consequently, we were unable to determine whether vertical wall pressure at the silo-hopper transition presented asymmetries and were thus obliged to consider it uniform around the entire perimeter. Once the model has been validated, independent readings will be taken from the vertical cells in order to study possible asymmetries, since the research team considers that such a study would be of interest, above all in the case of eccentric discharge.

The SCADA software developed permits the time interval between load cell readings to be selected, and it is also possible to establish different intervals between readings for filling, static conditions or discharge, independently. In the results field, the software generates a text file with the load cell readings and the moment they were taken spaced along each line. This file is subsequently processed in a spreadsheet.

In the tests described in this article, the system was programmed to read all load cells twice per second. This may appear to be an excessive number of readings, above all when the loaded silo is static. However, by also establishing this interval for static conditions we were able to determine how the grain settled from the surges produced during this stage, and at the same time to

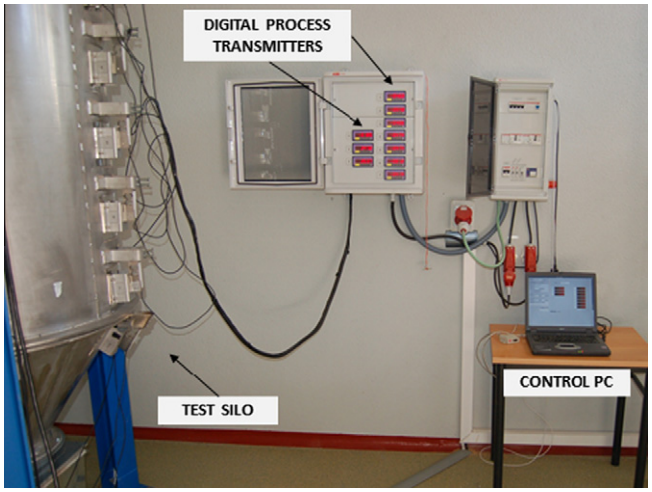

Fig. 10. Control system.

confirm that the prototype was functioning correctly, since the surges in vertical and horizontal pressure occurred in the same time, and were registered independently by the load cells. Readings from each load cell measuring normal wall pressures and located on the cylinder and hopper generatrix were taken independently, and readings from the load cells measuring vertical pressure and placed at three different heights were taken independently for each of the three heights.

2.3.5. Calibration

Calibration of the load cells was performed using two known weights, one in the first quarter of the cell service load and the other in the third quarter for confirmation.

In the case of the double bending beam load cells used to measure horizontal pressures, each cell was calibrated individually. To this end, each cell was attached to a platform and a known weight was applied in the first quarter of the service load in order to obtain the calibration constant. Once calibrated, a known weight was applied in the third quarter for confirmation. Although each cell carries a factory stamp bearing its calibration constant, we determined this parameter experimentally and found that the constant provided by the manufacturer coincided in all cases with the constant obtained experimentally.

In order to calibrate the tension/compression load cells used to obtain vertical pressures, we followed a similar procedure but with the difference that the three cells from each level were calibrated together with the known weights, rather than separately.

In order to confirm the absence of friction between the panels connected to the double bending beam load cells and the silo wall, we ran a sheet of paper around the entire perimeter in the space between the two pieces.

In order to verify the absence of friction between the rings, we ran a 1 mm thick metal sheet between the pieces. Since the sheet was thicker than maximum deflection at service load (<0.5 mm), this confirmed that these pieces would not come into contact during filling. This test should also be carried out when the full silo is in a static state and during filling and discharging, since if the load cell deformation coefficient provided by the manufacturer is not correct, the rings may come into contact due to excessive deformation and distort the readings.

2.4. Nomenclature

The nomenclature employed here follows the Eurocode and therefore the definition of parameters such as A, K, F, n_{zSk}, U, μ_m, γ and ϕ is omitted.

However, this article also includes specific aspects which are not considered in the code, and these different parameters are defined as follows:

- $F_{GA1,t}$: value of the force recorded by load cell GA1 at time t, kN.
- $F_{L1X,t}$: vertical force exerted on the load cells located at level L1 at each time t, kN.
- $p_{hct,t}$: mean value of normal cylinder wall pressure at time t at the silo-hopper union, kN/m^2.
- $p_{hGA1,t}$: normal wall pressure at time t on the load cell GA1, kN/m^2.
- $p_{hm,t}$: mean value of normal cylinder wall pressure at time t, kN/m^2.
- $p_{nht,t}$: value of mean normal hopper wall pressure at time t at the silo-hopper transition, kN/m^2.
- $p_{vt,t}$: vertical stress in the stored material at the silo-hopper transition at time t, kN/m^2.
- $p_{w,t}$: mean value of wall frictional traction at time t, kN/m^2.
- $S_{c,t}$: cylinder surface in contact with stored material at time t, m^2.
- SG: cylinder wall surface acting on each load cell, m^2.
- $SG0$: hopper wall surface acting on each load cell, m^2.
- W_{hsm}: weight of stored material between the outlet and the silo-hopper transition, zero in the case of flat bottom, kN.
- W_T: total weight of stored material, kN.
- V_c: internal cylinder volume, m^3.
- V_h: internal hopper volume, m^3.

2.5. Calculation

2.5.1. Normal wall pressures

Values for normal wall pressures in the cylinder and hopper at each point along the vertical generatrix are obtained by dividing the force registered at each of the load cells by the surface area of the wall on which it is acting; this latter is known since it corresponds to the surface area of the sheet.

For example, to obtain the cylinder wall pressure at the point where double bending beam load cell 1 is located (cell GA1), at time t, the following expression is used:

$$p_{hGA1,t} = \frac{F_{GA1,t}}{S_{GA1}} \tag{1}$$

And in the case of normal hopper wall pressure:

$$p_{nht,t} = \frac{F_{GA0,t}}{S_{GA0}} \tag{2}$$

2.5.2. Vertical force in the cylinder by unit of length

The mean vertical force in the lower part of the cylinder (silo-hopper transition) by unit of length at each time t, is obtained from readings provided by the tension/compression load cells located at level L1, using the following expression:

$$n_{zSk,t} = \frac{F_{L1A,t} + F_{L1B,t} + F_{L1C,t}}{U} \tag{3}$$

2.5.3. Vertical stress in the stored solid at the transition

Once the hopper is full, the mean vertical pressure of stored material at the silo-hopper transition for each time t, is obtained from readings provided by the tension/compression load cells located at levels L0 and L1, using the following expression:

$$p_{vt,t} = \frac{(F_{L0A,t} + F_{L0B,t} + F_{L0C,t}) - (F_{L1A,t} + F_{L1B,t} + F_{L1C,t}) - W_{hsm}}{A} \tag{4}$$

When using a flat bottom silo, as described in Couto et al. (2012), the pressure exerted by the grain on the base of the silo can be determined using the above equation, where the weight of the material stored in the hopper takes the value of zero.

The weight of the material stored in the hopper can be obtained in two ways: either from the volume and specific weight of the material, or directly from the readings provided by the vertical load cells located at level L0. The second option is possible because the time when hopper filling is completed is known, since it is at this moment that readings from the vertical load cells at level L1 start to show an increase in pressure, as do those from the cell GA1, located in the cylinder and used for reading normal cylinder wall pressure.

2.5.4. Wall frictional traction

The mean value of the frictional pressure exerted on the cylinder wall by stored material can be obtained for each time, even during filling and discharge, since the evolution over time of the cylinder surface in contact with the stored material is known, deduced from the known, constant speed of filling and discharge.

Mean frictional pressure is obtained using the following expression:

$$p_{w,t} = \frac{(F_{L1A,t} + F_{L1B,t} + F_{L1C,t})}{S_{c,t}} \quad (5)$$

2.5.5. Wall friction coefficient

The mean value for the grain-wall friction coefficient is obtained from the following expression:

$$\mu_m = \frac{p_{w,t}}{P_{hm,t}} \quad (6)$$

2.5.6. Lateral pressure ratio K and hopper pressure ratio F

The relationship between horizontal and vertical cylinder wall pressures on the cylinder wall, K, and on the hopper wall, F, at the silo-hopper transition at each time t, can be obtained from the following expressions:

$$K = \frac{p_{hGA1,t}}{p_{vt,t}} \quad (7)$$

$$F = \frac{p_{nht,t}}{p_{vt,t}} \quad (8)$$

2.5.7. Specific weight of stored material

Given that the silo volume is known and the slope angle of the stored material can be measured, the specific weight of the stored material when the silo is full and the stored material is static is obtained from vertical load cell readings from level L0 using the following expression:

$$\delta = \frac{(F_{L0A} + F_{L0B} + F_{L0C})}{V_c + V_h} = \frac{W_T}{V_c + V_h} \quad (9)$$

2.6. Description of the tests

In order to validate the prototype, tests were conducted using common wheat (*Triticum aestivum*), Galera R2 variety, with a minimum purity of 98%. The properties of this material were previously determined experimentally in the School of Agricultural Engineering (ESTIA) laboratories in accordance with the method proposed in Eurocode 1, part 4 (CEN, 2006). The values obtained were: specific weight, 8.38 kN/m^3; angle of repose, 34.22°; steel wall friction coefficient, 0.20; and humidity, 10.3%. The values obtained in these tests, both as regards the specific weight and grain-wall friction, were very close to those obtained in the experimental silo.

Using this granular material, 12 tests were conducted which consisted of collecting data during three different phases: during silo filling, under static conditions and during discharge. Silo filling was performed centrally at a constant speed. Once this phase was completed, the material was left inside the silo under static conditions, and lastly, the material was discharged. The silo outlet slide gate was fully opened for discharge, thus producing free-flowing discharge during the initial moments until the screw feeder hopper was filled (Fig. 4); subsequently, discharge occurred at a constant speed.

The behaviour and values obtained for the different parameters analysed were similar in all 12 tests: consequently, in order to avoid presenting an elevated number of figures or overloaded graphics, only the results obtained for two of the tests conducted will be given in the following section. The difference between the two tests shown is the length of time the material remained static inside the silo; in the first case, this was 21.8 h and in the second, 1.6 h.

In the last section, the results obtained experimentally are compared with Eurocode 1, part 4 (CEN, 2006). In order to calculate pressures in accordance with Eurocode 1, part 4, we used the unit weight of the stored material obtained in the tests, γ_m = 8.4 kN/m^3, a wall friction coefficient in the cylinder and hopper of μ = 0.24, an angle of internal friction of ϕ_i = 30°, a lateral pressure ratio K = 0.54, and the values indicated for wheat in Eurocode 1, part 4, Annex E, Table E.1: Particulate solids properties (CEN, 2006).

3. Results and discussion

In this section we present the results of two tests conducted following the procedures described in the preceding section. As mentioned above (Table 1), the only difference between the two tests was the length of time the granular material remained static inside the silo.

Figs. 11 and 12 show the normal silo wall pressures and the vertical pressures of the stored material at the silo-hopper transition in both tests during the three phases. As expected, normal wall pressures reached their highest values during discharge, at the hopper wall at the level of the silo-hopper transition, in accordance with European standards (CEN, 2006) and in agreement with international tests on real silos (Askegaard and Munch-Andersen, 1985; Härtl et al., 2008; Ramirez et al., 2010c; Zhong et al., 2001).

The same figures also show that in the interval between completion of filling and start of discharge, in other words, during the static phase, pressures inside the silo did not remain constant. This is because the material undergoes a process of settling inside the silo, a process which occurs in surges separated by increasingly longer intervals.

Table 2 gives the values obtained in the test for normal wall pressure and vertical pressure of the stored material at the silo-hopper transition at the end of filling and just before starting discharge, in other words, when static. As can be seen, vertical pressure of the stored material at the silo-hopper transition increased over time, and the same was true for normal hopper wall pressure. In contrast, the opposite was the case for normal cylinder wall pressure, which decreased over time. In other words, the cylinder walls released some of their load, increasing the weight borne by the hopper.

Observation of this phenomenon represents a novel discovery, and no reference to it has been found in the standards or in the numerous international publications which have been consulted. The authors conclude that this phenomenon should be studied in detail in order to determine the laws governing the behaviour observed.

Returning to the main focus of this article, that of experimentally testing and validating the theoretical design of the test station, observation of the surges in pressure during grain settling under static conditions reveals that all the load cells registered surges in both wall and vertical pressures at the same time, even though readings were taken independently. This represents clear evidence that pressure readings inside the silo were taken correctly, even given the instrumentation with which the silo was equipped, where readings of the analog signal sent by each cell were received by an independent reader, as was also the case for the three cells at each height, for vertical pressure readings. Furthermore, level L0 cell readings under static conditions were constant; in other words, the values given for weight did not reflect

Table 1
Length of time for each of the test phases.

	t (s)				t (h)
	Filling	Static	Discharge	Total	Total
Test I	350.0	78676.2	309.0	79335.2	22.04
Test II	350.5	5887.1	310.0	6547.6	1.82

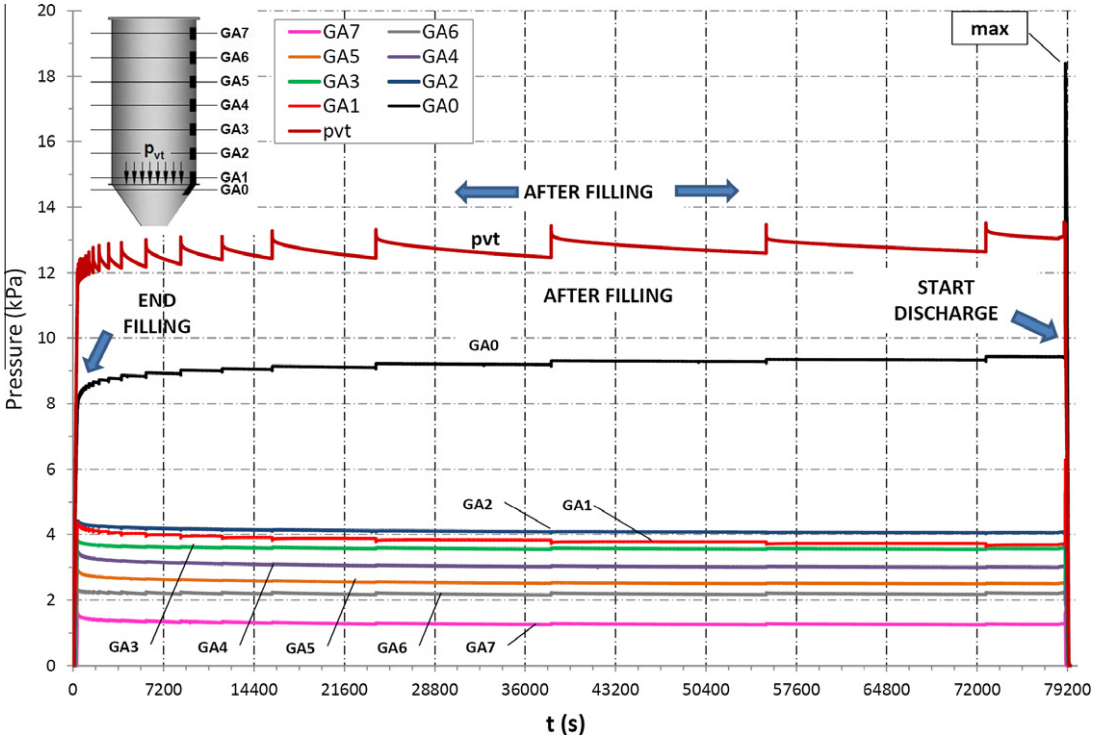

Fig. 11. Normal silo wall pressures ($p_{hGA,t}$) and vertical stress in the stored material at the transition ($p_{vt,t}$), at each time t. Test I.

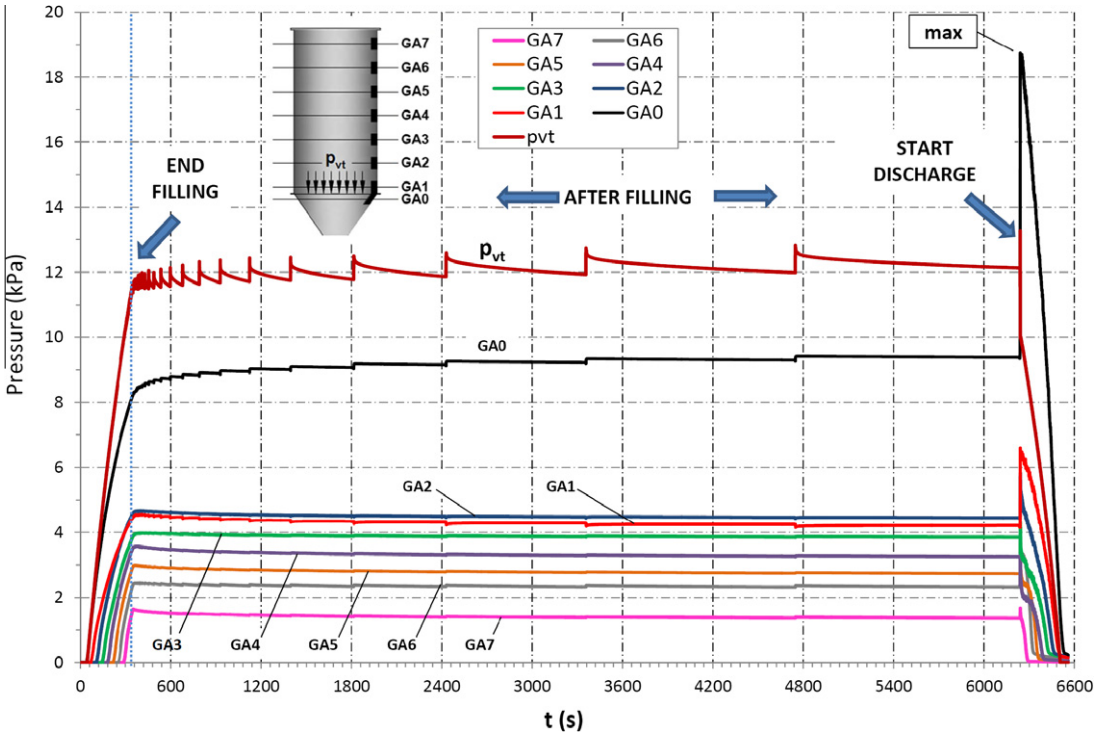

Fig. 12. Normal silo wall pressures ($p_{hGA,t}$) and vertical stress in the stored material at the transition ($p_{vt,t}$), at each time t. Test II.

these surges, clearly indicating that they were due to movement of the material inside the silo.

Another finding which supports our theory (Fig. 13) is that the frictional force against the wall was measured independently of lateral pressures and, as can be seen in the graphics, the reduction in normal cylinder wall pressure which occurred during these surges coincided in time with a reduction in the frictional force exerted on the wall of the cylinder, and thus with a reduction in the resulting vertical force value per unit perimeter at the level of the silo-hopper transition (mean value of resultant vertical stress per unit perimeter at transition). In contrast, at the same time, vertical pressure of the stored material at the silo-hopper

Table 2
Variations under static conditions of normal wall pressures at different heights, and of the vertical pressure of stored material at the silo-hopper transition (kN/m^2).

Test	End filling (kPa)		End static (kPa)		Δ (kPa)		Δ (%)	
	I	II	I	II	I	II	I	II
P_{hGA0}	7.80	8.27	9.39	9.44	1.59	1.17	20.3	14.2
P_{hGA1}	4.28	4.46	3.69	4.16	−0.59	−0.30	−13.8	−6.8
P_{hGA2}	4.37	4.60	4.07	4.44	−0.29	−0.17	−6.7	−3.6
P_{hGA3}	3.84	3.90	3.59	3.86	−0.24	−0.04	−6.3	−1.1
P_{hGA4}	3.48	3.53	3.03	3.26	−0.45	−0.27	−13.0	−7.7
P_{hGA5}	2.94	2.96	2.53	2.74	−0.41	−0.21	−13.8	−7.2
P_{hGA6}	2.32	2.41	2.25	2.36	−0.08	−0.05	−3.3	−2.0
P_{hGA7}	1.60	1.65	1.30	1.38	−0.30	−0.26	−18.7	−16.1
$p_{vt,t}$	11.74	11.53	13.49	12.13	1.75	0.60	14.9	5.2

transition inevitably increased, since the cylinder wall was releasing pressure.

By reducing the time interval of the graphic, Figs. 14 and 15 provide more detail of the evolution of pressure during filling and discharge in Test II. The results from Test I will not be discussed further here since they are similar to those obtained in Test II and in all the other 12 tests conducted (see Table 3). The aim of omitting these results is to avoid repetition or the inclusion of a large number of figures in the present article.

Table 3 shows the maximum variation in percentage with respect to the mean obtained from comparable four trials, since the speed of filling and discharge is the same, as is the dwell time of the material stored in static state inside the silo.

Figs. 14 and 15 also show the coherence between the results obtained during filling and discharge. Thus, Fig. 14 shows how, as hopper filling approached completion, readings began at GA0, immediately followed by the three vertical LI cells, from which vertical pressure of the stored material at the silo-hopper transition was obtained. From this point onwards, hopper filling was completed and cylinder filling began. The progress of filling is clearly visible since the readings given by the cylinder wall cells began to rise as the grain approached their level.

In the same figure it can be seen that silo filling occurred at a constant speed, since the GA cylinder cells placed at regular intervals around the wall began to detect stresses at regular time intervals. Once filling was completed and the screw conveyor motors disconnected, the phenomenon of grain settling began. As can be observed, the time interval between each surge became longer, a phenomenon which, as we mentioned earlier, continued to occur throughout the static phase of the test.

Coherence between the results obtained during discharge can also be observed in Fig. 15. Thus, as the cylinder was emptied, pressure readings at the GA cells, located at different heights of the cylinder wall, approached zero. Cylinder discharge was completed at p_{vt} and GA1 readings equalled zero at the point when hopper discharge began. Cell GA0, located in the hopper, continued to provide readings until the granular material fell below the level of the cell. Furthermore, for the same reason as in the case of filling, from the results obtained it can be deduced that discharge occurred at a constant speed.

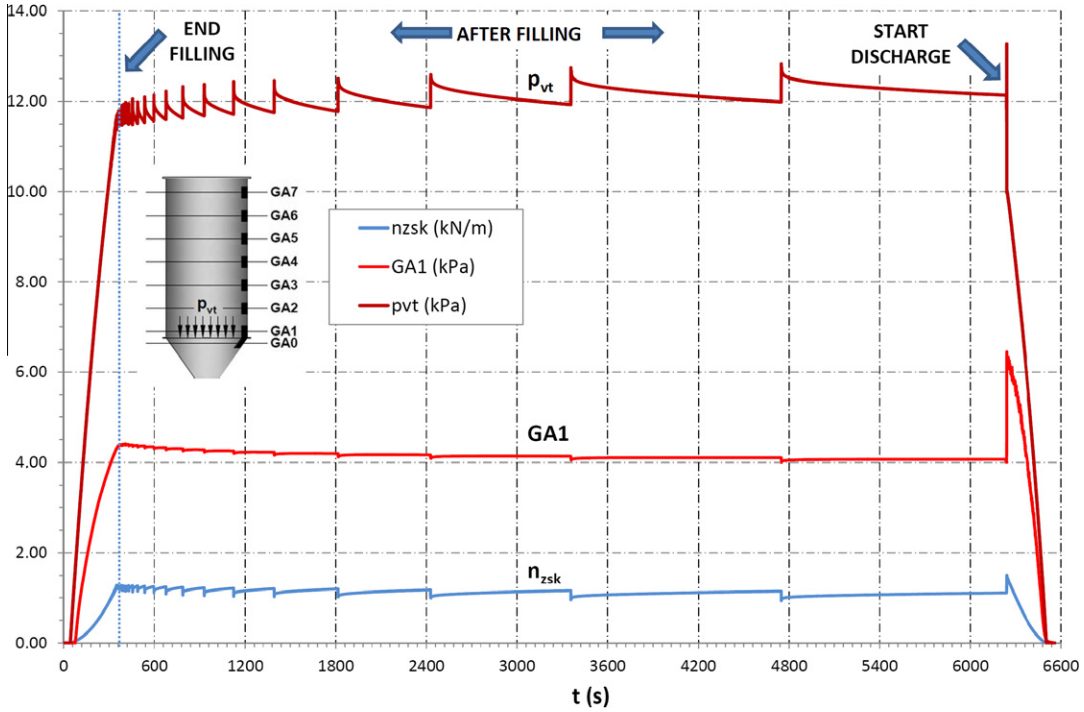

Fig. 13. Normal silo wall pressure al level GA1, vertical stresses in the stored material at the transition ($p_{vt,t}$) and mean value of resultant vertical stress per unit perimeter at transition ($n_{zsk,t}$) for each time "t". Test II.

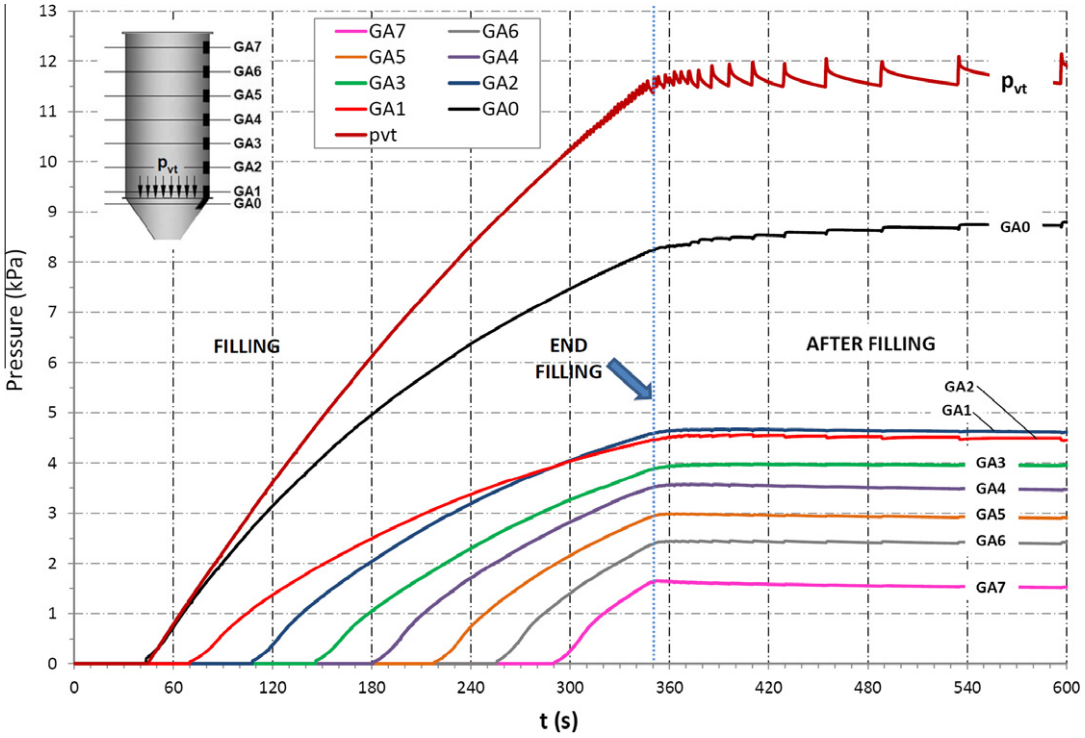

Fig. 14. Normal silo wall pressures ($p_{hGA,t}$) and vertical stresses in the stored material at the transition ($p_{vt,t}$) for each time "t" during filling. Test II.

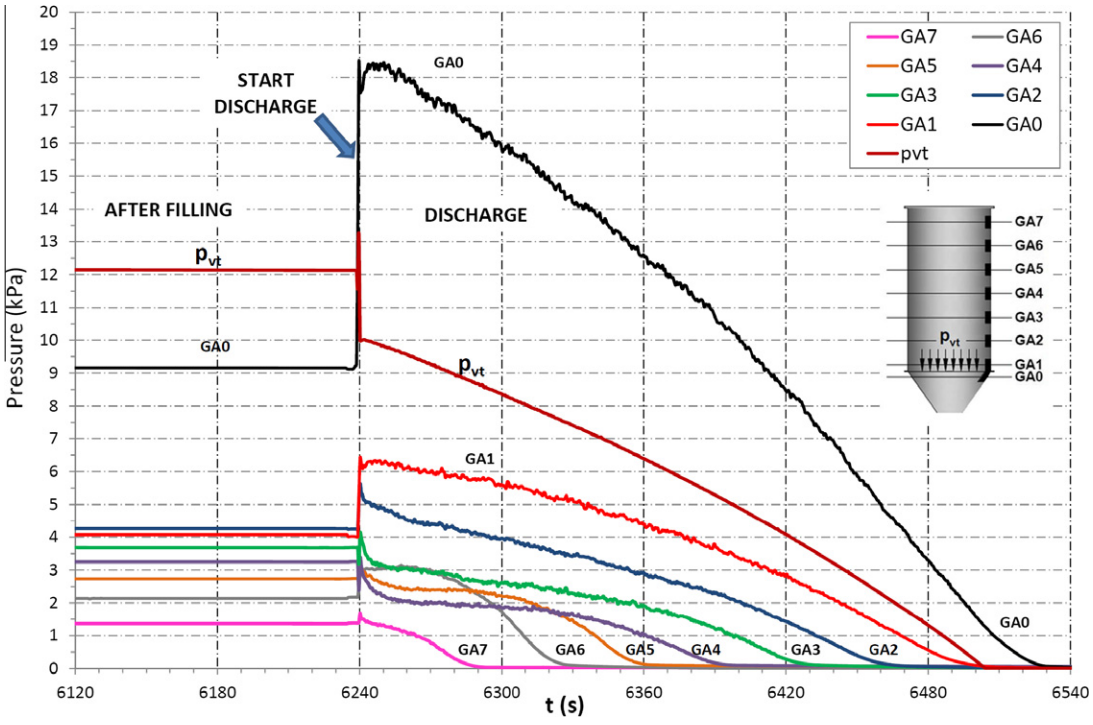

Fig. 15. Normal silo wall pressures ($p_{hGA,t}$) and vertical stresses in the stored material at the transition ($p_{vt,t}$) for each time "t" during discharge. Test II.

It can also be seen in Fig. 15 that the highest pressures inside the silo occurred at the beginning of discharge, a behaviour which is in agreement with Eurocode 1, part 4 (CEN, 2006), and with international publications on silos. However, the values reached were not in agreement, as can be seen in Figs. 17–19, as these were lower in the real-life tests, than those given in the European standard on silos, nevertheless, it should be borne in mind that the standard must ensure safety and consider extreme cases.

The extremely short time interval that we established for reading data during the test (0.5 s) enabled us to observe that the overpressure produced during discharge did not occur instantaneously (Fig. 15), to then decrease gradually, but rather, it reached a maximum value which remained almost constant for some seconds.

Another finding which supports the coherence of the results obtained is shown by the left-hand arrow at the bottom of Fig. 15, which indicates the start of discharge. It can be observed that at

Table 3
Maximum variation in % with respect to the mean of the maximum values obtained from comparable four trials, during filling, in static state and during discharge, of the normal wall pressures at different heights, and of the vertical pressure of material stored at the silo-hopper transition junction.

	Filling (%)	Static (%)	Discharge (%)
P_{hGA0}	0.31	0.52	0.47
P_{hGA1}	1.34	1.64	3.13
P_{hGA2}	0.81	1.16	1.98
P_{hGA3}	2.64	2.36	4.50
P_{hGA4}	1.61	2.13	6.75
P_{hGA5}	1.57	1.86	2.42
P_{hGA6}	0.12	0.63	0.62
P_{hGA7}	2.41	2.20	3.22
$p_{vt,t}$	3.02	2.90	3.25

that time, readings from the cells in the lower part of the silo, cells GA0 L0 and L1 (from which p_{vt} is obtained), began to vary, whilst readings from the cell in the upper part, GA7, began to vary approximately 1 s later (right-hand arrow at the bottom). This suggests that overpressure at the beginning of discharge was propagated from the lower to the upper part of the silo. Table 4 gives the numerical values reached during this increase in pressure, showing that the maximum increase in pressure occurred in the hopper wall at the silo-hopper transition, even doubling in some cases.

Figs. 16 and 17 show the behaviour of the other parameters involved in silo calculation according to the European standard (CEN, 2006). These data were obtained from the load cell readings as described in Section 2.5 of this article. Table 5 provides the numerical values reached at the end of filling and before starting discharge, and the maximum values obtained during the first 10 s of discharge, the time interval during which maximum pressures occur inside the silo. Thus, it can be seen that these parameters presented increased values in the first moments of discharge, and this increase was most marked in the case of the mean value of resultant vertical stress per unit perimeter at transition ($n_{zSk,t}$) and of the lateral pressure ratio at the transition (K) which increased by 35.5% and 92.7%, respectively.

Fig. 19 and Table 6 provide a comparison of the maximum pressures obtained during tests under static conditions and those obtained during discharge using Eurocode 1, part 4. As could be seen in the previous figures, the values obtained in real-life tests were lower than those obtained using the calculation methods proposed in the European standard. Thus, as shown in Table 6, the biggest differences were observed during discharge at normal pressures on the cylinder wall at the silo hopper junction, where variation with respect to the standard reached 75.7%.

Still considering Fig. 19, a curious finding can be observed: the discharge pressures registered in real-life tests did not follow a steady pattern of increasing wall pressures compared to pressure under static conditions, but rather the curve presented waves, and these were produced at the same height in both of the tests shown and in all the remaining tests (not shown). Initially, we thought that this might have been due to poor calibration of the cells located at this level, or to the existence of friction between the panels onto which the cells were mounted and the silo wall. Consequently, we checked the clearance between these elements and recalibrated the cells, but the same phenomenon was repeated. After interchanging the cells from different wall heights, the phenomenon still recurred. One explanation for this finding could be that the overpressure propagation pattern during discharge mentioned earlier, from the lower part to the upper part of the silo, produces increased pressures in certain areas, but constant or even reduced pressures in others.

In the analysis of data obtained from the 12 tests conducted, consisting of concentric filling, static conditions and centralised discharge, no significant differences in pressures were found between the different tests along the generatrix employed. From this we have concluded that in our case, no asymmetries of normal wall

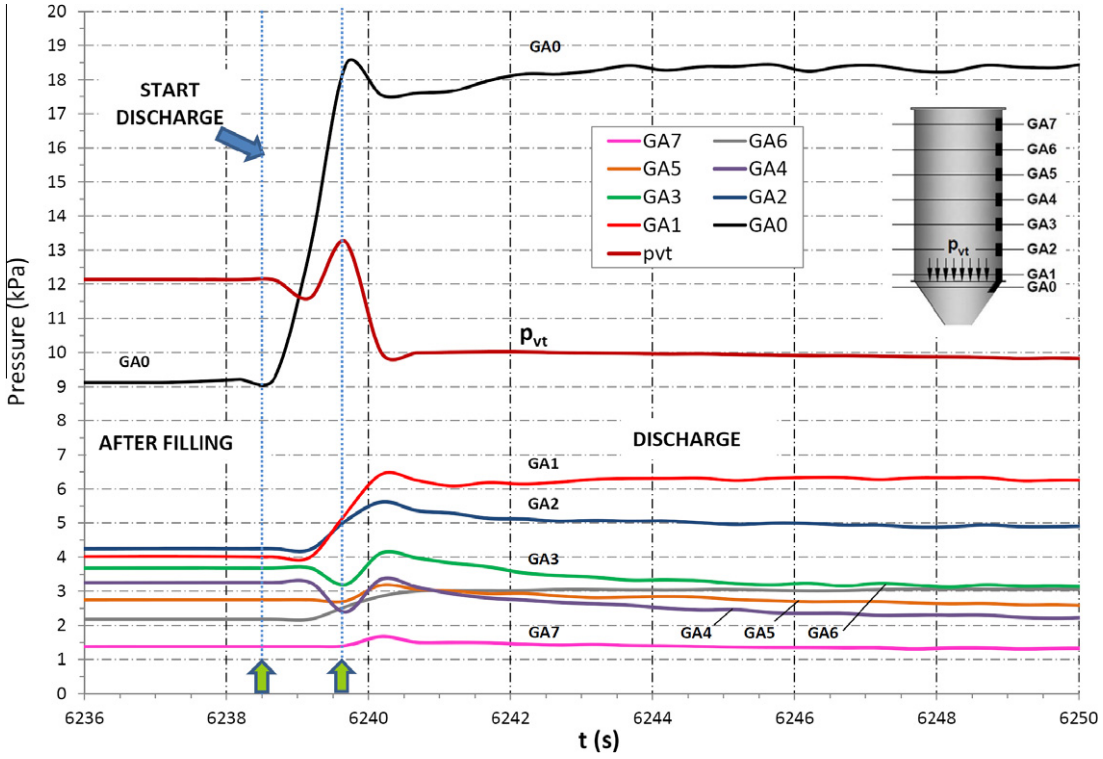

Fig. 16. Normal silo wall pressures ($p_{hGA,t}$) and vertical stresses in the stored material at the transition ($p_{vt,t}$) for each time "t" during the first seconds of discharge. Test II.

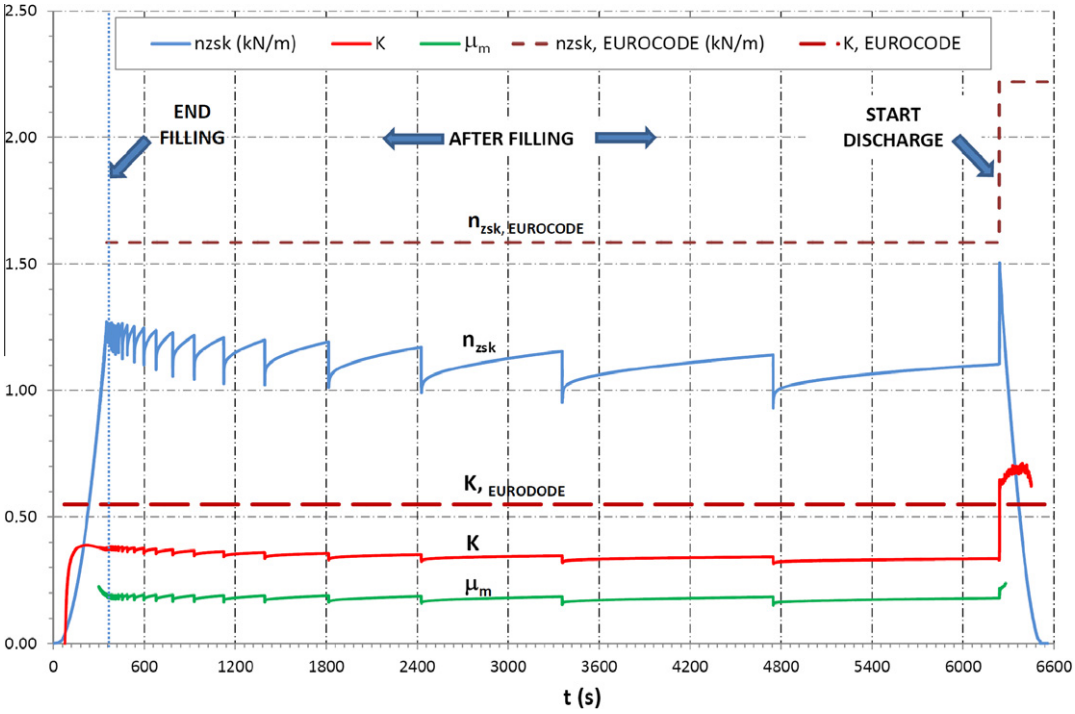

Fig. 17. Mean value of resultant vertical stress per unit perimeter at transition ($n_{zSk,t}$), lateral pressure ratio at the transition (K); mean value of the wall friction coefficient between the stored material and the cylinder wall (μ_m). Comparison between the values obtained Test II and using the Eurocode 1, part 4.

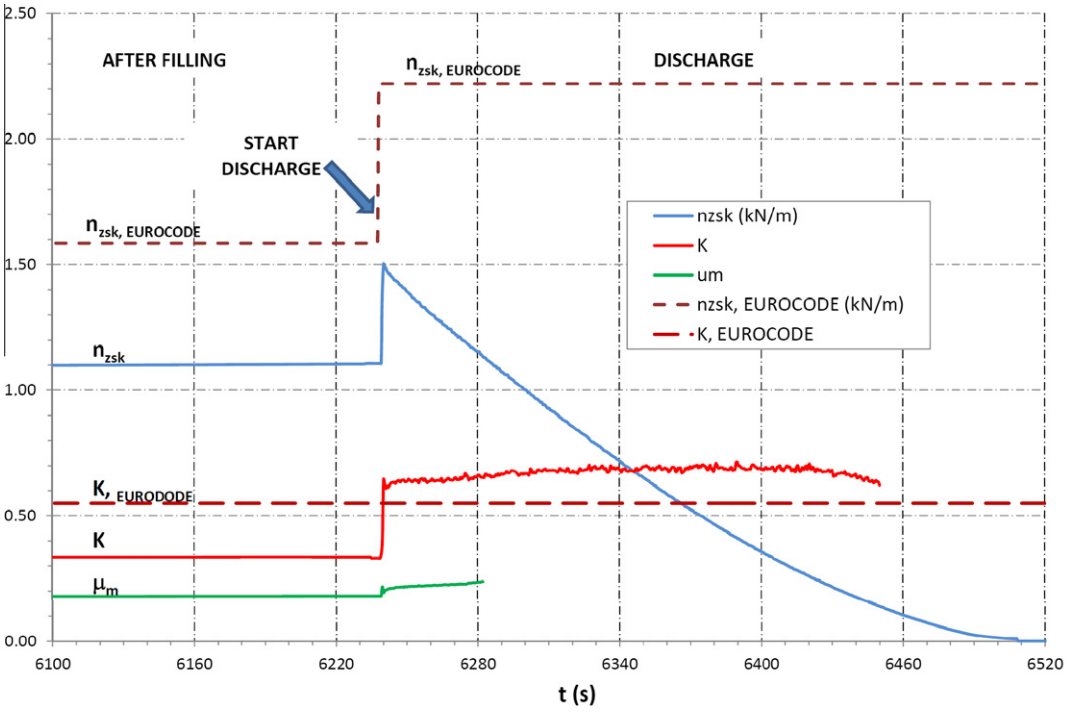

Fig. 18. Discharge. Mean value of resultant vertical stress per unit perimeter at transition ($n_{zSk,t}$), lateral pressure ratio at the transition (K); mean value of the wall friction coefficient between the stored material and the cylinder wall (μ_m). Comparison between the values obtained from Test II and using the Eurocode 1, part 4.

pressures occurred in the circumference of the silo, asymmetries which, in contrast, have been observed by several other authors under conditions of centralised discharge (Härtl et al., 2008; Ramirez et al., 2010c; Zhong et al., 2001). Their absence in our case may be due to the test conditions employed, where silo geometry and environmental conditions were strictly controlled, since the silo was located in a laboratory. Nevertheless, such asymmetries represent a phenomenon which merits further research in order to determine the conditions which lead to wall pressure asymmetries and the magnitude these attain.

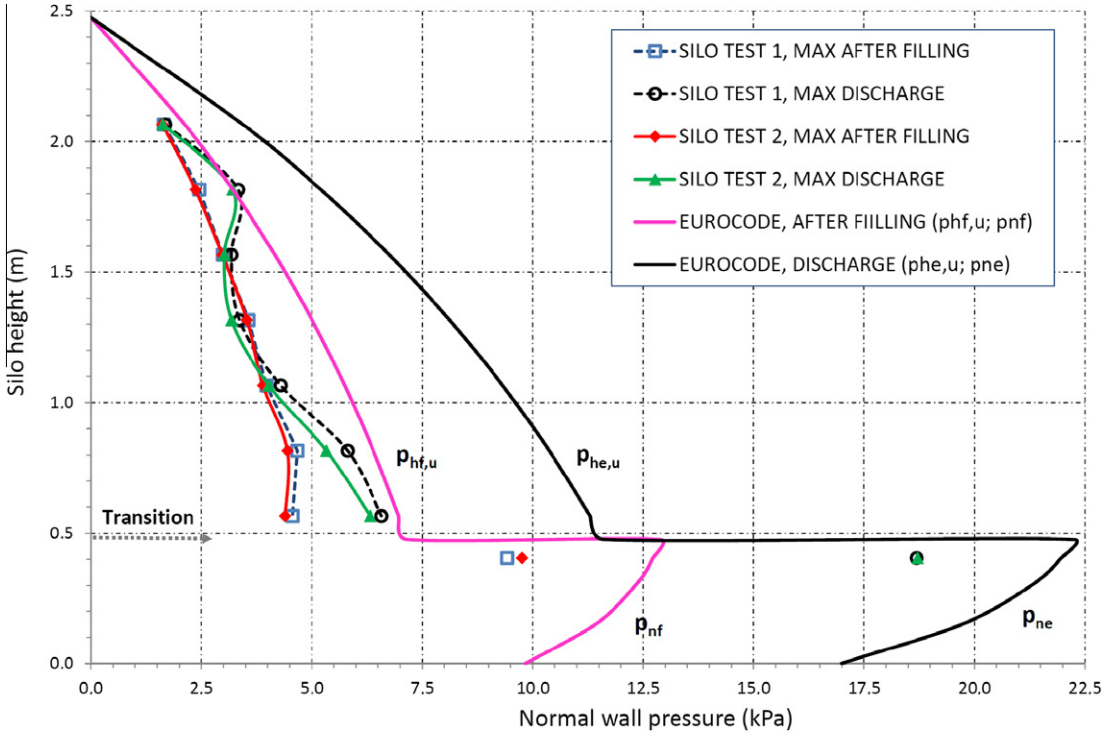

Fig. 19. Comparison between normal wall pressures obtained with the tests and using the Eurocode 1, part 4.

Table 4
Variations in pressure during discharge. Test II.

	End static (kPa)	Max. in discharge (kPa)	Δ (kPa)	Δ (%)
P_{hGA0}	9.21	18.46	9.25	100.4
P_{hGA1}	4.07	6.43	2.36	58.0
P_{hGA2}	4.26	5.62	1.36	31.9
P_{hGA3}	3.68	4.13	0.44	12.1
P_{hGA4}	3.25	3.36	0.11	3.4
P_{hGA5}	2.73	3.18	0.45	16.3
P_{hGA6}	2.14	3.15	1.01	47.0
P_{hGA7}	1.36	1.68	0.32	23.3
$p_{vt,t}$	12.14	13.24	1.10	9.1

4. Conclusions

The test station design proposed by the authors of the present article and described in Couto et al. (2012) has been validated for measuring silo pressure, and it offers multiple possibilities for future research.

Before discharge, in other words, during filling and when the material stored inside the silo is static, the highest normal cylinder wall pressures occurred just at the end of filling. In contrast, the opposite was true for the hopper wall, were normal wall pressures increased over storage time.

The highest pressures inside the silo occurred during the first seconds of discharge, in agreement with real-life tests conducted

Table 5
Mean value of resultant vertical stress per unit perimeter at transition ($n_{zSk,t}$); lateral pressure ratio at the transition (K) and mean value of coefficient of wall friction between particulate solid and the cylinder wall (μ_m). Test II and Eurocode 1, part 4.

	End filling	End static	Max. in the first 10 s of the discharge	Δ (%)
n_{zSk} (kN/m)	1.23	1.10	1.49	35.5
K	0.38	0.34	0.65	92.7
μ_m	0.19	0.18	0.22	22.0
$n_{zSk,EUROCODE}$ (kN/m)	1.59	2.22	2.22	39.6
$K_{EUROCODE}$	0.54	0.54	0.54	0

Table 6
Comparison between normal wall pressures and the mean value of resultant vertical stress per unit perimeter at transition ($n_{zSk,t}$), obtained with the tests and those given by the Eurocode 1, part 4.

	After filling			Discharge		
	Max. Test II	Eurocode	Δ (%)	Max. Test II	Eurocode	Δ (%)
P_{hGA0} (kPa)	9.21	12.72	38.1	18.46	21.96	18.9
P_{hGA1} (kPa)	4.41	6.96	57.8	6.43	11.30	75.7
n_{zSk} (kN/m)	1.27	1.59	24.8	1.50	2.22	47.8

by several other authors (Askegaard and Munch-Andersen, 1985; Härtl et al., 2008; Ramirez et al., 2010c; Wu and Schmidt, 1992; Zhong et al., 2001) and with the European standard on silos (CEN, 2006). The highest normal wall pressures occurred at the hopper wall, at the silo-hopper transition. This was also where the highest normal wall pressures were produced in the cylinder, although these pressures were considerably lower than those reached in the hopper. In our tests, normal hopper wall pressures were of the order of 180% higher than those obtained for the cylinder wall.

Under static conditions, the stored material undergoes a process of settling. During this process, the cylinder walls released pressure, increasing the normal wall pressure of the hopper and the vertical pressure of the stored material at the silo-hopper transition. This phenomenon occurred in surges over increasingly longer time intervals (Figs. 11 and 12 and Table 6). This aspect requires further in depth study before drawing definitive conclusions as it may be due to, or be amplified by, the specific design of the silo.

A study of pressure patterns under static conditions inside the silo due to grain settling (Figs. 11, 12, and 16), and of overpressure patterns along the vertical generatrix in the cylinder during discharge (Fig. 18), suggests that the increase in pressures observed in certain areas was not a consequence of chaotic behaviour but rather obeyed certain physical laws which have not yet been studied sufficiently. This point is considered in the Eurocode (CEN, 2006) in the section on Patch load, where these laws are taken into account both in static and dynamic states. They comprise a number of phenomena that produce asymmetries, among which are those discussed in this paragraph.

Acknowledgements

The authors thank the Spanish Research and Technology Commission (CICYT) (Research Project AGL2005-07430-C02-01/AGR) and the Regional Executive of Castilla y León (Research Project LE020A10-2) for financing this research.

We also thank the reviewers for their advice, which has undoubtedly contributed significantly to improving the quality of this publication.

References

Askegaard, V., Munch-Andersen, J., 1985. Results from tests with normal and shear stress cells in a medium-scale model silo. Powder Technology 44, 151–157.

Brown, C.J., Lahlouh, E.H., Rotter, J.M., 2000. Experiments on a square planform steel silo. Chemical Engineering Science 55, 4399–4413.

CEN, 2006. EN 1991–4:2006. Eurocode 1: Actions on Structures. Part 4: Silos and Tanks. European Committee for Standardization. Brussels.

Chen, J.F., Ooi, J.Y., Rotter, J.M., 1996. A rigorous statistical technique for inferring circular silo wall pressures from wall strain measurements. Engineering Structures 18, 321–331.

Chen, J.F., Rotter, J.M., Ooi, J.Y., Zhong, Z., 2005. Flow pattern measurement in a full scale silo containing iron ore. Chemical Engineering Science 60, 3029–3041.

Chen, J.F., Rotter, J.M., Ooi, J.Y., Zhong, Z., 2007. Correlation between the flow pattern and wall pressures in a full scale experimental silo. Engineering Structures 29, 2308–2320.

Coetzee, C.J., Els, D.N.J., 2009. Calibration of discrete element parameters and the modelling of silo discharge and bucket filling. Computers and Electronics in Agriculture 65, 198–212.

Couto, A., Ruiz, A., Aguado, P.J., 2012. Design and instrumentation of a mid-size test station for measuring static and dynamic pressures in silos under different conditions – Part I: Description. Computers and Electronics in Agriculture. http://dx.doi.org/10.1016/j.compag.2012.04.009.

Härtl, J., Ooi, J.Y., Rotter, J.M., Wojcik, M., Ding, S., Enstad, G.G., 2008. The influence of a cone-in-cone insert on flow pattern and wall pressure in a full-scale silo. Chemical Engineering Research and Design 86, 370–378.

Moya, M., Ayuga, F., Guaita, M., Aguado, P., 2002. Mechanical properties of granular agricultural materials. Transactions of the ASAE 45, 1569–1577.

Moya, M., Guaita, M., Aguado, P., Ayuga, F., 2006. Mechanical properties of granular agricultural materials, part 2. Transactions of the ASAE 49, 479–489.

Ooi, J.Y., Pham, L., Rotter, J.M., 1990. Systematic and random features of measured pressures on full-scale silo walls. Engineering Structures 12, 74–87.

Ramirez, A., Moya, M., Ayuga, F., 2009. Determination of the mechanical properties of powdered agricultural products and sugar. Particle & Particle Systems Characterization 26, 220–230.

Ramirez, A., Nielsen, J., Ayuga, F., 2010a. On the use of plate-type normal pressure cells in silos – Part 1: calibration and evaluation. Computers and Electronics in Agriculture 71, 71–76.

Ramirez, A., Nielsen, J., Ayuga, F., 2010b. On the use of plate-type normal pressure cells in silos – Part 2: validation for pressure measurements. Computers and Electronics in Agriculture 71, 64–70.

Ramirez, A., Nielsen, J., Ayuga, F., 2010c. Pressure measurements in steel silos with eccentric hoppers. Powder Technology 201, 7–20.

Rotter, J.M., Brown, C.J., Lahlouh, E.H., 2002. Patterns of wall pressure on filling a square planform steel silo. Engineering Structures 24, 135–150.

Schurich, T., Fürll, C., Enstad, G.G., 2001. Full scale silo tests and numerical simulations of the "cone in cone" concept for mass flow. In: Kalman, A.L.a.H. (Ed.), Handbook of Powder Technology. Elsevier Science B.V., pp. 75–180.

Teng, J.G., Lin, X., 2005. Fabrication of small models of large cylinders with extensive welding for buckling experiments. Thin-Walled Structures 43, 1091–1114.

Teng, J.G., Lin, X., Rotter, J.M., Ding, X.L., 2005. Analysis of geometric imperfections in full-scale welded steel silos. Engineering Structures 27, 938–950.

Teng, J.G., Zhao, Y., Lam, L., 2001. Techniques for buckling experiments on steel silo transition junctions. Thin-Walled Structures 39, 685–707.

Wu, J., Binbo, J., Chen, J., Yang, Y., 2009. Multi-scale study of particle flow in silos. Advanced Powder Technology 20, 62–73.

Wu, Y.H., Schmidt, L.C., 1992. A boundary element method for prediction of silo pressures. Computers and Structures 45, 315–323.

Yang, S.-C., Hsiau, S.-S., 2001. The simulation and experimental study of granular materials discharged from a silo with the placement of inserts. Powder Technology 120, 244–255.

Zhao, Y., Teng, J.G., 2004. Buckling experiments on steel silo transition junctions – I: experimental results. Journal of Constructional Steel Research 60, 1783–1801.

Zhong, Z., Ooi, J.Y., Rotter, J.M., 2001. The sensitivity of silo flow and wall stresses to filling method. Engineering Structures 23, 756–767.

ANEJO 4

Copia del artículo IV,

Experimental study of the pressures exerted by wheat stored in slender cylindrical silos, varying the flow rate of material during discharge. Comparison with Eurocode 1, part 4,

publicado en

Powder Technology 237 (2013) 450–467

Powder Technology 237 (2013) 450–467

Contents lists available at SciVerse ScienceDirect

Powder Technology

journal homepage: www.elsevier.com/locate/powtec

Experimental study of the pressures exerted by wheat stored in slender cylindrical silos, varying the flow rate of material during discharge. Comparison with Eurocode 1 part 4

A. Couto *, A. Ruiz, P.J. Aguado

Department of Agricultural Engineering and Sciences, ESTI Agricultural, University of Leon, Av. Portugal 41, 24071 León, Spain

ARTICLE INFO

Article history:
Received 16 July 2012
Received in revised form 12 December 2012
Accepted 15 December 2012
Available online 22 December 2012

Keywords:
Test silo
Silo pressures
Wheat storage
Discharge flow variation

ABSTRACT

In this article, we report the results and conclusions of studies conducted using a mid-size test station for assaying pressures in silos. Assays were conducted with wheat, obtaining results for pressures during loading, in static state and during discharge. In addition, different flow rates (kg/s) of the granular material were tested during discharge. The results obtained were compared with Eurocode 1, Part 4.

The test station basically consists of a mid-scale cylindrical silo equipped with load cells. This design enabled us to obtain most of the parameters governing the behaviour of stored material and subsequently to compare and validate the different theoretical calculation models and existing standards.

The results obtained indicate that in static state, the pressures inside the silo are not constant, and that varying the flow rate during discharge does not entail an associated variation in pressures. They also show that the state of overpressure during discharge is mainly due to an increment in the unit weight of the material in certain areas of the silo and, to a much lesser extent, to dilatancy. Furthermore, the pressure values obtained during discharge were higher than those obtained using the calculation method proposed in Eurocode 1, part 4.

© 2012 Elsevier B.V. All rights reserved.

1. Introduction

The question of calculating actions in silos used for the storage of particulate solids in order to determine their correct structural design has been a subject of enquiry since the end of the 19th century [1]. Since then, many advances in knowledge have been made but numerous aspects of silo structural design still remain unresolved [2–4].

Over the course of this research, it has been concluded that tests conducted with small scale silos are not suitable for determining pressures on the walls of life-size silos [5].

However, very few experimental installations in the world have full-scale silos [6–12] and very few assays have been conducted on them [7,11,13–19]. Such structures and tests demand a considerable investment, and although they have yielded extremely important results, many uncertainties still remain which require further research in order to reliably predict the behaviour of material stored in this kind of structure.

It is well known that the highest thrust forces are exerted on the walls during silo discharge [7,8,12,13,20,21].

However, despite the numerous studies which have been conducted, determining pressure during discharge continues to present considerable difficulties because this is a complex phenomenon that depends on how the material flows as well as other parameters such as initial solid volumetric weight and wall roughness [15,22].

Some authors have observed that the presence of shear zones influences the pressures on the silo walls [23]. These shear zones cause fluctuations in the lateral pressures on the walls, and may recur throughout the height of the silo, causing discontinuities in the curve of normal pressures on the wall [24].

The flow pattern can be of two types, mass flow or funnel flow [21]. This pattern influences the magnitude and distribution of the forces acting on the walls, and the parameters which exert most influence on the type of flow are the hopper angle and the friction angle between the material and the hopper wall. In mass flow, all the material moves, and this type of flow is typical for smooth walled hoppers with large outlets as well as being the most commonly employed in industrial processes because it is the most efficient discharge system and avoids dead zones that can alter the properties of the material stored [25].

In this article, we present the results of several assays conducted using an experimental cylindrical silo to determine the thrust forces exerted by the stored material on the walls. The material employed was common wheat (*Triticum aestivum*), using the variety Galera R2, produced and registered in Spain in 1999 by the company NICKERSON GEIE. Assays were performed in static state and during discharge, analysing the influence of variations in the flow rate (kg/s) of material during unloading. We also tested the effect of partial discharges on

* Corresponding author. Tel./fax: +34 987 29 10 00x5243.
E-mail addresses: acouy@unileon.es (A. Couto), aruip@unileon.es (A. Ruiz), pedro.aguado@unileon.es (P.J. Aguado).

0032-5910/$ – see front matter © 2012 Elsevier B.V. All rights reserved.
http://dx.doi.org/10.1016/j.powtec.2012.12.030

pressures. The results were compared with values obtained using the European standard for calculating actions in silos [21].

A mid-scale test station was used to carry out the assays. The installation basically consists of a mid-scale, cylindrical silo equipped with load cells to measure pressure, with which it was possible to obtain most of the parameters governing the behaviour of material stored in silos and to compare the values obtained with the different calculation models and standards which have been proposed. The silo was designed, built and validated by the same research team responsible for the present paper, and has been described and validated in detail in two previous publications [26,27].

2. Materials and methods

2.1. General description of the installation

The principle components of the test station consist of a silo for storing the material to be tested and another, experimental silo containing the instrumentation necessary for measuring the actions of the stored material. The stored material is transferred between both silos using two screw conveyors powered by electric motors (Fig. 1).

2.1.1. Geometry of the experimental silo

The geometry and dimensions of the test silo are shown in Figs. 2 and 3. The silo is cylindrical, with a central hopper. The silo body (a vertical cylinder) and the hopper independent and can be dismantled.

The silo walls were constructed from sheets of stainless steel 3 mm thick, whilst the cylinder, hopper and roof reinforcement rings were 50 mm wide and 10 mm thick. Given the dimensions and the type of material used for the walls, the silo can thus be considered a rigid, smooth-walled steel silo. According to the Eurocode classification, it corresponds to a slender silo, since the cylinder height/diameter ratio is equal to 2 (hc/dc = 2).

2.1.2. Measuring horizontal pressures

To measure normal wall pressures, a vertical generatrix was located on the cylinder wall, along which 7 readings were taken at the different heights indicated in Figs. 2–4, whilst hopper pressures were measured immediately below the silo–hopper transition, at the prolongation of the generatrix mentioned above for measuring cylinder pressures.

Double bending beam load cells were used to measure normal wall pressures. To this end, 150 × 150 mm openings were made in the wall, into which panels of the same curvature were inserted, leaving a small gap around the edges. This clearance was of approximately 1 mm, sufficiently large to prevent friction between the panels and the wall, and sufficiently small to prevent grains from entering the space and distorting measurement readings. The panels were attached to the

Fig. 2. Test silo.

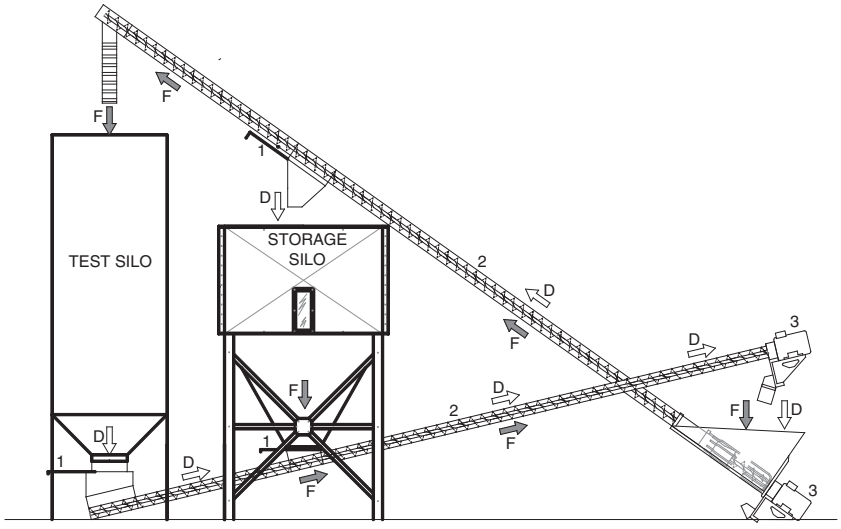

Fig. 1. General test station silo installation. 1: slide gate; 2: screw conveyor; 3: AC motor; F: filling; D: discharge.

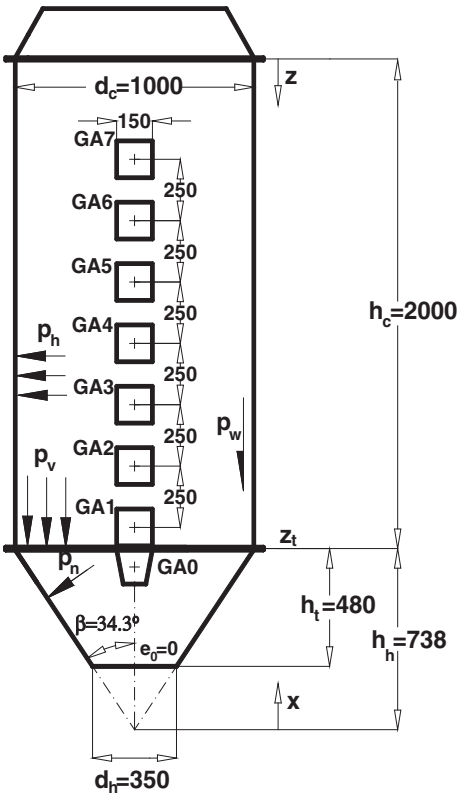

Fig. 3. Symbology, dimensions and points of measurement of normal cylinder wall pressures of the test silo.

load cells as indicated in Fig. 4. Hopper wall pressure readings were taken in the same way.

More detailed information related to this section is given in two previous articles published by the same research team [26,27], which describe the load cell model used, its technical specifications and how the cells were calibrated.

2.1.3. Measuring vertical forces

In order to measure vertical forces caused by friction of the stored material against the wall, the cylinder and hopper were connected by mounting the external reinforcing rings of each on the tension/compression load cells. The rings were very close but did not come into contact, and thus all vertical pressures were absorbed by the load cells (Figs. 4 and 5).

As in the previous section, more detailed information is provided in the two articles cited above [26,27].

In our first paper about the test station used for the experiments [26], which contains a description of the test station design, it was envisaged that horizontal pressure readings at the hopper and cylinder walls would be taken on four 90° generatrices, which would allow the study of discharge asymmetries and/or filling eccentricities. The second article [27] details the construction of a prototype based on the design previously described in order to validate its performance. Not all the elements originally envisaged were installed, although the possibility remained of incorporating them at a later date. This was the prototype used for the experiments reported in this paper. These experiments were performed with central filling and discharge, and the geometry of the silo was completely symmetrical; thus, the main difference between thrusts was produced along its height. It should also be borne in mind that given the symmetry of the silo, if there had been marked differences around the wall circumference, these would have been random and would have been detected due to the disparate values produced between two repetitions of the same assay. It should also be borne in mind that the silo flow is always non-symmetric although the silo geometry and filling process is symmetric.

2.2. Nomenclature

The nomenclature employed is in accordance with that used in the Eurocode [21], but this article also includes specific aspects which are not considered in the code. These different parameters are defined as follows:

A:	plan cross-sectional area of vertical walled segment, m^2.
F:	hopper pressure ratio.
K:	lateral pressure ratio.
U:	perimeter of the plan-cross section of the vertical walled segment, m.
W:	weight of stored material, kN.
W_E:	weight at the end of the phase, kN.
W_I:	weight after filling, kN.
W_{II}:	weight after discharge 1, kN.
W_S:	weight at the start of the phase, kN.
f:	grain flow during discharge (kg/s).
n_{zSk}:	mean value of vertical stress per perimeter unit at the silo-hopper transition, kN/m.
$p_{hGA1,t}$:	normal wall pressure at time t on the load cell GA1, kN/m^2.
$p_{vt,t}$:	vertical stress in the stored material at the silo–hopper transition at time t, kN/m^2.
γ:	value of the bulk unit weight of particulate solid, kN/m^3.
ϕ:	Angle of internal friction of particulate solid, °.

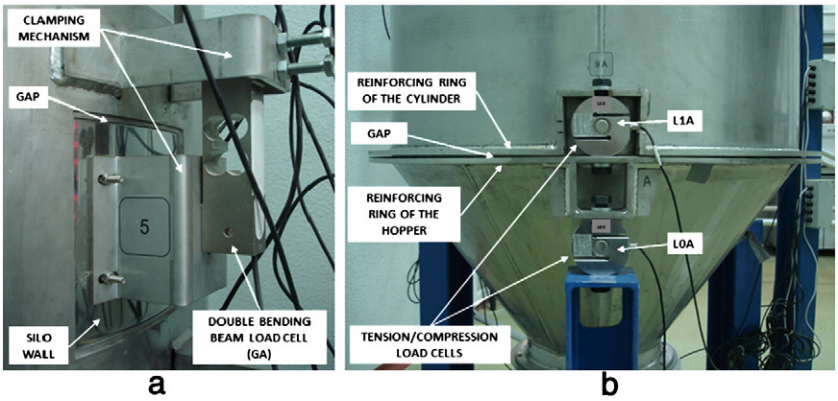

Fig. 4. Measurement of normal cylinder wall pressures (a) and vertical forces (b).

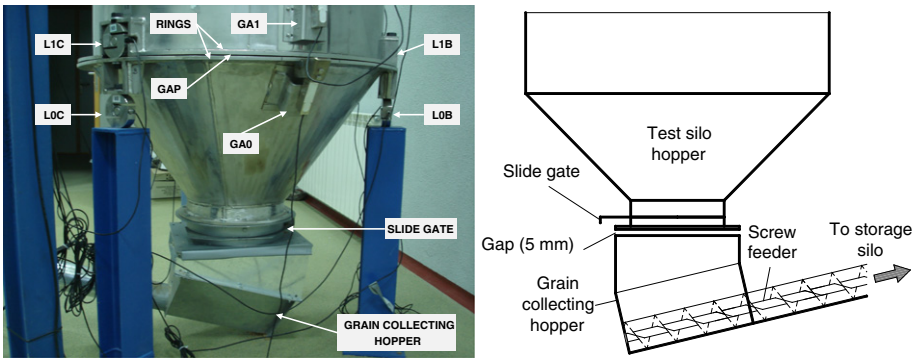

Fig. 5. Hopper and screw feeder hopper details.

μ_m: mean value of coefficient of wall friction between particulate solid and the cylinder wall.

2.3. Description of the tests

Tests were conducted using common wheat (*T. aestivum*), Galera R2 variety, with a minimum purity of 98%. The properties of this material were previously determined experimentally in the School of Agricultural Engineering (E.S.T.I.A.) laboratories in accordance with test methods proposed in Eurocode 1, part 4 Annex C [21]. The values obtained were: specific weight (see Fig. 6), angle of repose, 34.22°; steel wall friction coefficient, 0.20; internal friction angle, 30.17°; modulus of elasticity, 10,674.33 kPa and humidity, 10.3%. The values for specific weight and grain–wall friction obtained in these tests were very close to those obtained with the experimental silo (mean specific weight = 8.392 kN/m^3, μ = see Tables 1 and 2), and it was these values, obtained in laboratory tests, that were used to obtain pressures according to the calculation method proposed in the Eurocode. In the case of specific weight, the value employed in the calculations was 8.397 kN/m^3, a value that corresponds to the maximum particle packing density at a stress level corresponding to the location in the stored solid in the silo where maximum vertical stress after filling occurs, namely, vertical stress in the stored material at the silo–hopper transition.

Using the granular material described above, 21 assays were conducted, consisting of central loading and discharge of the silo, and these are described below.

In all assays, silo filling was accomplished using a screw conveyor ending in a vertical tube which was always centred during filling and was used to effect free discharge into the silo interior, as shown in Figs. 1 and 2. This method is commonly employed in this type of structure when the material stored is grain. A uniform filling speed (kg/s) was used in all cases and values for each trial are given in Tables 1–3.

In all cases, discharge was effected by gravity. A grain collecting device, separated from the silo by a clearance of 5 mm, was located beneath the outlet and transported the grain to the storage silo. This gap was sealed to prevent grain spilling though, but a flexible material was used in order to prevent the vibrations caused by rotation of the screw conveyor device from being transmitted to the test silo.

The 21 assays mentioned above were grouped into three types of tests which differed with regard to how discharge was achieved. Thus, in type I assays, following a period in static state, the material stored in the silo was completely discharged. In type II assays, a small amount of stored material, between 1.7% and 3.2% of the total, was discharged before halting the process. The grain was thus returned to static state before finally emptying the silo completely. Meanwhile, successive discharges were performed in type III assays, alternating each discharge with a period in static state. Then, after discharging approximately

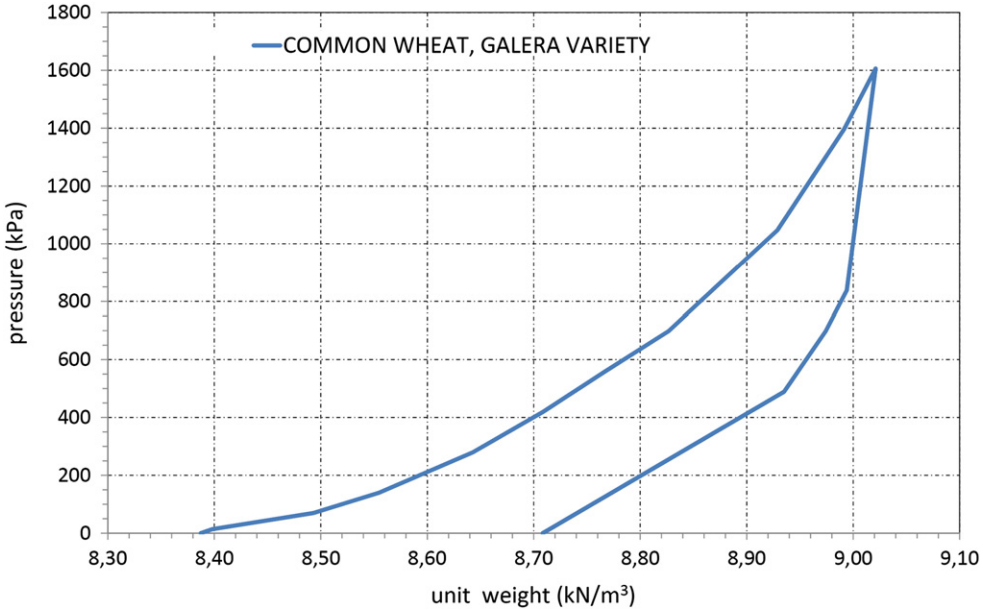

Fig. 6. Pressure–unit weight of the grain.

Table 1
Summary of results obtained in type I assays (tests 1 to 7).

			Normal wall pressures (kPa)								(kN/m)	(kPa)			
TEST 1	t (s)	f (kg/s)	P_{hGA7}	P_{hGA6}	P_{hGA5}	P_{hGA4}	P_{hGA3}	P_{hGA2}	P_{hGA1}	P_{hGA0}	n_{tsh}	$p_{vt,t}$	K	μ_m	Gate (PI)
Filling	360,2	4,17	1,52	2,54	3,05	3,44	3,75	4,22	4,22	8,75	1,25	11,78	0,38	0,21	(max. values)
Static	326,8	0	1,54	2,58	3,1	3,5	3,81	4,28	4,28	9,15	1,28	12,34	0,37	0,2	(max. values)
			1,39	2,49	2,98	3,35	3,67	4,18	4,15	8,76	1,11	11,65	0,34	0,18	(min. values)
Discharge	312,0	4,82	1,43	3,35	3,55	3,5	5,08	5,81	7,6	18,65	2,06	12,09	0,82	0,28	(max. values)
Weight after filling (kN)	14,75														
			Normal wall pressures (kPa)								(kN/m)	(kPa)			
TEST 2	t (s)	f (kg/s)	P_{hGA7}	P_{hGA6}	P_{hGA5}	P_{hGA4}	P_{hGA3}	P_{hGA2}	P_{hGA1}	P_{hGA0}	n_{tsh}	$p_{vt,t}$	K	μ_m	Gate (PI)
Filling	363,7	4,16	1,59	2,53	2,95	3,33	3,96	4,16	4,11	8,70	1,09	12,51	0,34	0,18	(max. values)
Static	348,7	0	1,61	2,55	2,99	3,36	3,99	4,18	4,14	9,05	1,17	13,08	0,34	0,18	(max. values)
			1,46	2,47	2,86	3,21	3,85	4,08	4,00	8,71	0,95	12,22	0,31	0,15	(min. values)
Discharge	311,2	4,86	1,74	3,39	3,72	4,01	5,56	6,05	7,14	18,82	1,95	12,90	0,74	0,22	(max. values)
Weight after filling (kN)	14,84														
			Normal wall pressures (kPa)								(kN/m)	(kPa)			
TEST 3	t (s)	f (kg/s)	P_{hGA7}	P_{hGA6}	P_{hGA5}	P_{hGA4}	P_{hGA3}	P_{hGA2}	P_{hGA1}	P_{hGA0}	n_{tsh}	$p_{vt,t}$	K	μ_m	Gate (PII)
Filling	365,7	4,15	1,61	2,56	3,14	3,48	4,15	4,45	4,47	9,20	1,16	12,59	0,40	0,19	(max. values)
Static	361,2	0	1,59	2,57	3,14	3,49	4,16	4,46	4,49	9,61	1,15	13,01	0,36	0,17	(max. values)
			1,48	2,49	2,78	3,33	4,06	4,38	4,36	9,22	0,98	12,33	0,33	0,15	(min. values)
Discharge	318,5	4,77	1,50	3,46	3,05	3,39	5,59	6,37	7,98	21,09	1,63	12,28	0,84	0,21	(max. values)
Weight after filling (kN)	14,89														
			Normal wall pressures (kPa)								(kN/m)	(kPa)			
TEST 4	t (s)	f (kg/s)	P_{hGA7}	P_{hGA6}	P_{hGA5}	P_{hGA4}	P_{hGA3}	P_{hGA2}	P_{hGA1}	P_{hGA0}	n_{tsh}	$p_{vt,t}$	K	μ_m	Gate (PII)
Filling	363,1	4,17	1,62	2,53	3,00	3,39	4,10	4,42	4,23	8,71	1,11	12,47	0,39	0,18	(max. values)
Static	339,1	0	1,64	2,57	3,04	3,43	4,15	4,46	4,28	9,04	1,18	13,00	0,35	0,18	(max. values)
			1,49	2,49	2,90	3,30	4,04	4,37	4,15	8,72	0,98	12,19	0,32	0,15	(min. values)
Discharge	319,6	4,74	1,51	3,40	2,99	3,33	5,43	6,21	7,76	20,87	1,61	12,78	0,81	0,22	(max. values)
Weight after filling (kN)	14,86														
			Normal wall pressures (kPa)								(kN/m)	(kPa)			
TEST 5	t (s)	f (kg/s)	P_{hGA7}	P_{hGA6}	P_{hGA5}	P_{hGA4}	P_{hGA3}	P_{hGA2}	P_{hGA1}	P_{hGA0}	n_{tsh}	$p_{vt,t}$	K	μ_m	Gate (PIII)
Filling	364,2	4,15	1,61	2,51	2,95	3,35	4,10	4,21	4,24	8,84	1,10	12,50	0,39	0,18	(max. values)
Static	323,0	0	1,62	2,55	2,98	3,39	4,15	4,25	4,28	9,28	1,17	13,06	0,35	0,18	(max. values)
			1,47	2,48	2,84	3,24	4,04	4,16	4,14	8,85	0,96	12,21	0,32	0,15	(min. values)
Discharge	710,3	2,13	1,49	3,49	2,88	3,28	4,89	5,91	7,80	22,26	1,46	12,75	0,78	0,21	(max. values)
Weight after filling (kN)	14,84														
			Normal wall pressures (kPa)								(kN/m)	(kPa)			
TEST 6	t (s)	f (kg/s)	P_{hGA7}	P_{hGA6}	P_{hGA5}	P_{hGA4}	P_{hGA3}	P_{hGA2}	P_{hGA1}	P_{hGA0}	n_{tsh}	$p_{vt,t}$	K	μ_m	Gate (PIII)
Filling	367,7	4,12	1,62	2,62	3,20	3,58	3,97	4,39	4,40	8,94	1,18	12,19	0,40	0,19	(max. values)
Static	342,8	0	1,63	2,66	3,24	3,62	4,02	4,44	4,46	9,24	1,25	12,78	0,37	0,19	(max. values)
			1,48	2,59	3,13	3,50	3,69	4,35	4,35	8,95	1,04	11,93	0,34	0,16	(min. values)
Discharge	715,3	2,12	1,50	3,44	3,18	3,53	5,30	6,45	8,20	21,76	1,56	12,53	0,83	0,22	(max. values)
Weight after filling (kN)	14,87														
			Normal wall pressures (kPa)								(kN/m)	(kPa)			
TEST 7	t (s)	f (kg/s)	P_{hGA7}	P_{hGA6}	P_{hGA5}	P_{hGA4}	P_{hGA3}	P_{hGA2}	P_{hGA1}	P_{hGA0}	n_{tsh}	$p_{vt,t}$	K	μ_m	Gate (PIV)
Filling	363,6	4,17	1,68	2,63	3,04	3,29	4,10	4,13	4,32	8,61	1,01	12,87	0,40	0,17	(max. values)
Static	328,6	0	1,69	2,64	3,05	3,31	4,11	4,17	4,35	8,85	1,07	13,35	0,34	0,17	(max. values)
			1,53	2,55	2,92	3,17	4,00	4,07	4,18	8,61	0,89	12,63	0,31	0,14	(min. values)
Discharge	2526,1	0,60	1,54	3,63	2,95	3,21	4,42	5,93	8,23	24,77	1,27	13,19	0,77	0,19	(max. values)
Weight after filling (kN)	14,86														

15% of the material, the silo was refilled and the process was repeated before a final refill and complete discharge in a single step.

The rationale for performing these three types of assays was to mimic the common use made in practice of these structures, since although silos are sometimes completely emptied in a single step after filling, discharge is also frequently halted after partial emptying of the stored material, or the silo may even be refilled before it has been completely emptied of the material it contains. Simulation of the actual use made of these structures has enabled us to obtain novel findings which we describe in the following paragraphs.

2.3.1. Type I assays

In a first set of assays (type I, tests 1 to 7), the silo was loaded with granular material and then, after a pause of approximately 5 min, the material was discharged varying the grain flow rate (kg/s) between tests. To unload the material, the motors driving the screw conveyors were switched on and the outlet slide gate was opened. The grain collecting hopper (Figs. 5 and 7) remained free of material in all the assays. The grain flow rate was varied by varying the degree to which the outlet slide gate was opened, and 4 different positions were tested: fully open, or position PI (tests 1 and 2), PII (tests 3 and 4), PIII (tests 5 and 6) and PIV (test 7). Fig. 7 shows a diagram of this type of test when the slide gate was opened to position 1 (PI). The duration of each phase (loading–static–discharge), position of the outlet gate and discharge flow rate for each of these positions in the different tests are given in Table 1.

2.3.2. Type II assays

As with the assays described above, in a second set of assays, called type II (tests 8 to 20), the grain flow rate (kg/s) was varied and the same four outlet gate opening positions were used, but unlike the previous tests, discharge was performed in two stages. In the first stage, the grain outlet gate was opened with the discharge device motors switched off, so that unloading was interrupted once the hopper discharge device had become filled to capacity, and the granular material returned to static state. The dwell time in this phase varied between the different tests. In the second stage, discharge was resumed by switching on the motors once the hopper discharge device was full. Fig. 8 shows a diagram of this type of test when the gate was opened to position 1 (PI). Dwell times in each of the phases, position of the outlet gate and discharge flow rates in the different assays are given in Table 2.

2.3.3. Type III assays

Finally, we performed a test called type III (test 21), consisting of loading the silo, effecting a partial discharge of approximately 2.10 kN and then reloading to the initial level, repeating the process 2 times. The two partial discharges were performed in seven stages of 0.3 kN each. To achieve this, the grain outlet gate was opened to position 3 (PIII) with the unloading device switched on, thus preventing the collection hopper from becoming filled to capacity, and approximately 0.3 kN of grain was discharged before closing the gate, leaving the material in static state for 5 min and repeating the process. These stages were repeated 7 times, in other words, until a partial discharge of 2.1 kN had been achieved. Then, the silo was refilled to the initial level and the process was repeated. Finally, the silo was once again reloaded and a complete discharge was effected in a single stage. The data obtained from this assay are shown in Table 3.

3. Results and discussion

In this section, we report and discuss the results of the three types of assays performed following the procedures outlined in the previous section. The shape of the curves obtained for each set of type I and type II assays was similar, and only the dwell time in each of the static–discharge stages and the maximum and minimum values attained varied. Thus, in order to avoid an excessive number of figures, only the curves corresponding to one assay of each type are shown. All other data is given in Tables 1 and 4, which show the duration of the various phases of each assay, the flow rate of the material discharged, the weight of the material stored in each phase and a summary of the results obtained in each stage.

In all the assays it was observed that during discharge, all of the stored material was moving and thus the results correspond to a mass flow pattern.

Fig. 9 shows the shape of the curves obtained in type I assays (tests 1 to 7), and gives normal silo wall pressures and vertical stress in the stored material at the silo–hopper transition. Table 1 gives a summary of the conditions and results obtained in the type I assays.

As expected, the normal wall pressure underwent considerable variation at the beginning of discharge, reaching highest values at the hopper wall, at the level of the silo–hopper transition, which is consistent with European standards [21] and with international tests on real silos [7,8,12,13]. As can be seen in Table 4, there was an increase of up to 179.8% at the hopper wall and of up to 89.3% in the lower section of the cylinder. It can also be seen that in the cells located in the lower section of the cylinder (cells GA0 to GA3), the increase in pressure was always positive, whereas in the upper part of the cylinder there were some areas for which, at certain heights, almost constant or even decreasing pressures with respect to the static state were recorded, rather than increases. This suggests that in the experiments reported here, the phenomenon described above was due to a variation in the initial particle packing density during discharge, increasing or decreasing in determined areas with respect to the previous static state. Note that slight variations in the specific weight (unit weight) are associated with large variations in pressure (see Fig. 6).

This phenomenon was confirmed by the results obtained from the type II and III assays, which are described below. In a silo of infinite height, we believe that this phenomenon of increased pressure in some areas rather than others would be repeated at intervals throughout the silo height, and this is consistent with the results obtained by Wojcik

Table 2
Summary of results obtained in type II assays (tests 8 to 20).

			Normal wall pressures (kPa)								(kN/m)	(kPa)			
TEST 8	**t (s)**	**f (kg/s)**	P_{hGA7}	P_{hGA6}	P_{hGA5}	P_{hGA4}	P_{hGA3}	P_{hGA2}	P_{hGA1}	P_{hGA0}	n_{zsk}	$p_{vt,t}$	K	μ_m	**Gate (PI)**
Filling	362,4	4,17	1,51	2,37	2,97	3,45	3,87	4,09	4,12	8,09	1,08	12,55	0,39	0,18	(max. values)
Static 1	312,4	0	1,53	2,43	2,97	3,46	3,89	4,12	4,14	8,55	1,14	13,11	0,34	0,18	(max. values)
			1,37	2,36	2,85	3,31	3,78	4,02	3,98	8,10	0,94	12,31	0,30	0,16	(min. values)
Discharge 1	4,5	10,42	1,54	3,08	3,67	4,03	5,88	6,46	7,28	19,01	1,75	12,75	0,67	0,29	(max. values)
Static 2	355,2	0	1,46	3,05	3,59	3,93	5,39	6,05	6,91	19,02	1,29	12,20	0,61	0,16	(max. values)
			1,28	2,91	3,36	3,70	5,09	5,65	6,28	18,81	1,02	11,11	0,52	0,13	(min. values)
Discharge 2	310,5	4,72	1,29	3,46	3,37	3,70	5,04	5,54	7,17	20,54	1,56	10,51	0,87	0,24	(max. values)
Weight after filling (kN)	**14,830**														
Weight after Discharge I (kN)	**14,370**														
W_I-W_{II} (kN)	**0,460**														

			Normal wall pressures (kPa)								(kN/m)	(kPa)			
TEST 9	**t (s)**	**f (kg/s)**	P_{hGA7}	P_{hGA6}	P_{hGA5}	P_{hGA4}	P_{hGA3}	P_{hGA2}	P_{hGA1}	P_{hGA0}	n_{zsk}	$p_{vt,t}$	K	μ_m	**Gate (PI)**
Filling	363,7	4,17	1,51	2,51	3,02	3,27	3,89	4,11	4,20	8,39	1,12	12,44	0,41	0,19	(max. values)
Static 1	4041,9	0	1,53	2,55	3,06	3,32	3,92	4,15	4,23	9,02	1,18	13,54	0,35	0,19	(max. values)
			1,24	2,38	2,74	2,97	3,62	3,87	3,85	8,40	0,85	12,20	0,29	0,14	(min. values)
Discharge 1	4,5	10,51	1,46	3,04	3,57	3,58	5,51	6,67	7,63	18,90	1,67	13,14	0,71	0,29	(max. values)
Static 2	383,1	0	1,39	2,95	3,48	3,49	5,34	6,10	7,29	19,30	1,36	11,87	0,65	0,17	(max. values)
			1,27	2,84	3,32	3,34	5,09	5,78	6,73	18,59	1,12	10,92	0,57	0,15	(min. values)
Discharge 2	309,6	4,75	1,28	3,42	3,33	3,35	5,08	5,77	7,52	20,19	1,61	10,50	0,77	0,24	(max. values)
Weight after filling (kN)	**14,877**														
Weight after Discharge I (kN)	**14,411**														
W_I-W_{II} (kN)	**0,466**														

			Normal wall pressures (kPa)								(kN/m)	(kPa)			
TEST 10	**t (s)**	**f (kg/s)**	P_{hGA7}	P_{hGA6}	P_{hGA5}	P_{hGA4}	P_{hGA3}	P_{hGA2}	P_{hGA1}	P_{hGA0}	n_{zsk}	$p_{vt,t}$	K	μ_m	**Gate (PI)**
Filling	364,7	4,16	1,63	2,56	3,03	3,44	4,08	4,28	4,40	9,22	1,14	12,37	0,75	0,19	(max. values)
Static 1	158,3	0	1,63	2,59	3,06	3,46	4,12	4,32	4,44	9,54	1,21	12,77	0,37	0,18	(max. values)
			1,51	2,53	2,96	3,35	4,02	4,24	4,37	9,23	1,04	12,09	0,34	0,16	(min. values)
Discharge 1	5,0	8,90	1,53	3,11	3,27	3,46	5,59	6,31	7,27	19,85	1,96	12,39	0,72	0,27	(max. values)
Static 2	80992,2	0	1,33	3,04	3,07	3,28	5,28	5,98	7,04	19,87	1,37	13,26	0,64	0,18	(max. values)
			1,02	2,44	2,62	2,83	4,53	5,08	5,71	19,24	0,78	10,84	0,43	0,12	(min. values)
Discharge 2	312,5	4,71	1,23	3,62	3,04	2,94	5,17	5,25	8,04	21,99	1,55	13,09	0,87	0,23	(max. values)
Weight after filling (kN)	**14,878**														
Weight after Discharge I (kN)	**14,440**														
W_I-W_{II} (kN)	**0,438**														

			Normal wall pressures (kPa)								(kN/m)	(kPa)			
TEST 11	**t (s)**	**f (kg/s)**	P_{hGA7}	P_{hGA6}	P_{hGA5}	P_{hGA4}	P_{hGA3}	P_{hGA2}	P_{hGA1}	P_{hGA0}	n_{zsk}	$p_{vt,t}$	K	μ_m	**Gate (PI)**
Filling	363,5	4,16	1,60	2,55	3,01	3,57	4,08	4,36	4,11	8,35	1,06	12,66	0,39	0,19	(max. values)
Static 1	344,1	0	1,60	2,58	3,03	3,60	4,13	4,46	4,12	8,63	1,11	13,20	0,33	0,17	(max. values)
			1,48	2,52	2,91	3,41	4,00	4,30	4,01	8,25	0,92	12,46	0,30	0,15	(min. values)
Discharge 1	5,5	8,46	1,49	3,08	3,35	3,48	5,46	6,38	7,19	19,46	1,73	12,97	0,66	0,28	(max. values)
Static 2	260193,1	0	1,41	3,04	3,31	3,43	5,10	5,91	6,99	19,46	1,28	13,93	0,61	0,17	(max. values)
			1,00	2,68	2,70	2,80	4,34	4,92	5,27	19,16	0,59	11,20	0,38	0,09	(min. values)
Discharge 2	311,0	4,72	1,21	3,48	2,96	2,82	4,39	5,22	8,06	23,14	1,47	13,59	0,78	0,24	(max. values)
Weight after filling (kN)	**14,850**														
Weight after Discharge I (kN)	**14,393**														
W_I-W_{II} (kN)	**0,457**														

			Normal wall pressures (kPa)								(kN/m)	(kPa)			
TEST 12	**t (s)**	**f (kg/s)**	P_{hGA7}	P_{hGA6}	P_{hGA5}	P_{hGA4}	P_{hGA3}	P_{hGA2}	P_{hGA1}	P_{hGA0}	n_{zsk}	$p_{vt,t}$	K	μ_m	**Gate (PII)**
Filling	362,1	4,18	1,57	2,53	2,97	3,26	3,91	4,00	4,13	8,26	1,10	12,50	0,38	0,19	(max. values)
Static 1	302,6	0	1,58	2,53	2,98	3,30	3,93	4,04	4,16	8,69	1,16	13,06	0,34	0,19	(max. values)
			1,43	2,47	2,88	3,18	3,83	3,95	4,01	8,26	0,96	12,24	0,31	0,16	(min. values)
Discharge 1	18,0	1,54	1,44	2,82	2,90	3,19	4,81	5,89	7,18	22,03	1,55	12,72	0,68	0,22	(max. values)
Static 2	279,5	0	1,06	2,83	2,58	2,28	4,52	5,64	6,82	22,39	1,29	12,39	0,58	0,19	(max. values)
			0,98	2,74	2,51	2,25	4,34	5,35	6,31	21,90	1,04	11,36	0,51	0,15	(min. values)
Discharge 2	317,0	4,68	1,17	3,46	2,61	2,26	4,87	5,94	7,79	23,12	1,54	12,20	0,78	0,23	(max. values)
Weight after filling (kN)	**14,835**														
Weight after Discharge I (kN)	**14,564**														
W_I-W_{II} (kN)	**0,271**														

			Normal wall pressures (kPa)								(kN/m)	(kPa)			
TEST 13	**t (s)**	**f (kg/s)**	P_{hGA7}	P_{hGA6}	P_{hGA5}	P_{hGA4}	P_{hGA3}	P_{hGA2}	P_{hGA1}	P_{hGA0}	n_{zsk}	$p_{vt,t}$	K	μ_m	**Gate (PII)**
Filling	375,6	4,02	1,51	2,54	3,12	3,54	4,40	4,46	4,25	8,43	1,04	12,71	0,42	0,18	(max. values)
Static 1	342,2	0	1,51	2,54	3,12	3,55	4,37	4,44	4,20	8,86	1,08	13,25	0,33	0,16	(max. values)
			1,37	2,47	2,97	3,40	4,19	4,29	3,98	8,43	0,90	12,55	0,30	0,14	(min. values)
Discharge 1	13,0	2,09	1,39	2,98	2,99	3,42	4,66	5,70	6,70	21,56	1,49	13,11	0,63	0,22	(max. values)
Static 2	84131,8	0	1,06	3,00	2,71	2,09	4,40	5,47	6,45	23,61	1,24	13,73	0,54	0,19	(max. values)
			0,79	2,64	2,39	1,91	3,84	4,61	4,93	21,37	0,70	11,54	0,36	0,12	(min. values)
Discharge 2	336,6	4,41	1,16	3,41	2,62	1,96	4,34	5,25	7,70	25,99	1,45	13,20	0,74	0,24	(max. values)
Weight after filling (kN)	**14,815**														
Weight after Discharge I (kN)	**14,548**														
W_I-W_{II} (kN)	**0,267**														

			Normal wall pressures (kPa)								(kN/m)	(kPa)			
TEST 14	**t (s)**	**f (kg/s)**	P_{hGA7}	P_{hGA6}	P_{hGA5}	P_{hGA4}	P_{hGA3}	P_{hGA2}	P_{hGA1}	P_{hGA0}	n_{zsk}	$p_{vt,t}$	K	μ_m	**Gate (PIII)**
Filling	363,2	4,17	1,55	2,54	2,94	3,30	3,97	4,14	4,05	8,33	1,10	12,51	0,38	0,19	(max. values)
Static 1	321,5	0	1,56	2,56	2,98	3,36	4,01	4,18	4,11	8,79	1,17	13,04	0,34	0,19	(max. values)
			1,42	2,48	2,88	3,20	3,90	4,07	3,99	8,33	0,97	12,23	0,31	0,16	(min. values)
Discharge 1	24,1	1,11	1,43	2,74	2,85	3,14	4,64	5,97	7,18	22,57	1,46	12,04	0,66	0,22	(max. values)
Static 2	352,6	0	1,02	2,74	2,58	2,23	4,46	5,66	6,91	22,74	1,34	12,27	0,60	0,20	(max. values)
			0,96	2,65	2,52	2,20	4,33	5,40	6,46	22,37	1,08	11,22	0,53	0,16	(min. values)
Discharge 2	608,7	2,45	1,13	3,49	2,58	2,22	4,84	6,00	7,79	23,46	1,48	11,85	0,79	0,22	(max. values)
Weight after filling (kN)	**14,865**														
Weight after Discharge I (kN)	**14,603**														
W_I-W_{II} (kN)	**0,262**														

(continued on next page)

Table 2 (*continued*)

			Normal wall pressures (kPa)								(kN/m)	(kPa)			
TEST 15	**t (s)**	**f (kg/s)**	P_{hGA7}	P_{hGA6}	P_{hGA5}	P_{hGA4}	P_{hGA3}	P_{hGA2}	P_{hGA1}	P_{hGA0}	n_{zsk}	$p_{vt,t}$	K	μ_m	**Gate (PIII)**
Filling	369,1	4,09	1,52	2,49	2,95	3,32	4,03	4,57	4,27	9,05	1,01	12,87	0,43	0,18	(max. values)
Static 1	405,2	0	1,58	2,49	2,95	3,32	4,04	4,55	4,22	9,34	1,05	13,34	0,33	0,16	(max. values)
			1,41	2,45	2,84	3,20	3,93	4,41	4,04	9,07	0,87	12,64	0,30	0,14	(min. values)
Discharge 1	26,0	1,00	1,42	3,06	2,85	3,21	4,16	5,65	6,93	22,86	1,34	13,04	0,61	0,20	(max. values)
Static 2	78923,8	0	0,98	3,08	2,47	1,96	3,97	5,30	6,52	23,23	1,26	13,70	0,55	0,20	(max. values)
			0,79	2,72	2,21	1,83	3,75	4,66	4,98	22,56	0,70	11,45	0,37	0,12	(min. values)
Discharge 2	749,2	1,98	1,11	3,55	2,64	1,83	4,09	5,39	8,01	24,89	1,33	13,40	0,73	0,22	(max. values)
Weight after filling (kN)	**14,794**														
Weight after Discharge I (kN)	**14,538**														
W_I-W_{II} (kN)	**0,256**														

			Normal wall pressures (kPa)								(kN/m)	(kPa)			
TEST 16	**t (s)**	**f (kg/s)**	P_{hGA7}	P_{hGA6}	P_{hGA5}	P_{hGA4}	P_{hGA3}	P_{hGA2}	P_{hGA1}	P_{hGA0}	n_{zsk}	$p_{vt,t}$	K	μ_m	**Gate (PIII)**
Filling	364,6	4,15	1,63	2,50	3,11	3,54	4,29	4,25	4,10	8,36	1,03	12,76	0,39	0,18	(max. values)
Static 1	750,9	0	1,64	2,54	3,12	3,55	4,30	4,29	4,13	8,81	1,09	13,38	0,33	0,17	(max. values)
			1,46	2,48	2,96	3,32	4,10	4,13	3,94	8,37	0,88	12,54	0,29	0,14	(min. values)
Discharge 1	28,0	0,96	1,47	2,92	2,98	3,34	4,70	5,98	7,29	23,55	1,37	13,04	0,65	0,20	(max. values)
Static 2	267696,0	0	1,03	2,94	2,64	2,15	4,49	5,81	7,07	24,22	1,29	13,99	0,59	0,19	(max. values)
			0,83	2,57	2,32	1,92	3,68	4,35	5,28	23,28	0,64	11,41	0,38	0,11	(min. values)
Discharge 2	741,2	2,01	1,20	3,46	2,65	1,96	4,39	5,99	8,89	26,62	1,36	13,67	0,93	0,21	(max. values)
Weight after filling (kN)	**14,847**														
Weight after Discharge I (kN)	**14,583**														
W_I-W_{II} (kN)	**0,264**														

			Normal wall pressures (kPa)								(kN/m)	(kPa)			
TEST 17	**t (s)**	**f (kg/s)**	P_{hGA7}	P_{hGA6}	P_{hGA5}	P_{hGA4}	P_{hGA3}	P_{hGA2}	P_{hGA1}	P_{hGA0}	n_{zsk}	$p_{vt,t}$	K	μ_m	**Gate (PIV)**
Filling	376,2	4,01	1,53	2,62	3,02	3,69	3,97	4,47	4,73	8,44	1,02	12,76	0,43	0,16	(max. values)
Static 1	339,1	0	1,55	2,79	3,02	3,68	3,99	4,48	4,69	8,83	1,07	13,27	0,37	0,16	(max. values)
			1,40	2,67	2,89	3,49	3,87	4,35	4,45	8,44	0,89	12,55	0,34	0,14	(min. values)
Discharge 1	71,6	0,35	1,41	3,03	2,90	3,52	3,93	5,65	7,50	23,37	1,24	12,92	0,64	0,19	(max. values)
Static 2	228,9	0	0,90	3,07	2,44	1,90	3,64	5,41	7,19	23,74	1,20	12,52	0,59	0,18	(max. values)
			0,86	2,98	2,39	1,88	3,59	5,27	6,82	23,38	1,00	11,72	0,55	0,15	(min. values)
Discharge 2	3047,4	0,49	0,96	3,49	2,57	1,90	4,10	5,62	7,99	24,05	1,25	12,31	0,99	0,20	(max. values)
Weight after filling (kN)	**14,804**														
Weight after Discharge I (kN)	**14,556**														
W_I-W_{II} (kN)	**0,248**														

			Normal wall pressures (kPa)								(kN/m)	(kPa)			
TEST 18	**t (s)**	**f (kg/s)**	P_{hGA7}	P_{hGA6}	P_{hGA5}	P_{hGA4}	P_{hGA3}	P_{hGA2}	P_{hGA1}	P_{hGA0}	n_{zsk}	$p_{vt,t}$	K	μ_m	**Gate (PIV)**
Filling	369,6	4,10	1,57	2,56	3,14	3,37	3,93	4,21	4,44	8,30	1,07	12,65	0,40	0,17	(max. values)
Static 1	320,6	0	1,58	2,60	3,19	3,40	3,97	4,23	4,44	8,51	1,10	13,19	0,35	0,17	(max. values)
			1,43	2,51	3,02	3,26	3,86	4,11	4,20	7,52	0,93	12,49	0,32	0,15	(min. values)
Discharge 1	68,1	0,38	1,43	3,10	3,03	3,28	4,17	5,73	7,34	24,30	1,27	13,13	0,63	0,20	(max. values)
Static 2	289,0	0	0,90	3,13	2,60	1,97	3,97	5,37	6,91	24,84	1,20	12,49	0,57	0,18	(max. values)
			0,86	3,05	2,53	1,95	3,87	5,20	6,51	24,22	1,02	11,80	0,52	0,16	(min. values)
Discharge 2	2611,5	0,57	1,01	3,62	2,58	1,97	4,18	5,61	8,13	25,46	1,29	12,17	0,92	0,19	(max. values)
Weight after filling (kN)	**14,860**														
Weight after Discharge I (kN)	**14,610**														
W_I-W_{II} (kN)	**0,251**														

			Normal wall pressures (kPa)								(kN/m)	(kPa)			
TEST 19	**t (s)**	**f (kg/s)**	P_{hGA7}	P_{hGA6}	P_{hGA5}	P_{hGA4}	P_{hGA3}	P_{hGA2}	P_{hGA1}	P_{hGA0}	n_{zsk}	$p_{vt,t}$	K	μ_m	**Gate (PIV)**
Filling	374,2	4,03	1,53	2,60	2,96	3,50	4,28	4,84	4,22	9,17	1,02	12,78	0,41	0,16	(max. values)
Static 1	345,6	0	1,54	2,72	2,96	3,50	4,29	4,82	4,24	9,53	1,07	13,32	0,34	0,16	(max. values)
			1,40	2,60	2,82	3,33	4,12	4,58	4,02	9,17	0,88	12,56	0,30	0,14	(min. values)
Discharge 1	66,1	0,38	1,41	3,04	2,85	3,36	4,15	5,55	7,04	23,32	1,23	13,24	0,60	0,19	(max. values)
Static 2	75154,3	0	0,91	3,05	2,43	1,91	3,64	5,24	6,54	23,64	1,23	13,57	0,55	0,19	(max. values)
			0,74	2,69	2,13	1,62	3,00	4,27	5,30	22,78	0,74	11,62	0,39	0,13	(min. values)
Discharge 2	2309,9	0,64	0,99	3,65	2,56	1,83	3,62	5,20	7,96	25,02	1,23	12,85	0,93	0,21	(max. values)
Weight after filling (kN)	**14,807**														
Weight after Discharge I (kN)	**14,561**														
W_I-W_{II} (kN)	**0,246**														

			Normal wall pressures (kPa)								(kN/m)	(kPa)			
TEST 20	**t (s)**	**f (kg/s)**	P_{hGA7}	P_{hGA6}	P_{hGA5}	P_{hGA4}	P_{hGA3}	P_{hGA2}	P_{hGA1}	P_{hGA0}	n_{zsk}	$p_{vt,t}$	K	μ_m	**Gate (PIV)**
Filling	367,2	4,12	1,50	2,48	3,06	3,27	3,92	4,41	4,10	9,53	1,05	12,69	0,44	0,19	(max. values)
Static 1	345,6	0	1,51	2,48	3,06	3,28	3,93	4,39	4,13	9,70	1,09	13,20	0,33	0,17	(max. values)
			1,36	2,42	2,92	3,16	3,83	4,24	4,01	9,40	0,92	12,54	0,30	0,15	(min. values)
Discharge 1	51,6	0,47	1,37	2,71	2,95	3,20	4,39	5,90	7,38	22,20	1,34	12,84	0,66	0,20	(max. values)
Static 2	252531,2	0	0,88	2,73	2,53	1,91	4,16	5,55	7,14	22,75	1,26	14,11	0,60	0,19	(max. values)
			0,70	2,37	2,06	1,55	3,32	4,13	5,26	21,93	0,62	11,54	0,38	0,11	(min. values)
Discharge 2	1886,9	0,79	1,04	3,62	2,52	1,67	3,86	5,55	8,82	25,66	1,30	12,01	0,98	0,21	(max. values)
Weight after filling (kN)	**14,830**														
Weight after Discharge I (kN)	**14,595**														
W_I-W_{II} (kN)	**0,236**														

[24], which indicated the presence of these areas alternating in height along the length of the cylinder wall.

Fig. 9 also shows that in static state, the vertical stress in the stored material at the level of the silo–hopper transition increased over time, as did the normal hopper wall pressure. The opposite occurred in the case of normal cylinder wall pressures, as these decreased over time. In other words, in static state the cylinder walls discharged their load, increasing the weight resting on the hopper, and this was due to resettling of the grain in the silo, a phenomenon which has already been discussed in more detail in a previous publication [27].

Focusing on flow rates during discharge, it will first be observed that for the same outlet position, the flow rate varied slightly between

Table 3
Summary of results obtained in the type III assay (test 21).

						Normal wall pressures (kPa)								n_{zsk}	$p_{vt,t}$	K	
TEST 21	t (s)	t_T (s)	W_s (kN)	W_E (kN)	f (kg/s)	P_{hGA7}	P_{hGA6}	P_{hGA5}	P_{hGA4}	P_{hGA3}	P_{hGA2}	P_{hGA1}	P_{hGA0}	(kN/m)	(kPa)		Gate (PIII)
Filling 1	373,1	373,1	0,000	14,815	4,05	1,56	2,57	2,83	3,59	4,18	4,36	4,19	8,13	1,01	12,81	0,43	(max. values)
After filling 1	333,0	706,1	14,815	14,815	0	1,58	2,59	2,84	3,59	4,21	4,43	4,40	8,88	1,07	13,23	0,35	(max. values)
						1,41	2,52	2,75	3,42	4,05	4,28	4,15	8,13	0,91	12,58	0,32	(min. values)
Discharge 1	23,0	729,2	14,815	14,505	1,37	1,43	2,90	2,76	3,43	4,25	5,71	7,05	22,83	1,38	13,31	0,64	(max. values)
Static 1	260,9	990,1	14,505	14,505	0	1,06	2,94	2,45	2,17	4,25	5,60	6,94	23,18	1,25	12,53	0,60	(max. values)
						0,93	2,82	2,37	1,99	4,05	5,25	6,23	21,22	0,98	11,48	0,50	(min. values)
Discharge 2	15,0	1005,1	14,505	14,232	1,85	1,06	3,07	2,40	2,07	4,21	5,53	7,30	23,68	1,39	12,37	0,68	(max. values)
Static 2	340,6	1345,7	14,232	14,232	0	1,06	3,08	2,31	1,82	4,21	5,53	7,24	22,45	1,26	12,32	0,63	(max. values)
						0,96	2,91	2,24	1,75	4,06	5,32	6,66	22,11	0,95	11,06	0,54	(min. values)
Discharge 3	17,0	1362,7	14,232	13,911	1,92	1,07	3,35	2,36	1,83	4,16	5,34	7,55	23,54	1,39	12,21	0,72	(max. values)
Static 3	343,1	1705,8	13,911	13,911	0	1,06	3,30	2,36	1,86	4,16	5,27	7,09	21,73	1,26	11,87	0,64	(max. values)
						0,98	3,18	2,30	1,83	4,06	5,12	6,68	21,43	0,96	10,68	0,56	(min. values)
Discharge 4	16,0	1721,9	13,911	13,631	1,78	1,02	3,48	2,36	1,88	4,07	5,13	7,41	23,01	1,36	11,48	0,73	(max. values)
Static 4	274,4	1996,3	13,631	13,631	0	0,99	3,31	2,35	1,93	4,00	5,07	7,06	21,66	1,27	11,64	0,67	(max. values)
						0,91	3,18	2,29	1,90	3,89	4,93	6,67	21,29	0,93	10,29	0,57	(min. values)
Discharge 5	17,5	2013,8	13,631	13,344	1,67	0,94	3,49	2,52	1,90	3,93	4,95	7,19	22,63	1,32	11,63	0,72	(max. values)
Static 5	343,6	2357,4	13,344	13,344	0	0,82	3,25	2,51	1,83	3,93	4,86	6,96	20,89	1,25	11,34	0,68	(max. values)
						0,76	3,14	2,45	1,81	3,83	4,73	6,59	20,51	0,91	9,98	0,58	(min. values)
Discharge 6	17,0	2374,4	13,344	13,041	1,81	0,81	3,45	2,51	1,81	3,84	4,75	7,13	22,13	1,28	11,12	0,73	(max. values)
Static 6	286,0	2660,4	13,041	13,041	0	0,60	3,14	2,51	1,80	3,69	4,70	6,90	20,52	1,20	10,94	0,69	(max. values)
						0,56	2,98	2,45	1,78	3,60	4,58	6,71	20,18	0,92	9,78	0,61	(min. values)
Discharge 7	16,5	2676,9	13,041	12,748	1,80	0,57	3,29	2,52	1,79	3,79	4,62	6,97	21,57	1,24	11,07	0,73	(max. values)
Static 7	300,0	2977,0	12,748	12,748	0	0,30	2,93	2,54	1,81	3,72	4,63	6,71	20,18	1,18	10,58	0,69	(max. values)
						0,29	2,83	2,50	1,78	3,65	4,54	6,52	19,83	0,91	9,50	0,63	(min. values)
Filling 2	60,1	3037,1	12,748	14,811	3,50	1,59	3,42	3,02	3,17	4,07	4,61	6,52	20,37	1,19	12,39	0,69	(max. values)
After filling 2	338,0	3375,1	14,811	14,811	0	1,57	3,48	3,16	3,22	4,33	4,64	6,34	20,52	1,18	12,66	0,52	(max. values)
						1,39	3,37	3,05	3,10	4,07	4,59	6,23	20,36	1,05	12,12	0,49	(min. values)
Discharge 8	18,5	3393,6	14,811	14,519	1,60	1,40	4,22	3,12	3,12	4,23	5,27	7,60	23,18	1,54	12,42	0,71	(max. values)
Static 8	339,2	3732,9	14,519	14,519	0	1,23	4,19	3,13	2,42	4,06	5,26	7,50	22,32	1,35	12,31	0,66	(max. values)
						1,15	4,04	3,09	2,34	4,00	5,12	7,04	22,07	1,04	11,10	0,57	(min. values)
Discharge 9	18,0	3750,9	14,519	14,209	1,75	1,18	4,42	3,17	2,42	4,01	5,13	7,68	23,60	1,47	12,08	0,73	(max. values)
Static 9	342,6	4093,5	14,209	14,209	0	1,13	4,44	3,25	2,49	4,07	5,12	7,37	22,07	1,38	11,92	0,68	(max. values)
						1,05	4,14	3,19	2,12	4,01	5,00	6,98	21,70	1,04	10,56	0,59	(min. values)
Discharge 10	15,5	4109,0	14,209	13,925	1,86	1,09	4,49	3,20	2,46	4,17	5,01	7,54	23,27	1,46	11,54	0,73	(max. values)
Static 10	341,1	4450,1	13,925	13,925	0	1,05	4,42	3,22	2,23	4,25	4,97	7,38	21,63	1,36	11,70	0,69	(max. values)
						0,97	4,17	3,17	2,04	4,17	4,85	6,95	21,29	1,01	10,30	0,59	(min. values)
Discharge 11	16,0	4466,1	13,925	13,631	1,87	1,01	4,48	3,39	2,23	4,23	5,03	7,41	22,86	1,42	11,27	0,73	(max. values)
Static 11	343,1	4809,2	13,631	13,631	0	0,97	4,11	3,40	2,22	4,24	5,03	7,06	21,31	1,29	11,46	0,68	(max. values)
						0,91	2,91	3,35	2,16	4,15	4,90	6,69	20,99	0,97	10,18	0,58	(min. values)
Discharge 12	16,5	4825,8	13,631	13,332	1,84	0,92	3,96	3,50	2,27	4,17	4,92	7,10	22,44	1,37	11,07	0,72	(max. values)
Static 12	344,1	5169,8	13,332	13,332	0	0,80	3,61	3,50	2,39	4,08	4,61	7,01	20,91	1,28	11,21	0,69	(max. values)
						0,74	3,42	3,41	2,35	4,00	4,49	6,60	20,55	0,94	9,83	0,59	(min. values)
Discharge 13	18,0	5187,9	13,332	13,030	1,71	0,78	3,82	3,46	2,36	4,25	4,72	7,03	22,17	1,32	11,22	0,73	(max. values)
Static 13	340,5	5528,4	13,030	13,030	0	0,60	3,35	3,45	2,29	4,24	4,65	6,79	20,40	1,25	10,72	0,69	(max. values)
						0,57	3,24	3,39	2,27	4,16	4,55	6,61	20,07	0,97	9,60	0,63	(min. values)
Discharge 14	16,0	5544,4	13,030	12,742	1,83	0,58	3,53	3,41	2,30	4,16	4,55	6,89	21,44	1,29	10,30	0,73	(max. values)
Static 14	338,6	5883,0	12,742	12,742	0	0,35	3,15	3,40	2,37	4,08	4,47	6,66	20,05	1,22	10,48	0,69	(max. values)
						0,33	3,01	3,32	2,33	4,01	4,39	6,47	19,72	0,94	9,35	0,63	(min. values)
Filling 3	61,1	5944,2	12,742	14,812	3,45	1,50	3,40	3,89	3,49	4,50	4,49	6,49	20,22	1,22	12,25	0,69	(max. values)
After filling 3	308,5	6252,7	14,812	14,812	0	1,50	3,40	3,90	3,48	4,50	4,49	6,30	20,26	1,23	12,58	0,53	(max. values)
						1,39	3,31	3,82	3,38	4,42	4,43	6,25	20,23	1,07	11,95	0,50	(min. values)
Discharge 15	644,1	6896,8	14,812	0,000	2,34	1,40	4,35	4,03	3,40	4,73	5,48	7,52	22,69	1,56	12,39	0,80	(max. values)

one test and another (Table 1). This was because the outlet gate was opened manually to a previously marked point and was not therefore open to exactly the same degree for each position assayed. It will also be seen that when tests were conducted with the slide gate at positions PI and PII, the flow rate was practically the same, and this was because the flow rate coincided with the maximum quantity of material the discharge device was capable of evacuating. In PI assays, the flow rate was much higher during the initial moments because discharge was free-flowing, with the result that the flow of material was greater than the screw conveyor could carry and the discharge hopper became completely filled. When the hopper discharge device became filled to capacity, unloading then continued at a constant rate which coincided with the assay conducted in position PII, which was the maximum flow rate that the screw conveyor could evacuate. In assays conducted with the outlet gate in position PII, the opening discharged material into the hopper discharge device at a rate which coincided approximately with the maximum rate that the screw conveyor was capable of evacuating. In the assays conducted in positions PIII and PIV, the rate of material discharged was lower than that which the discharge device was capable of evacuating, and thus the hopper was never filled to capacity.

Fig. 10 shows the maximum normal wall pressures registered during discharge at the silo–hopper transition for each of the discharge flow rates tested in type I assays. It can be seen that pressures on the hopper wall (GA0) decreased linearly as the discharge flow rate increased ($r^2 = 0.778$), whereas the maximum pressures reached on the cylinder wall (GA1) were virtually constant, independently of the discharge flow rate. This was an unexpected result, but is a true reflection of what actually happens, at least in this type of silo. We are now conducting assays with maize and the results are similar to those obtained with wheat as far as flow is concerned. What did clearly vary according to the flow rate were the peaks in pressure

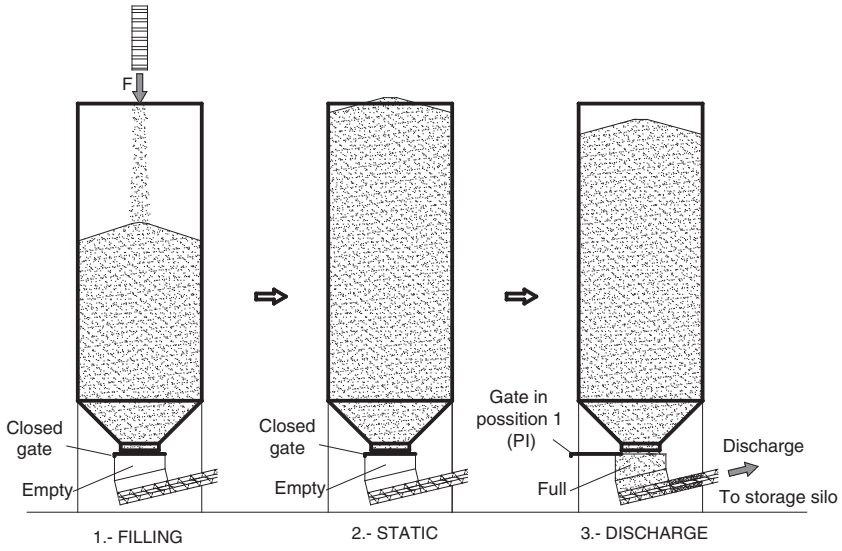

Fig. 7. Diagram of type I assays with the outlet gate in position 1 (PI).

which occurred along the cylinder wall above GA1, a phenomenon which is depicted in Fig. 13. The reason for this is that when the outlet opening was at its widest, substantial overpressures were registered by some of the upper load cells, and as the opening was gradually reduced these overpressures decreased whilst those below increased. This was probably because the material in the upper sections descended more rapidly, leading to areas of discontinuity which, as has been observed by other authors, are associated with discontinuities in the pressure curves [24,28].

Thus, according to our results and in contrary to what might be expected, a rapid discharge does not imply higher overpressures on the silo wall.

Fig. 11 shows the trends followed by the other parameters involved in the calculation of silos according to the European standard [21]. The value of K is given for the silo loading phase, from when hopper loading had ended and filling of the cylinder had begun, and for during discharge until the silo had been completely unloaded, intervals at which this parameter is relevant. As regards the value of μ, this is given for loading from the moment when the level of grain rose above GA7, i.e., from the moment that the forces registered by this cell related to pressures on the wall since the grain acts on the entire surface of the wall connected to this cell, until the grain had dropped again to the same level during discharge. Note also that in static state, the value of n_{ZSK} was not constant but rather decreased, due to the phenomenon discussed earlier of grain resettling, whereby the cylinder walls discharge their load during static state, increasing the weight resting on the hopper. This phenomenon has previously been discussed by Sugita, who reported that "for 5 or 6 hours after loading the silo, pressures in the upper sections decreased and increased on the sloping wall of the hopper".

Fig. 11 also shows the increase in the value of K during discharge, which is logical since the vertical pressure on the stored material dropped at the beginning of discharge while the normal cylinder wall pressure at the silo hopper transition increased. A comparison is also given with the results obtained using the Eurocode [21], showing that the value of n_{ZSK} was below that given in the European standard whereas the proposed value of K was far exceeded during discharge.

When the maximum variation in these parameters obtained during discharge compared with the maximum values obtained in static state was analysed, it could be seen that these parameters presented an increase during the first moments of discharge, which was more pronounced in the case of the mean value of resultant vertical stress per unit perimeter at the transition ($n_{zSk,t}$) and of the lateral pressure ratio at the transition (K), reaching 67.2% and 115.8%, respectively.

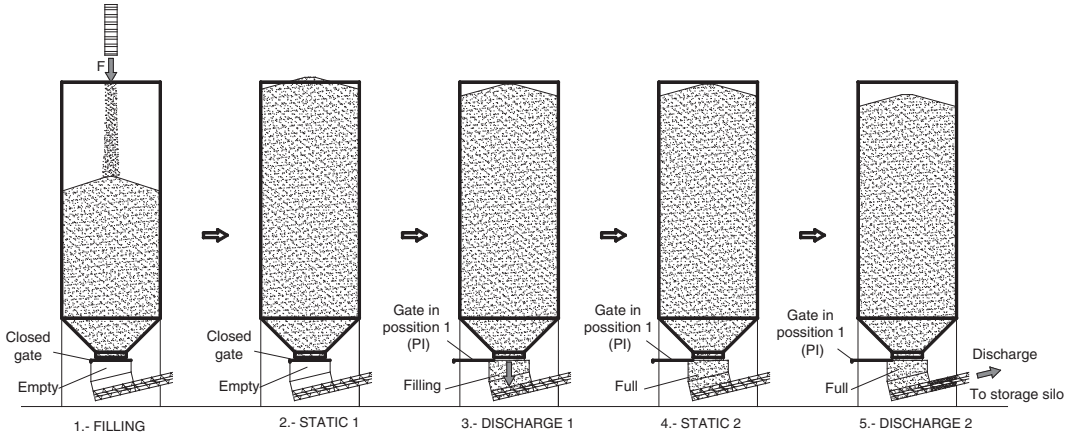

Fig. 8. Diagram of type II assays with the outlet gate in position 1 (PI).

Table 4
Maximum variation in normal wall pressure during discharge compared with maximum values obtained in static state. Type I assays.

	P_{hGA7}	P_{hGA6}	P_{hGA5}	P_{hGA4}	P_{hGA3}	P_{hGA2}	P_{hGA1}	P_{hGA0}
TEST 1	-7,1%	29,8%	14,5%	0,0%	33,3%	35,7%	77,6%	103,8%
TEST 2	8,0%	32,8%	24,7%	19,4%	39,3%	44,6%	72,3%	107,9%
TEST 3	-7,0%	34,9%	-2,8%	-2,7%	34,4%	42,9%	77,8%	119,5%
TEST 4	-7,9%	32,4%	-1,8%	-2,8%	31,0%	39,4%	81,5%	130,7%
TEST 5	-8,1%	36,6%	-3,4%	-3,0%	17,7%	38,8%	82,0%	139,8%
TEST 6	-8,4%	29,3%	-2,0%	-2,6%	31,6%	45,2%	83,8%	135,4%
TEST 7	-9,0%	37,5%	-3,5%	-3,0%	7,5%	42,1%	89,3%	179,8%

Fig. 12 shows the shape of the curves obtained in the type II assays, in which, as explained in Section 2.3.2., discharge was performed in two stages. The results are given in Table 2. In the loading phase and the first phase in static state, the results obtained in type I and II assays were comparable and similar: consequently, in order to avoid repetition, these will not be discussed again here.

As can be seen in Table 2, in assays conducted with the outlet gate in position I (PI), approximately 0.45 kN of wheat was evacuated during the initial discharge, whereas in assays conducted with the gate in PII, PIII, and PIV, around 0.26 kN was discharged. This difference is explained by the fact that with the gate in PI, the outlet was completely open and the hopper discharge device was completely filled, whereas when the outlet gate was in all the other positions, discharge was effected through a small opening and eventually the material reached the same level as the opening, blocking it and stopping the flow of grain. It can also be seen that as with the type I assays, for the same outlet gate position, the flow rate varied slightly between one test and another, which was due to the same reason discussed above for type I assays.

The curves shown in Fig. 12 also indicate that once the initial discharge was halted, lateral pressures during the second static phase did not return to the previous static state values. See, for example, the results of tests 11, 16 or 20, in which the second static state was maintained for over 70 h without attaining initial pressure values. This phenomenon should be borne in mind when developing new numerical theories and methods for calculating pressures during silo discharge since it indicates that the movement of material within the silo during the initial discharge induces changes in solid unit weight, which increases or decreases in certain areas along the height of the silo, and the main variations in pressure that occur inside the silo are primarily due to this phenomenon rather than to an increase in volume caused by lateral displacement of the particles during discharge, a phenomenon known as dilatancy, since if this latter were responsible, initial values would be recovered once discharge was halted. The magnitude of this increase in pressure depends on the initial solid unit weight. In other words, the above statement would not be true if the material attained critical density as a result of the pressure levels reached in the lower parts of the cylinder. In this case, it might be that the pressure increase was entirely due to dilatancy, and thus when discharge was halted, the static state pressure levels would be restored.

A similar phenomenon has been described by Pieper and Wenzel [29], who reported that "When discharge was stopped, the pressure was recorded in that moment about maintained for 15 h", although unlike us, they did not state initial pressures that were not recovered. The experiments were carried out using cylindrical metal silos measuring 23.6 in. (60 cm) in diameter and 121 in. (302.5 cm) high, employing grain and sand as the stored material.

It can also be seen in Fig. 12 that the resettling of grain inside the silo in static state, previously discussed for type I assays, continued to occur in the second static state, which explains the abrupt steps present in the curves. This figure includes the curve for the weight of the material stored, for the different phases. As can be seen, such steps do not occur in this curve and this, together with other reasons which we have reported previously elsewhere [27], indicate that the resettling was not due to interference in electronic readings.

Table 5 shows the maximum variation in normal wall pressure during each of the discharges with respect to the previous static state. As in the previous assays, the normal wall pressure presented a substantial

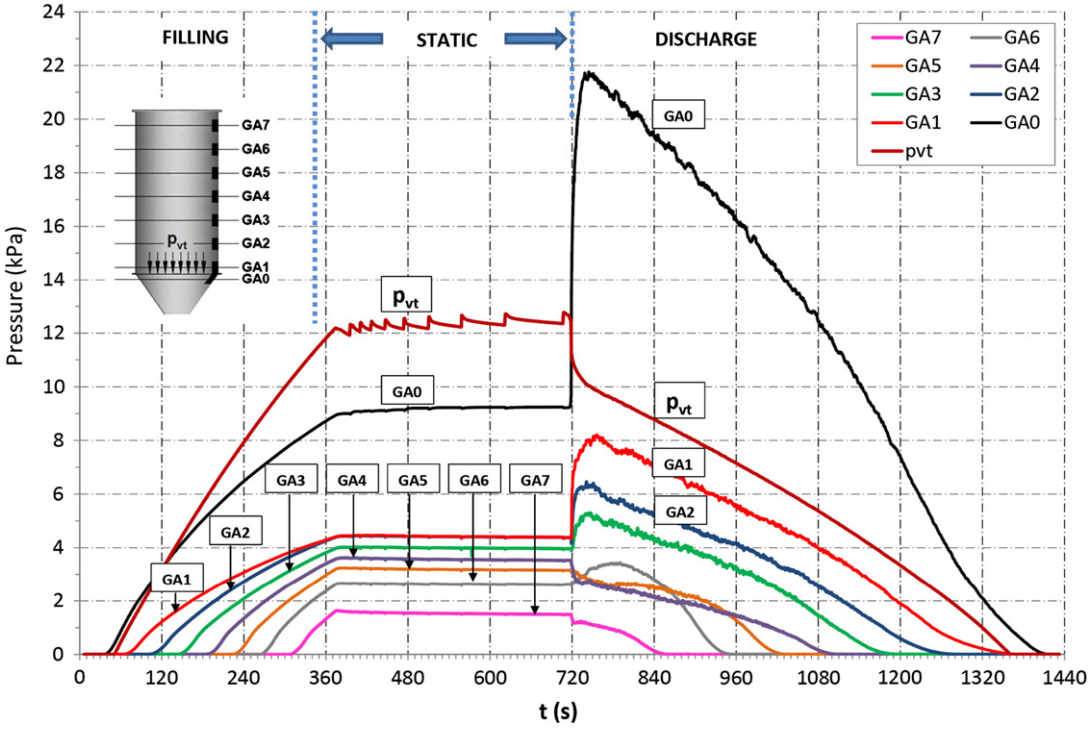

Fig. 9. Normal silo wall pressures ($p_{hGA,t}$) and vertical stress in the stored material at the transition ($p_{vt,t}$), at each time t. Type I assay, test 6.

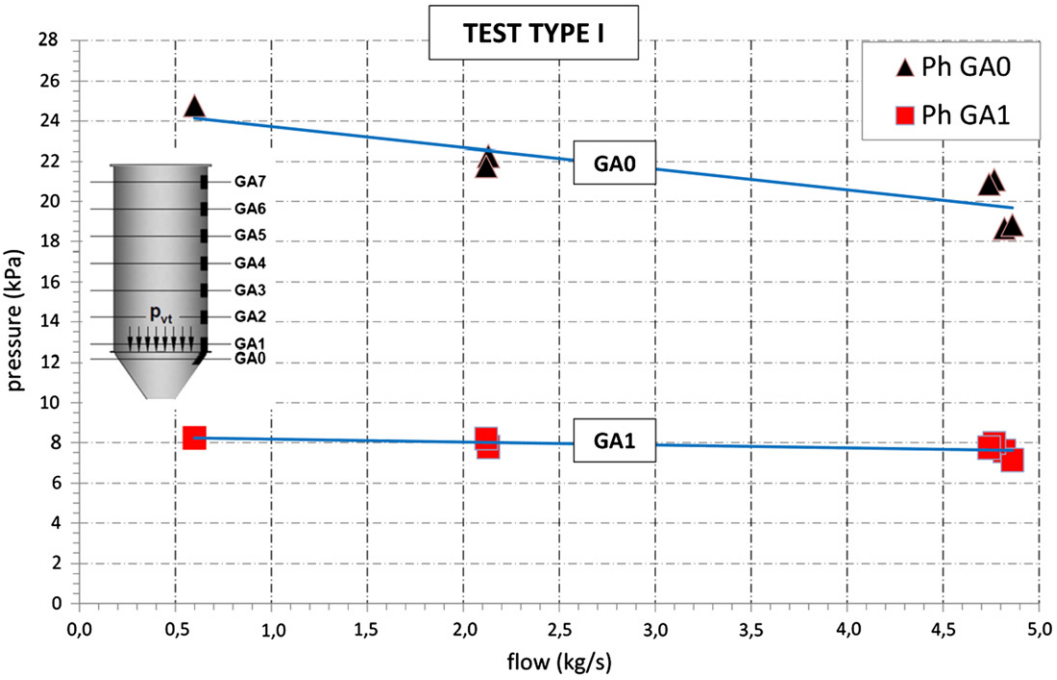

Fig. 10. Regression lines obtained from the maximum normal pressures on the cylinder wall and the hopper at the silo–hopper transition recorded in the assays, for each discharge flow rate. Type I assays.

variation at the beginning of the first discharge, reaching values and pressure distributions inside the silo similar to those described for type I assays. However, the variation in pressure following the second discharge was much smaller and, as will be seen in the type III assay, initial pressures were recovered on returning to static state. Consequently, we believe that this second increase in pressure can be attributed to dilatancy.

Table 5 also shows that in contrast to what happened in the type I assays, in which the increase in pressure recorded by the cells in the lower section of the cylinder (cells GA0 to GA3) was always positive whereas in the upper section of the cylinder the pressure remained almost constant or even fell at some points, in these assays, and more specifically in tests 17 and 19, the GA3 cells began to register pressures below those recorded for static state.

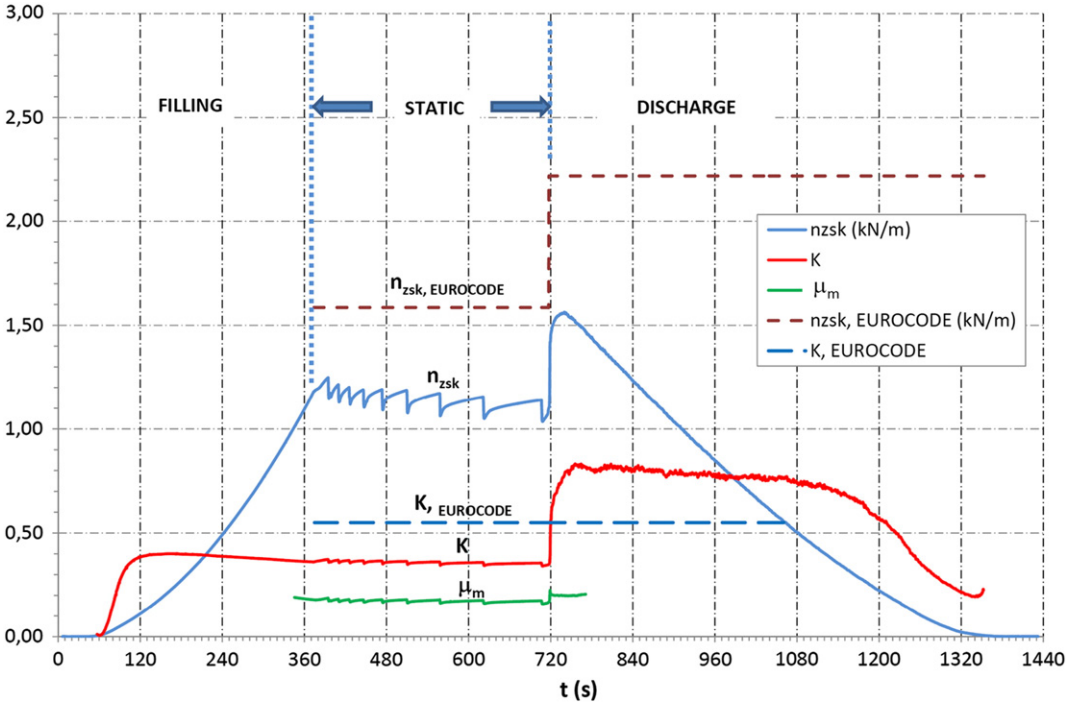

Fig. 11. Mean value of resultant vertical stress per unit perimeter at the transition ($n_{zSk,t}$), lateral pressure ratio at the transition (K); mean value of the wall friction coefficient between the stored material and the cylinder wall (μ_m). Comparison between the values obtained in test 4 and those obtained using Eurocode 1, part 4. Type I assays.

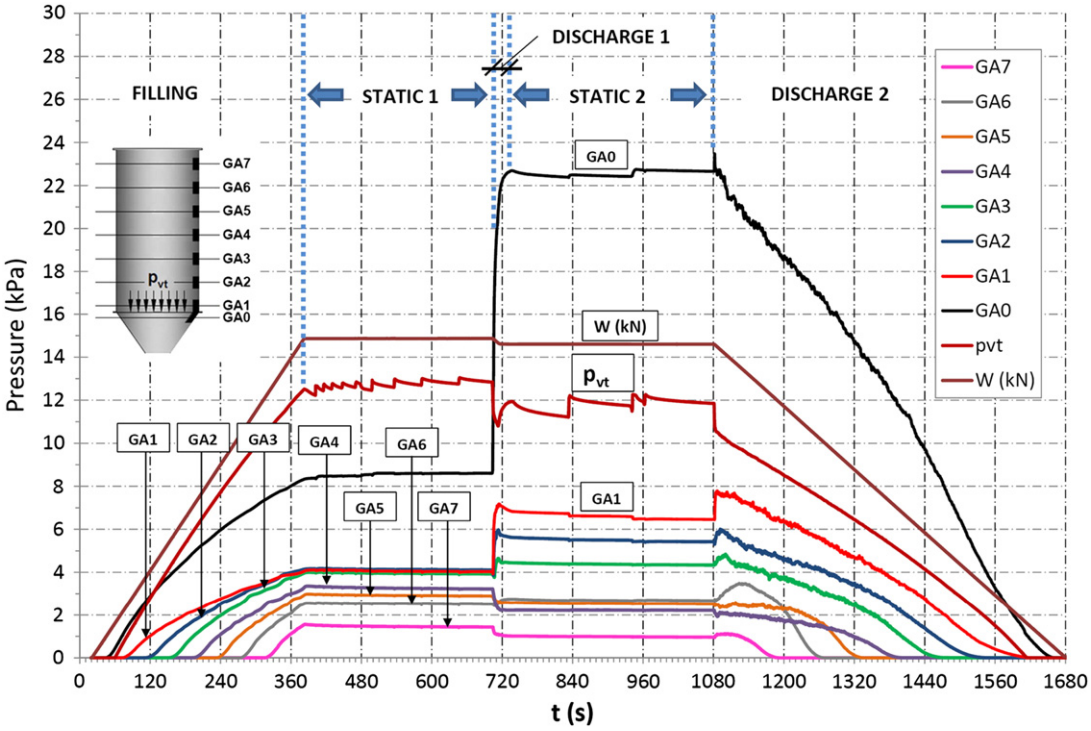

Fig. 12. Normal silo wall pressures ($p_{hGA,t}$) and vertical stress in the stored material at the transition ($p_{vt,t}$), at each time t. Type II assay, test 14.

Fig. 13 presents an analysis of the maximum variation in wall pressure during discharge 1 with respect to the previous static state in type II assays with the outlet gate positioned at either extreme, i.e., with the outlet gate in PI and PIV. As can be observed in the Figure, the curves for the same degree of outlet opening present a similar pattern which is clearly different from the pattern presented by curves for the other opening. The shape of these curves supports the explanation that the variation in pressures during discharge is mainly due to an increase or decrease in the specific weight of the grain in some areas rather than in others. Thus, a slower discharge produces a greater increase in the unit weight of the material at the level of the hopper, which in turn leads to a greater increase in pressure in these areas. However, up to the level of GA2, the trend was reversed, and pressures lower than those in static state were registered at a lower cylinder height than in assays where discharge occurred more rapidly. On the other hand, with faster discharge (greater degree of outlet gate opening), more movement occurred in the upper layers and the material did not have time to achieve such a large increase in *unit weight* in the hopper as was produced with a slow discharge.

Table 5
Maximum variation in normal pressure on the wall during discharge 1 with respect to pressures in static state 1 (ΔS1–D1) and during discharge 2 with respect to static state 2 (ΔS2–D2).

		P_{hGA7}	P_{hGA6}	P_{hGA5}	P_{hGA4}	P_{hGA3}	P_{hGA2}	P_{hGA1}	P_{hGA0}
TEST 8	Δ(D1-S1)	0,7%	26,7%	23,6%	16,5%	51,2%	56,8%	75,8%	122,3%
	Δ(D2-S2)	-11,6%	13,4%	-6,1%	-5,9%	-6,5%	-8,4%	3,8%	8,0%
TEST 9	Δ(D1-S1)	-4,3%	18,9%	16,6%	7,8%	40,6%	60,7%	80,6%	109,5%
	Δ(D2-S2)	-7,7%	16,1%	-4,5%	-3,8%	-4,7%	-5,4%	3,1%	4,6%
TEST 10	Δ(D1-S1)	-6,5%	19,8%	6,8%	0,1%	35,5%	46,3%	63,7%	108,1%
	Δ(D2-S2)	-7,7%	19,3%	-1,1%	-10,5%	-2,1%	-12,3%	14,3%	10,7%
TEST 11	Δ(D1-S1)	-7,2%	19,3%	10,8%	-3,2%	32,3%	42,9%	74,4%	125,5%
	Δ(D2-S2)	-14,0%	14,4%	-10,6%	-17,7%	-13,9%	-11,7%	15,2%	18,9%
TEST 12	Δ(D1-S1)	-8,8%	11,4%	-2,6%	-3,3%	22,2%	45,8%	72,7%	153,5%
	Δ(D2-S2)	10,9%	22,1%	1,2%	-1,0%	7,9%	5,4%	14,1%	3,3%
TEST 13	Δ(D1-S1)	-8,4%	17,5%	-4,1%	-3,7%	6,4%	28,3%	59,5%	143,3%
	Δ(D2-S2)	9,8%	13,7%	-3,5%	-6,0%	-1,3%	-4,1%	19,4%	10,1%
TEST 14	Δ(D1-S1)	-8,2%	6,9%	-4,5%	-6,6%	15,9%	43,0%	74,6%	156,7%
	Δ(D2-S2)	10,2%	27,2%	0,1%	-0,6%	8,6%	6,1%	12,7%	3,2%
TEST 15	Δ(D1-S1)	-10,2%	22,8%	-3,6%	-3,6%	3,0%	24,2%	64,3%	144,7%
	Δ(D2-S2)	13,6%	15,6%	6,7%	-6,4%	2,8%	1,7%	22,9%	7,1%
TEST 16	Δ(D1-S1)	-10,3%	15,2%	-4,3%	-5,7%	9,4%	39,6%	76,4%	167,4%
	Δ(D2-S2)	16,3%	17,5%	0,3%	-8,6%	-2,1%	3,1%	25,8%	9,9%
TEST 17	Δ(D1-S1)	-9,1%	8,8%	-3,8%	-4,3%	-1,6%	26,0%	60,1%	164,5%
	Δ(D2-S2)	6,0%	13,8%	5,4%	0,2%	12,7%	3,8%	11,0%	1,3%
TEST 18	Δ(D1-S1)	-9,2%	19,5%	-5,0%	-3,6%	5,0%	35,6%	65,2%	185,6%
	Δ(D2-S2)	11,9%	15,8%	-0,8%	-0,3%	5,3%	4,6%	17,7%	2,5%
TEST 19	Δ(D1-S1)	-8,6%	11,8%	-3,8%	-3,9%	-3,1%	15,1%	65,8%	144,8%
	Δ(D2-S2)	8,2%	19,6%	5,1%	-4,5%	-0,4%	-0,8%	21,7%	5,9%
TEST 20	Δ(D1-S1)	-9,0%	9,1%	-3,7%	-2,6%	11,7%	34,4%	78,8%	128,9%
	Δ(D2-S2)	17,2%	32,3%	-0,3%	-12,4%	-7,2%	0,0%	23,4%	12,8%

Minimum pressures were also observed at the height of the GA4 cell. Throughout the experiments, we repeatedly checked that calibration of the load cells, and of the GA4 cell in particular, was correct. We believe that this phenomenon was due to the variations in specific weight that occurred during discharge, increasing in some areas at the expense of a decrease or the formation of a gap in others, and that in a slender silo of infinite height this effect would be repeated along the entire height of the silo.

Fig. 14 gives the maximum normal wall pressures in the lower section of the silo (GA0 and GA1) recorded throughout the entire test (maximum for both discharges), for each discharge flow rate. As in the type I assays, pressures on the hopper wall (GA0) decreased linearly as the discharge rate increased ($r^2 = 0.423$), whereas pressures in the cylinder (GA1) remained virtually constant, independently of the rate of discharge.

As in the previous case, it is therefore concluded that a slow discharge does not imply lower pressures than those produced during a rapid discharge.

Fig. 15 shows the values obtained for the parameters K, n_{ZSK} and μ, compared with the values proposed in the Eurocode [21]. For the same

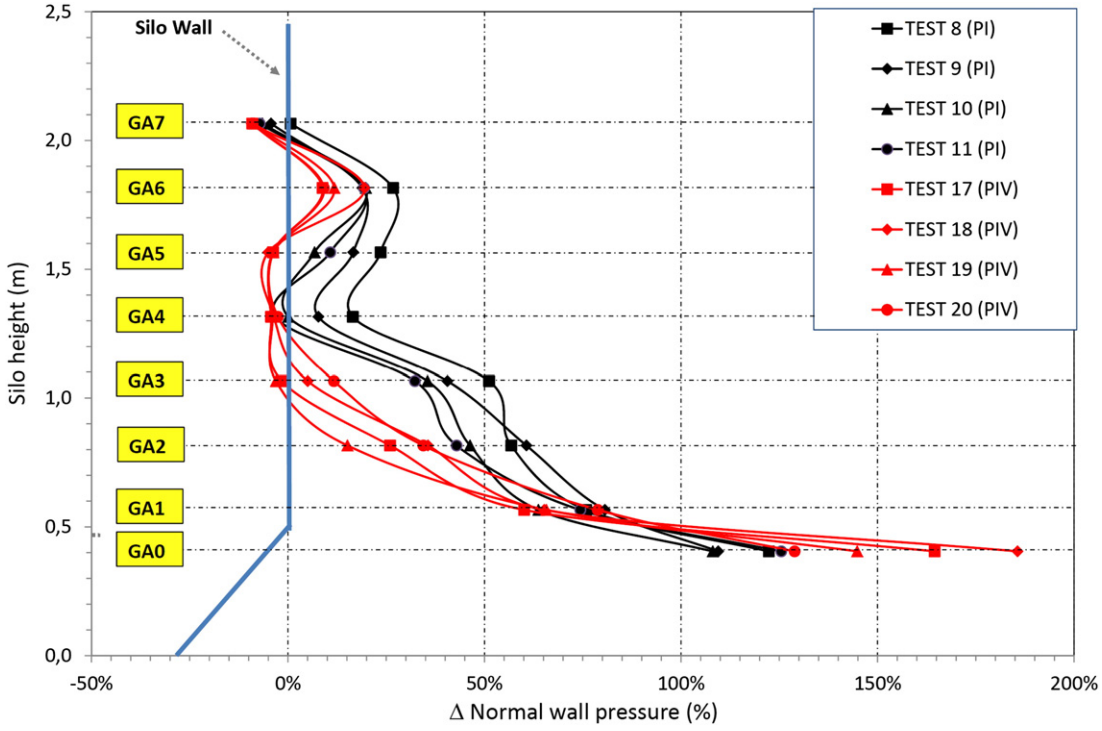

Fig. 13. Maximum variation in wall pressure during the first discharge with respect to the previous static state. Type II assays with the outlet gate in positions PI and PIV.

reason as that discussed for type I assays, the value of K and μ throughout the assay are not shown. In the Figure, it can be seen that in static state 2, the value of n_{ZSK} was not constant but rather decreased, due to the phenomenon discussed above of resettling of the grain. This parameter attained its maximum values at the beginning of the discharge, for both the discharges that comprised the test: however, at no time were the values proposed in the Eurocode for this parameter achieved. Focusing on the value of K, it can be seen that this underwent a sharp increase in the first discharge, exceeding the value obtained using the calculation method proposed in the Eurocode. Furthermore, this value did not fall to that obtained during the previous static state, which is logical since the normal cylinder wall pressure at the silo–hopper transition was not

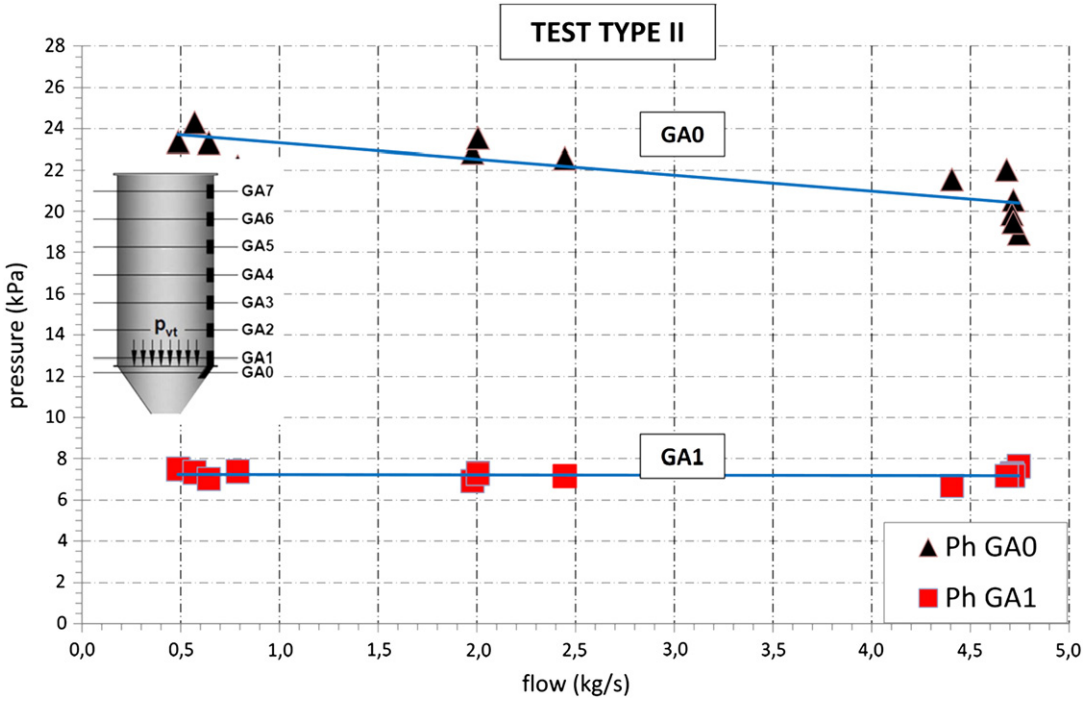

Fig. 14. Regression lines obtained from the maximum normal pressures on the cylinder wall and the hopper wall at the silo–hopper transition registered during the assays (discharge 1 and discharge 2), for each discharge flow rate. Type II assays.

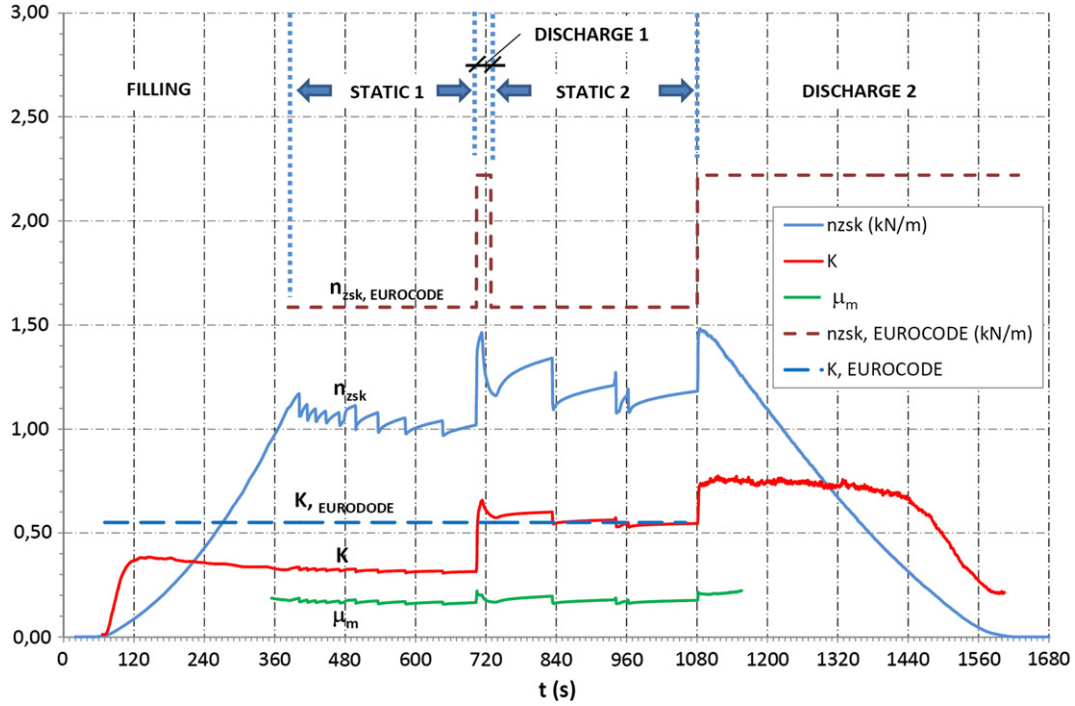

Fig. 15. Mean value of resultant vertical stress per unit perimeter at the transition ($n_{zSk,t}$), lateral pressure ratio at the transition (K); mean value of the wall friction coefficient between the stored material and the cylinder wall (μ_m). Comparison between the values obtained in test 14 and those obtained using Eurocode 1, part 4. Type II assay.

recovered either, whereas vertical stress in the stored material (p_{vt}) did decrease (Fig. 12). As regards the grain to wall coefficient of friction value, it can be observed that this remained virtually constant throughout the assay, presenting temporary increases at the beginning of each of the discharges.

Another of the main results obtained from the type II assays was that with the discharge of a small amount of material from the silo, in this case ranging from 1.7% to 3.2%, a state of overpressure was produced in the silo with maximum values similar to those attained when a complete discharge was effected. These pressures barely decreased until the

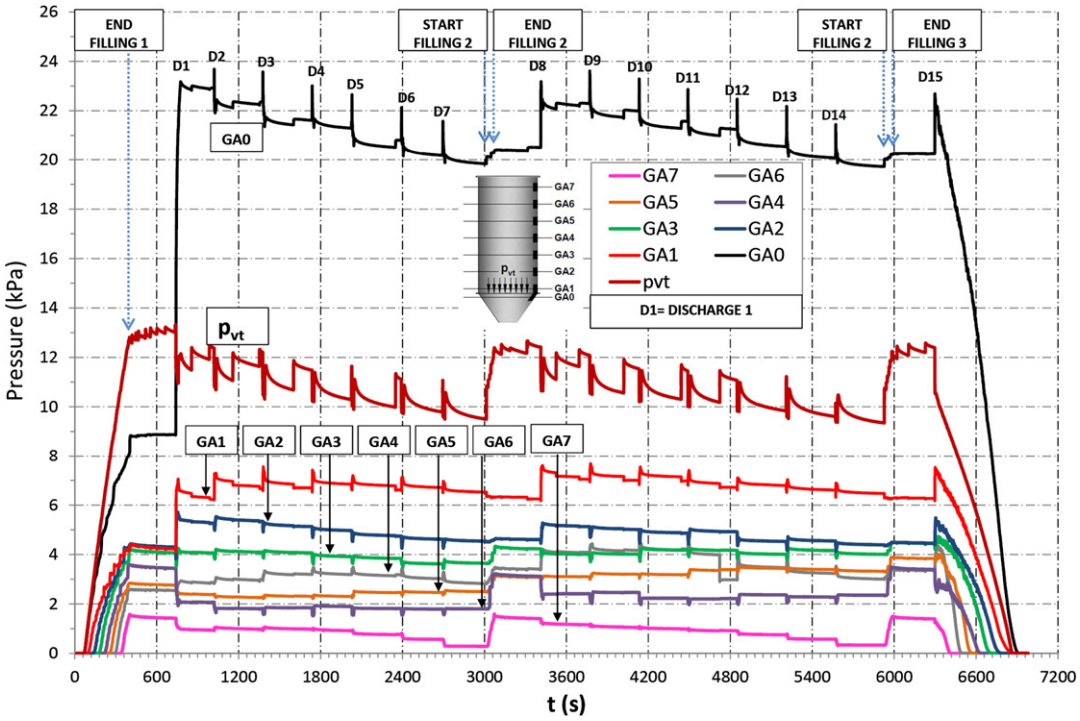

Fig. 16. Normal silo wall pressures ($p_{hGA,t}$) and vertical stress in the stored material at the transition ($p_{vt,t}$), at each time t. Type III assay, test 21.

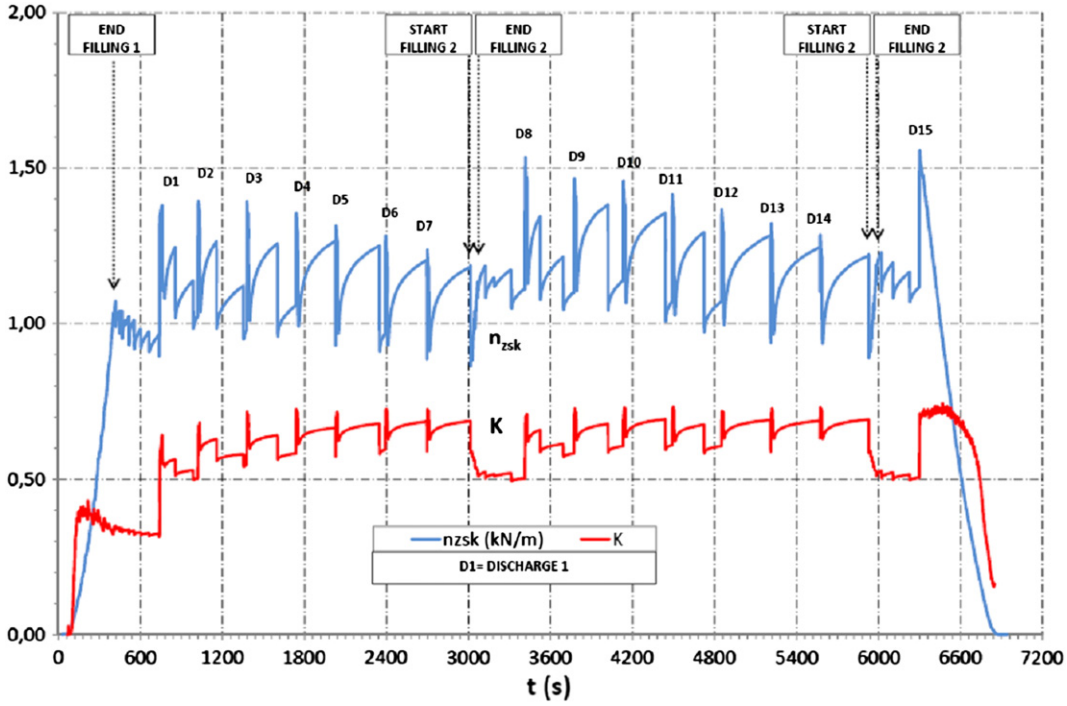

Fig. 17. Mean value of resultant vertical stress per unit perimeter at the transition ($n_{zSk,t}$), lateral pressure ratio at the transition (K), values obtained in type III assay, test 21 and using Eurocode 1, part 4.

silo was once again empty, and furthermore, during the second discharge the maximum pressure values were even higher. This aspect should be taken into account in the design of silos, since in practice, the material stored in silos is not always discharged all at the same time, but is rather discharged in several stages according to the need or demand for the material stored.

Figs. 16 and 17 show the curves obtained for the various parameters discussed above for the type III assay, and Table 3 shows the duration of the different phases and the corresponding numerical results. As expected in view of the previous results, following the first discharge, static state pressures did not return to the initial values obtained at the end of the first loading. At the silo–hopper transition (GA0–GA1),

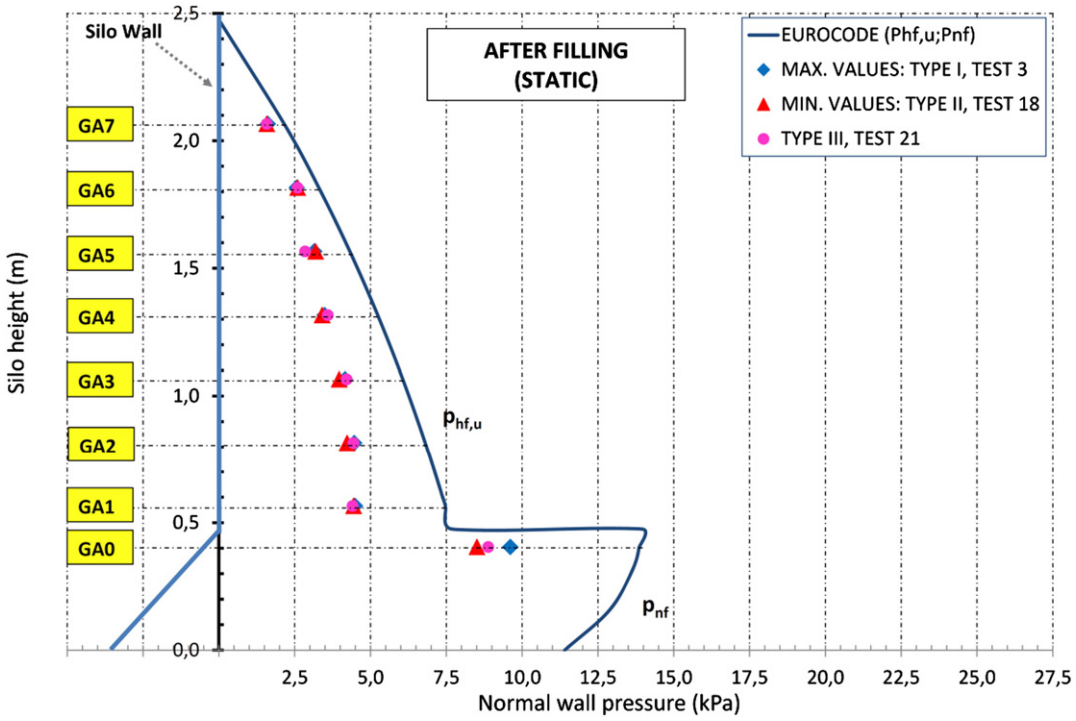

Fig. 18. Maximum values of normal wall pressures after the first loading, compared with Eurocode 1, part 4.

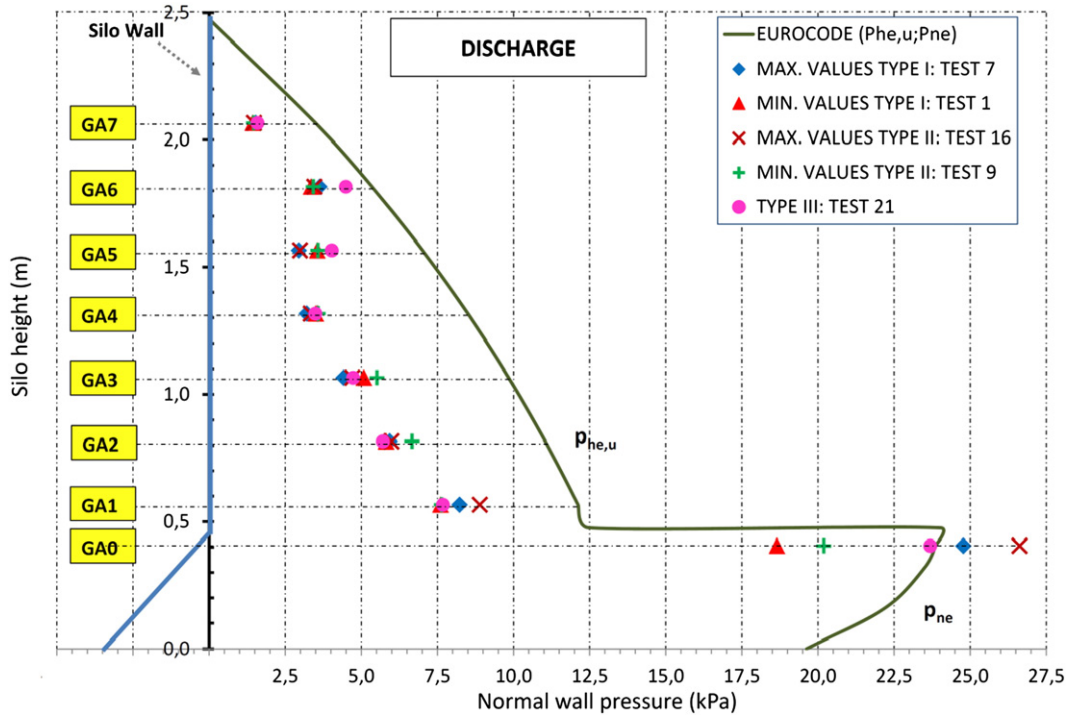

Fig. 19. Maximum values of normal wall pressures obtained during discharge throughout the entire test, compared with Eurocode 1, part 4.

it can be seen that pressures decreased after successive discharges, but this drop was due to progressive emptying of the silo (weight loss). In the successive discharges carried out, it can be seen that peaks in pressures appeared that rapidly disappeared again on returning to static state. These temporary increases in pressure were due to an increase in volume caused by lateral displacement of the grain, a phenomenon known as dilatancy. In other words, a process occurs inside the silo during discharge which is similar to what would happen if loose granular material were subjected to shear stress in a triaxial apparatus: the shearing induces an increase in the material's specific gravity, and after successive shearing episodes a weight which could be called "critical" is obtained. Once this has happened, further episodes will lead to an increase in volume.

To summarise, from an interpretation of the curves it can be deduced that at the beginning of the first discharge the granular material was compacted in the lower sections of the silo, increasing in weight

Table 6
Comparison between the maximum normal wall pressures at the level of the silo–hopper transition obtained in assays during discharge and using Eurocode 1, part 4.

	LEVEL P_{hGA1}			LEVEL P_{hGA0}		
	Eurocode	TESTS	Δ(%)	Eurocode	TESTS	Δ(%)
TEST 1	12,12	7,60	-37,29%	23,86	18,65	-21,84%
TEST 2	12,12	7,14	-41,06%	23,86	18,82	-21,12%
TEST 3	12,12	7,98	-34,17%	23,86	21,09	-11,62%
TEST 4	12,12	7,76	-35,94%	23,86	20,87	-12,55%
TEST 5	12,12	7,80	-35,67%	23,86	22,26	-6,72%
TEST 6	12,12	8,20	-32,32%	23,86	21,76	-8,80%
TEST 7	12,12	8,23	-32,09%	23,86	24,77	3,82%
TEST 8	12,12	7,28	-39,93%	23,86	20,54	-13,92%
TEST 9	12,12	7,63	-37,00%	23,86	20,19	-15,39%
TEST 10	12,12	8,04	-33,63%	23,86	21,99	-7,85%
TEST 11	12,12	8,06	-33,51%	23,86	23,14	-3,02%
TEST 12	12,12	7,79	-35,74%	23,86	23,12	-3,11%
TEST 13	12,12	7,70	-36,42%	23,86	25,99	8,93%
TEST 14	12,12	7,79	-35,75%	23,86	23,46	-1,67%
TEST 15	12,12	8,01	-33,88%	23,86	24,89	4,30%
TEST 16	12,12	8,89	-26,62%	23,86	26,62	11,56%
TEST 17	12,12	7,99	-34,10%	23,86	24,05	0,79%
TEST 18	12,12	8,13	-32,87%	23,86	25,46	6,68%
TEST 19	12,12	7,96	-34,30%	23,86	25,02	4,87%
TEST 20	12,12	8,82	-27,26%	23,86	25,66	7,52%
TEST 21	12,12	7,68	-36,63%	23,86	23,68	-0,75%

until reaching a critical value, and it is this phenomenon which was mainly responsible for the increase in pressures in this area, a state that was not reversed when discharge was halted. Once this state had been reached, successive discharges no longer caused an increase in specific weight in these zones but rather induced an increase in volume due to the displacement of particles, and this would be responsible for the peaks in pressure that occurred and which returned to initial values when the discharge was stopped. This decrease in pressure in the upper sections was due to migration of the material located here to areas which were compacted, and in view of the curves shown in Fig. 13, we believe that in a silo of infinite height, areas of increased and decreased pressures would alternate along the length of its walls.

It can be seen in Table 5 that due to an increase in the *specific weight of the material* during the first discharge, an increase in pressure was registered at GA0 which ranged from 108.1% to 185.6%, and at GA1 from 59.5% and 80.6%, depending on the test in question. The same Table shows the pressure also that increase during the second discharge occurred, attributed to dilatancy, which at GA0 ranged from 1.3% to 18.9% and from 3.1% at GA1 to 25.8%.

Careful observation of the curves obtained from the cells in the upper section of the silo (GA6–GA7) would seem to indicate that the pressure decreased during successive discharges with respect to the previous static state, which would not support the theory outlined above. However, if a detailed examination of the data shown in Table 3 is conducted, it will be seen that during each discharge, the pressure increased slightly with respect to the previous static state, which corresponds to the minimum value recorded. In other words, dilatancy produced a slight temporary rise in pressure during discharge, but this was much less as the grain was less compacted in these areas.

In Figs. 18 and 19, the normal wall pressures obtained in the assays are compared with Eurocode 1, Part 4 [21]. Fig. 18 shows the maximum pressures obtained in static state assays conducted following the first loading. In this phase, the three types of assays were similar and thus to avoid lack of clarity in the graph only the type III assay is shown together with type I and II assays in which higher and lower pressure values were obtained. As can be seen, at all heights and in all cases, the pressures were lower than those obtained using the calculation method proposed in the Eurocode.

Fig. 19 shows the maximum pressures obtained in discharge phase assays throughout the entire test. In this case, the curves shown for assays give maximum and minimum values for each type, since in this phase they were not analogous. Table 6 presents a comparison between the maximum normal wall pressures at the level of the silo–hopper transition obtained in assays during discharge and those obtained using Eurocode 1, part 4. As can be seen, during discharge, the normal cylinder wall pressure at the level of the silo–hopper transition obtained in the assays was always below that given in the Eurocode. However, at the same level, the normal hopper wall pressures exceeded those given in the Eurocode in 8 of the tests, reaching a value greater than 11.56% with respect to the calculation method proposed in the Eurocode. It is possible that this phenomenon may be due to the small size of the test silo and that it would not occur in a larger silo, since the lower the pressure levels, the higher the internal friction angle and dilatancy angle, and consequently, wall pressures rise.

The assays described in this paper are not totally comparable with other experiments conducted using real silos, since this would require the use of silos of similar dimensions, the same stored material and the same kind of assay, circumstances which are not fulfilled by any published article worldwide. Nevertheless, some aspects are comparable. Thus, as expected, normal wall pressure underwent considerable variation at the beginning of discharge, reaching highest values at the hopper wall, at the level of the silo–hopper transition, which is consistent with European standards [21] and with international tests on real silos [7,8,12,13]. Another aspect that coincides with the results obtained by Wojcik [24] is the fact that during discharge, almost constant or even decreasing pressures were registered in the upper part of the cylinder compared to during static state. Those areas where the pressure decreased represented discontinuities or gaps caused because the material from the lower layers subsided due to the discharge whilst at the same time the upper layers stopped subsiding due to friction with the wall. In a silo of infinite height, this phenomenon would be repeated alternately throughout the entire height of the silo. This finding coincides with the results obtained by Wojcik [24], who conducted tests on a silo full of sand. During discharge, gaps were detected in the sand, which had initially been dense in static state. These gaps or rupture zones alternated in height along the entire length of the cylinder wall and took the shape of an arrow pointing towards the upper part of the silo. Another aspect which is also comparable and has been described by other authors is the fact that a small discharge of material caused a change in pressures in the silo that did not revert when the silo returned to a static state. This phenomenon has been described by Pieper and Wenzel [29], who reported the following: “When discharge was halted, the pressure registered in that instant remained constant for 15 h”.

4. Conclusions

Pressures were not constant in the static state, since the grain underwent a process of resettling at increasingly wider spaced intervals.

In contrast to other tests, in the assays conducted, a reduced flow rate (kg/s) of the granular material during discharge did not entail an associated decrease in pressures on the silo wall, but rather the opposite.

Variations in flow speed (kg/s) produced changes in pressure distribution inside the silo. Thus, greater thrusts were recorded in the silo–hopper transition and lower thrusts on the wall at a slow speed than at a high flow speed.

At the beginning of discharge, the granular material underwent a process of variation in *unit weight*, where *unit weight* increased in some areas more than others or even decreased, and it was this effect which was primarily responsible for the variations in pressure inside the silo during discharge. Even if discharge was halted at this point, the silo did not recover the previous pressure values, and attained a state of overpressure similar to that produced when complete discharge was effected in a single step.

Once the material had reached a certain degree of *unit weight*, which could be called “critical”, variations in pressure during discharge were due to the phenomenon known as dilatancy, i.e., the increase in volume caused by dilatancy in a vertical direction due to the presence of stiff walls.

During discharge, the normal hopper wall pressures at the level of the silo–hopper transition can exceed those obtained using the calculation method proposed in the Eurocode 1, part 4.

Acknowledgements

The authors thank the Spanish Research and Technology Commission (CICYT) (Research Project AGL2005-07430-C02-01/AGR) and the Regional Executive of Castile and León (Research Project LE020A10-2) for financing this research.

References

[1] H.A. Janssen, Versuch über Getreidedruck in Sillozellen, Zeitschrift des Vereins Deutscher Ingenieure 39 (1895) 1045–1049.
[2] F. Ayuga, Some Unresolved Problems in the Design of Steel Cylindrical Silos, Crc Press-Taylor & Francis Group, Boca Raton, 2008.
[3] A. Dogangun, Z. Karaca, A. Durmus, H. Sezen, Cause of damage and failures in silo structures, Journal of Performance of Constructed Facilities 23 (2) (Mar–Apr 2009) 65–71.
[4] J. Nielsen, From Silo Phenomena to Load Models, 2008, 2008.
[5] J. Nielsen, V. Askegaard, Scale errors in model tests on granular media with special reference to silo models, Powder Technology 16 (1) (1977) 123–130.
[6] C.J. Brown, E.H. Lahlouh, J.M. Rotter, Experiments on a square planform steel silo, Chemical Engineering Science 55 (20) (2000) 4399–4413.

[7] J. Härtl, J.Y. Ooi, J.M. Rotter, M. Wojcik, S. Ding, G.G. Enstad, The influence of a cone-in-cone insert on flow pattern and wall pressure in a full-scale silo, Chemical Engineering Research and Design 86 (4) (2008) 370–378.
[8] A. Ramirez, J. Nielsen, F. Ayuga, Pressure measurements in steel silos with eccentric hoppers, Powder Technology 201 (1) (Jul 2010) 7–20.
[9] T. Schurich, C. Fürll, G.G. Enstad, Full scale silo tests and numerical simulations of the "cone in cone" concept for mass flow, in: Kalman ALaH (Ed.), Handbook of Powder Technology, Elsevier Science B.V., 2001, pp. 175–180.
[10] J.G. Teng, F. Chan, Plastic buckling strength of T-section transition ringbeams in steel silos and tanks, Engineering Structures 23 (3) (Mar 2001) 280–297.
[11] J.G. Teng, X. Lin, J.M. Rotter, X.L. Ding, Analysis of geometric imperfections in full-scale welded steel silos, Engineering Structures 27 (6) (May 2005) 938–950.
[12] Z. Zhong, J.Y. Ooi, J.M. Rotter, The sensitivity of silo flow and wall stresses to filling method, Engineering Structures 23 (7) (Jul 2001) 756–767.
[13] V. Askegaard, J. Munch-Andersen, Results from tests with normal and shear stress cells in a medium-scale model silo, Powder Technology 44 (2) (1985) 151–157.
[14] J.F. Chen, J.M. Rotter, J.Y. Ooi, Z. Zhong, Flow pattern measurement in a full scale silo containing iron ore, Chemical Engineering Science 60 (11) (2005) 3029–3041.
[15] J.F. Chen, J.M. Rotter, J.Y. Ooi, Z. Zhong, Correlation between the flow pattern and wall pressures in a full scale experimental silo, Engineering Structures 29 (9) (Sep 2007) 2308–2320.
[16] J.Y. Ooi, L. Pham, J.M. Rotter, Systematic and random features of measured pressures on full-scale silo walls, Engineering Structures 12 (2) (1990) 74–87.
[17] J.M. Rotter, C.J. Brown, E.H. Lahlouh, Patterns of wall pressure on filling a square planform steel silo, Engineering Structures 24 (2) (Feb 2002) 135–150.
[18] J. Wu, J. Binbo, J. Chen, Y. Yang, Multi-scale study of particle flow in silos, Advanced Powder Technology 20 (1) (2009) 62–73.
[19] S.-C. Yang, S.-S. Hsiau, The simulation and experimental study of granular materials discharged from a silo with the placement of inserts, Powder Technology 120 (3) (2001) 244–255.
[20] F. Ayuga, M. Guaita, P.J. Aguado, A. Couto, Discharge and the eccentricity of the hopper influence on the silo wall pressures, Journal of the Engineering Mechanics Division, ASCE 127 (10) (Oct 2001) 1067–1074.
[21] CEN. EN 1991-4:2006, Eurocode 1: Actions on structures. Part 4: Silos and Tanks, European Committee for Standardization, Brussels, 2006.
[22] A.W. Jenike, J.R. Johanson, On theory of bin loads, Mechanical Engineering 91 (1) (1969) 43.
[23] C. Slominski, M. Niedostatkiewicz, J. Tejchman, Application of particle image velocimetry (PIV) for deformation measurement during granular silo flow, Powder Technology 173 (1) (2007) 1–18.
[24] M. Wójcik, J. Tejchman, Modeling of shear localization during confined granular flow in silos within non-local hypoplasticity, Powder Technology 192 (3) (2009) 298–310.
[25] M. Wójcik, J. Tejchman, G.G. Enstad, Confined granular flow in silos with inserts. Full-scale experiments, Powder Technology 222 (2012) 15–36.
[26] A. Couto, A. Ruiz, P.J. Aguado, Design and instrumentation of a mid-size test station for measuring static and dynamic pressures in silos under different conditions — Part I: description, Computers and Electronics in Agriculture 85 (0) (2012) 164–173, (7//).
[27] A. Ruiz, A. Couto, P.J. Aguado, Design and instrumentation of a mid-size test station for measuring static and dynamic pressures in silos under different conditions — Part II: construction and validation, Computers and Electronics in Agriculture 85 (0) (2012) 174–187, (7//).
[28] M. Sugita, Flow and pressures of noncohesive granular materials in funnel-flow bins, Mechanical Engineering 94 (12) (1972) 60.
[29] K. Pieper, F. Wenzel, Druckverhaltnisse in Silozellen, Verlag von Wilhelm Ernst & Sohn, Berlin, Munich, 1964.